Stony Brook University

Anti-catabolic Role of Ultrasonic Mechanical Perturbation in Prevention of Bone Loss and Turnover in OVX Rat Model: A Combined Empirical, Nanomechanical and Micro-numerical Simulation Approach

A Dissertation Presented

by

Suzanne Lynn Ferreri

to

The Graduate School

in partial fulfillment of the

Requirements

for the Degree of

Doctor of Philosophy

in

Biomedical Engineering

Stony Brook University

August 2009

Stony Brook University

The Graduate School

Suzanne Lynn Ferreri

We, the dissertation committee for the above candidate for the

Doctor of Philosophy degree,
hereby recommend acceptance of this dissertation.

Yi-Xian Qin, Ph.D., Advisor
Professor
Department of Biomedical Engineering

Stefan Judex, Ph.D., Committee Chair
Associate Professor
Department of Biomedical Engineering

Clinton T. Rubin, Ph.D.
Professor and Chair
Department of Biomedical Engineering

X. Edward Guo, Ph.D., External Member
Professor
Department of Biomedical Engineering
Columbia University

This dissertation is accepted by the Graduate School

Lawrence Martin
Dean of the Graduate School

Abstract of the Dissertation

Anti-catabolic Role of Ultrasonic Mechanical Perturbation in Prevention of Bone Loss and Turnover in the OVX Rat Model: A Combined Empirical, Nanomechanical and Micro-numerical Simulation Approach

by

Suzanne Lynn Ferreri
Doctor of Philosophy
in
Biomedical Engineering
Stony Brook University

2009

Osteoporosis is a disease characterized by decreased bone mass and progressive erosion of the microstructure. As a result, bone is at higher risk for developing chronic and traumatic fractures at key skeletal sites such as the hip, spine and wrist. Current therapies, including hormonal and pharmacologic approaches, are not site-specific and often cause adverse side effects. Therefore, it is necessary to develop complementary and alternative, site-specific interventions for the treatment of osteopenic bone loss and microstructural deterioration. Therapeutic ultrasound may offer a potential non-pharmacologic, site-specific intervention.

The overall goal of this dissertation is to explore the therapeutic potential of LIPUS for treatment of bone loss associated with estrogen deficient osteopenia. The principal hypothesis is that therapeutic ultrasound improves bone quantity and quality under conditions of estrogen deficient osteopenia, and that intensity and pulse duration play a role in bone's adaptive response.

This hypothesis was tested in a series of specific aims. The first two aims address the role of ultrasound pulse duration in mediating bone's response to estrogen deficient osteopenia. In **Aim #1**, we determine the effect of pulse duration on morphology and mechanical properties using *μCT* and *μFE. In* **Aim #2**, we determine the effect of pulse duration on tissue level mechanical properties using *nanoindentation.* The second two aims address the role of signal intensity in bone's response. In **Aim #3**, we determine the effect of signal intensity on morphology and mechanical properties using *μCT* and *μFE. In* **Aim #4**, we determine the effect of signal intensity on tissue level mechanical properties using *nanoindentation*. Lastly, in **Aim #5**, we determine ultrasound wave propagation in the rat lumbar vertebra using *computational simulations*.

The results show that both 0.5MHz signals (~0.1mW/cm^2) and 1.5MHz signals (>30mW/cm^2) mediate changes to bone morphology and mechanical properties. At the tissue level, however, only higher intensity signals (>30mW/cm^2) mediate loss of tissue level modulus. Results indicate that bone's response is sensitive to changes in signal intensity but not pulse duration. The results also show that bone's response to locally

applied ultrasound was site specific and did not drive a systemic adaptive response. Lastly, we demonstrated that computational models could be used to describe how ultrasound signals propagate in geometrically complex tissues and that 1.5MHz signals had greater signal attenuation compared to 0.5MHz signals. Computational approaches could offer a means for developing individualized, site specific and targeted therapies which consider a patient's individual bone status in the optimization of a treatment protocol. These results suggest that ultrasound may provide a targeted therapy for treatment of skeletal sites prone to chronic and traumatic fractures.

Table of Contents

List of Figures

List of Tables

Chapter 1:

Introduction and Background

1.1 The Socioeconomic Impact of Osteoporosis

Osteoporosis is a systemic skeletal disease, which results in compromised bone quality and an increased susceptibility to chronic and traumatic fractures [3, 4]. Osteoporosis related fractures represent an important clinical challenge as they are associated with decreased mobility, prolonged disability and increased mortality [5, 6]. The presence of osteoporosis is pervasive in American society and is estimated to affect nearly 10 million individuals, with an additional 34 million individuals experiencing low bone mass [6]. Particularly affected are post-menopausal women. It is also a worldwide health problem in musculoskeletal system [7, 8]. It has been shown that in the ten years following menopause, women experience an increased rate of bone loss, approximately 2% per year [9]. Furthermore, it has been shown that Caucasian women, age 50 or older, are at higher risk for dying of an osteoporosis related fracture than from breast cancer and stroke combined [6, 10]. As a result hormonal (estrogen), pharmachologic [11] and mechanical vibration [12] treatments have been developed. However, such treatments have been known to have adverse side effects and are not specific to key skeletal sites known to experience fracture, such as the hip, spine and wrist. Furthermore, these treatments do not improve long-term bone quality, nor do they decrease the risk for fracture. Therefore, it is necessary to develop complementary and alternative, site-specific interventions for the treatment of osteopenic bone loss and microstructural deterioration.

1.2. The Pathophysiology of Osteoporosis in Bone

Bone is a dynamic tissue which undergoes a constant state of remodeling which, is balanced by both resorption and formation. In normal healthy tissue, there exists a balance between bone resorption and formation rates. In healthy tissue, the bone remodeling process repairs microdamage incurred due to normal daily activity [3]. However, in the case of post-menopausal osteoporosis, reductions in hormone levels of estrogen and testosterone lead to a decoupling in bone modeling/remodeling activities, which ultimately results in decreased overall bone quality [13]. Although a systemic disease, osteoporosis is known to present uniquely at key skeletal sites prone to fracture. Bone loss has also been shown to be greater in areas with larger regions of cancellous bone (i.e. spine, forearms) as opposed to regions dominated by a cortex (diaphysis in long bones). It is believed that bone loss is the result of higher rates of bone turnover. This is not surprising as bone turnover is a surface driven mechanism and trabecular bone has greater surface area; therefore trabecular bone is more susceptible to net bone loss.

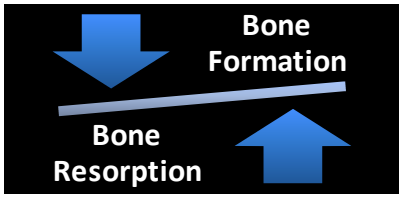

Figure 1. 2: *Changes to osteoporotic bone are the result of an imbalance in the rates of bone formation and bone resorption leading to net bone loss.*

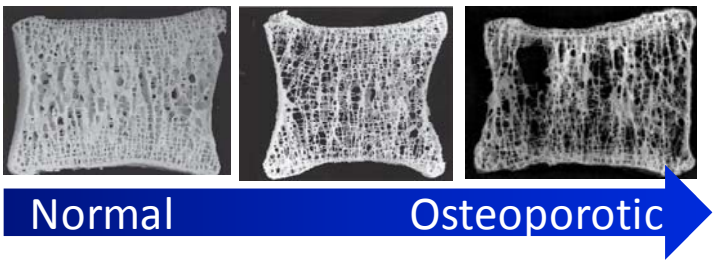

Figure 1.2: *Micrographs of human vertebra at progressive stages of osteoporosis [1].*

1.3. Mechanotransduction: Mechanical Loading and Bone Fluid Flow in Bone

Bone has been shown to be responsive to mechanical stimuli, adapting it's mass and morphology to its dominant loading conditions over time [14]. In addition, dynamically applied signals have been shown to induce an osteogenic response, while statically applied signals may have the opposite effect, resulting in net bone resorption [15]. In addition, bone's response has been shown to be sensitive to loading rate, strain magnitude, strain gradient and loading history [16-22]. The introduction of rest periods between loading bouts has also been show to have osteogenic potential [23-25].

Fluid flow within bone's microvasculature could also drive

. One potential mechanism involves dynamic bone fluid flows within the vascular and lacuno-canaclicular porosities. In general, it is believed that bone fluid flow (BFF) acts in two ways. First, BFF plays a role in the movement of nutrients and waste to and from bone cells. Changes in this process could result in alterations in cellular function. A second mechanism is that bone fluid flow can generate pressure gradients within the lacunar-canalicular porosities which may then result in fluid stresses that can be sensed by inter-calunar cellular processes or the osteocyte membrane itself [26-30].

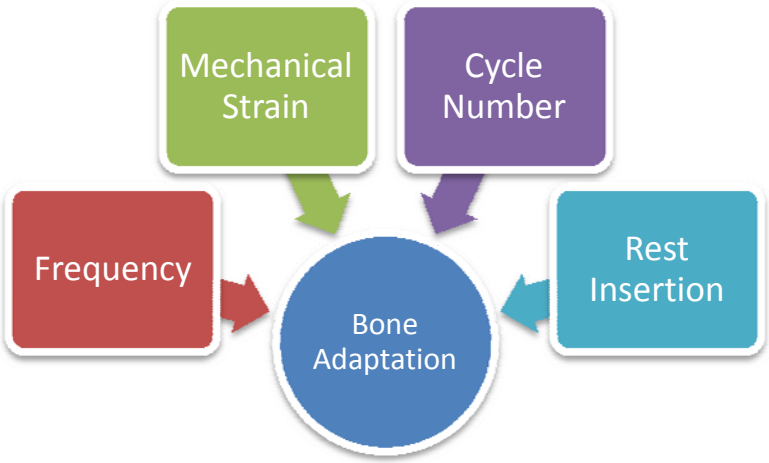

Figure 1.3: *Schematic depicting contributing mechanical loading parameters in mechanical strain driven bone adaptation.*

1.4 Biophysical Effects of Ultrasound

1.4.1 The effects of ultrasound in vitro and ex vivo

In vitro studies have shown that LIPUS is capable of increasing osteoblast proliferation and stimulating endochondral ossification in excised tissues [31-34]. It has also been shown that ultrasound signal intensity plays an important role in modulating the response of osteoblasts in vitro [35, 36]. It is unclear what role ultrasound signal parameters such as pulse duration or duty cycle play in bone's response. Bone and bone cells have been shown to be sensitive to the ratio of on cycles to off cycles applied during low amplitude, high frequency vibrations in vitro [23]. In addition, at ultrasound frequencies, membrane permeability may be associated with changes in duty cycle [37]. Harle et al also showed that alkaline phosphatase expression was linked to ultrasound signal intensity [38]. In vitro studies also suggest that ultrasound signal intensity may play a role in the response of osteoblasts in cell culture [34, 36, 39]. In vitro studies have shown that ultrasound delivered at spatial-averaged temporal-averaged intensities (I_{SATA}) ranging from 0.01 to 10mW/cm^2 is capable of enhancing endochondral bone formation for ex vivo tissues and in cell culture [31-34, 40, 41].

1.4.2 The role of ultrasound in fracture healing

Several studies have shown that low intensity ultrasound can be used in the treatment of fractures and fracture nonunion. Clinical studies have found that LIPUS ultrasound signals (I_{SATA} 30mW/cm^2, 1.5MHz pulsed US) could reduce healing time of fractures of the tibial diaphysis [42, 43] and distal radius [44-46]. Studies have shown that ultrasound is capable of enhancing endochondral bone formation, mineral density and mechanical strength [47-52]. Another application of therapeutic ultrasound is that of the treatment of fracture non-unions. Ultrasound has been shown to be effective in improving outcomes for fracture non-unions [53, 54]. The ultrasound signals used are typically characterized by 1.5MHz signals pulsed at 1kHz and 200µs pulses with I_{SATA} between 30 and 65mW/cm^2 [55-57]. Subsequently, LIPUS has been approved by the US food and drug administration (FDA) for the treatment of fracture non-unions.

1.4.3 Ultrasound as a therapy for intact/non-fractured bone

Studies have also addressed the use of ultrasound to treat bone in vivo. However, the results of these studies are inconclusive and the therapeutic potential of ultrasound for intact bone remains unclear. One study investigated the effect of therapeutic ultrasound (1 MHz signal delivered in 10µs bursts at 3.3kHz pulse repetition rate and 30mW/cm^2 I_{SATA}) in the human calcaneus in response to spinal cord injury and found no differences in parameters assessed using QUS and DEXA [58]. A second study investigated the effect of ultrasound (1.5 MHz signal delivered in 200µs bursts at 1 kHz pulse repetition rate and 30mW/cm^2 I_{SATA}) on growing bone in rats and found no differences in bone length or bone mineral content [59]. A third study investigated the effect of continuous ultrasound (1 MHz signal and 125mW/cm^2 I_{SATA}) in rats following sciatic neurectomy and found no differences in parameters measured using DEXA and

histomorphometry [60]. Interestingly, this study observed a significant difference in growth plate thickness between treated and control groups [60]. A fourth study investigated the effect of ultrasound (1 MHz signal delivered in 200µs bursts at 1 kHz pulse repetition rate and 30mW/cm^2 I_{SATA}) in rats following ovariectomy and found no differences in parameters measured with DEXA or histomorphometry [61].

Another study investigating the effects of ultrasound (1.5 MHz signal delivered in 200µs bursts at 1 kHz pulse repetition rate and 30mW/cm^2 I_{SATA}) also found no significant differences in bone mineral content (BMC) [62]. However, this study identified a significant increase in new bone formation and bone volume fraction using histomorphometric techniques and scanning electron microscopy (SEM) [62]. Finally, a study investigating the use of a commercially available system found that ultrasound (1.5 MHz signal delivered in 200µs bursts at 1 kHz pulse repetition rate and 30mW/cm^2 I_{SATA}) was capable of increasing BMC as determined by DEXA in the proximal femur of bedridden patients compared to contra lateral controls [63].

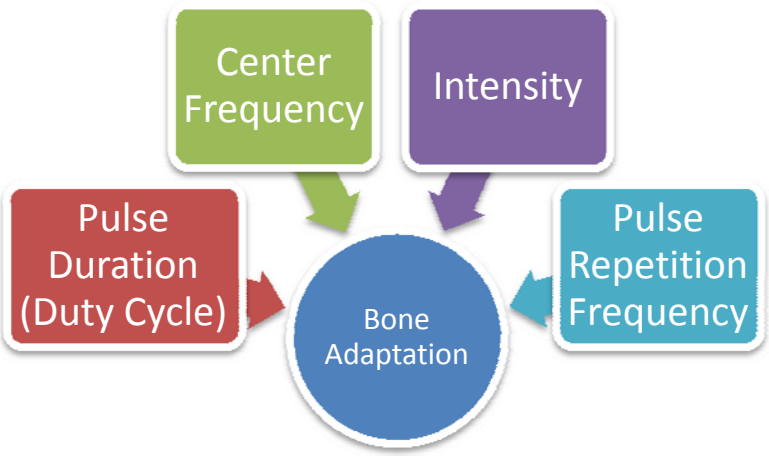

Figure 1.4: *Schematic depicting contributing ultrasound signal parameters involved in bone adaptation.*

1.4.4 Musculoskeletal sensitivity to ultrasound signal parameters

Bone has been shown to be sensitive to differences in ultrasound signal intensity. Yang et al, described improvements in mechanical strength parameters following fracture in groups treated with 50mW/cm^2 but not 100mW/cm^2 [64]. Pulse duration may also play a role in bone's response. Bone and bone cells have been shown to be sensitive to the ratio of on to off cycles applied during low amplitude, high frequency vibrations in vitro [23] and in vivo [24, 25]. In addition, at ultrasound frequencies, membrane permeability may be associated with changes in duty cycle [37].

Ultrasound carrier frequency has also been shown to be a critical factor in regulating bone's response. One study found no differences in bone's healing response for 0.5 and 1.5 MHz signals [48]. In another study, Tsai et al, showed improvements in mineral apposition rates at three weeks post fracture for 1.5 MHz signals over 3 MHz signals [65]. Subsequently, the 1.5MHz signal is the most commonly used signal for stimulating osteogenesis in vitro.

1.5. Experimental Approaches in the Study of Osteoporosis and Osteopenia

1.5.1 The OVX rat model of postmenopausal osteoporosis

Ovariectomy (OVX) in the mature rat is a well characterized modification in which removal of the ovaries leads to decreased levels of estrogen. Similar to post-menopausal osteoporosis in humans, this alteration in hormone levels results in an uncoupling of the balance between bone modeling and remodeling, which leads to increased bone resorption, net bone loss and decreased bone quality. Bone loss and microstructural erosion occurs at a greater rate in cancellous bone compared to cortical bone [66, 67].

OVX modification has also been shown to demonstrate skeletal site specificity. At the proximal tibia, bone volume fraction (BVF), connectivity density (Conn.D.) and trabecular number (Tb.N.) were shown to decline 40%, 45% and 30% within the first two weeks post-OVX [66, 67]. However at approximately 90 days post OVX, the rate of trabecular bone loss in the proximal tibia plateaus. Bone loss in the lumbar spine however, has been shown to be more gradual with significant differences (30% to 40%) in BVF occurring within the first two to four weeks post OVX [68] when measured using μCT techniques. In addition, significant differences were identified in BVF at 4 weeks post OVX using histomorphometric techniques [69, 70] and in bone mineral density (BMD) using DEXA scanning [71]. Mechanical properties were also shown to be compromised at 28 days [68] and 3 months post OVX [72-74].

While bone loss in the OVX rat model can be on the order of 40% within the first four weeks following OVX, bone loss associated with human post-menopausal osteopenia is much slower, occurring at a rate of 2% per year in the first ten years following menopause. This expedited rate of bone loss makes the OVX rat an efficient and more economical option for research addressing the skeletal changes of estrogen deficient osteopenia. It is important to note, however, that while bone loss in humans is often followed by fracture, this is not the case in rats. OVX rats seldom experience bone loss related fractures. Thus, one must consider this observation when extrapolating the effects of long tern OVX in the rat to that of humans.

1.5.2 The rat lumbar vertebra as an analogue for osteopenia in the human spine

The OVX rat is a commonly used animal model for the study of bone remodeling in response to disease progression and prophylaxis or treatment. There are a number of factors, however, that limit the extrapolation of data from morphological and biomechanical studies in the rat, to humans. First, the rat spine is an order of magnitude smaller than that of the human. While anatomically similar, this difference in size could lead to dramatically different biomechanics and therefore an altered adaptation affecting homeostatic loading conditions. Second, while we use the rat lumbar vertebra as an analogue to bone loss in the human spine, chronic compression fractures of the spine in humans primarily occur at the thoracic spine. The preferred use of the rat lumbar spine is primarily due to the small size of rat thoracic vertebra and the

limited volume of trabecular bone. Third, there are differences in the number of lumbar vertebra in the rat and human spines. The human lumbar vertebra is composed of five vertebrae, while the rat has seven lumbar vertebrae.

The overall structure of each vertebra is however, similar in rats and humans. Each vertebra is divided into two regions, the anterior portion, known as the vertebral body, and the posterior aspect, referred to as the vertebral arch. The endplates of each vertebral body form the attachment sites for intervertebral disks. In the human, the vertebral endplates are parallel, while in the rat the anterior edge of the superior surface is inferior to the posterior edge and the anterior edge of the inferior surface is superior to the posterior edge. The vertebral body and arch are connected by a region of cortical bone and together form the vertebral foramen. The vertebral foramen forms a cylindrical space that houses the spinal cord. In humans, the lateral sides of the vertebral foramen are primarily composed of cortical bone, while in the rat, this area contains cancellous bone within a cortical shell at the midpoint along the length of the vertebra. Each vertebral body also contains a series of vertebral processes, or bony structures, which protrude from the vertebral arch and allow for the attachment of muscles and the articulating of joint surfaces. In both species, the spinous process protrudes posteriorly; however, in the rat the spinous process is angled superiorly. On each side of the vertebral arch protrudes a transverse process. In the human, this structure protrudes laterally, while in the rat, they are superiorly antero-lateral. Trabecular bone within the vertebral body is primarily oriented in the superior-inferior direction in both species. This observation is one of the key justifications for the use of a quadruped in the study of biomechanics and disease progression in a bipedal animal [75]. It is thought that the muscle forces required to maintain natural posture create a similar mechanical loading environment in the vertebra of both species.

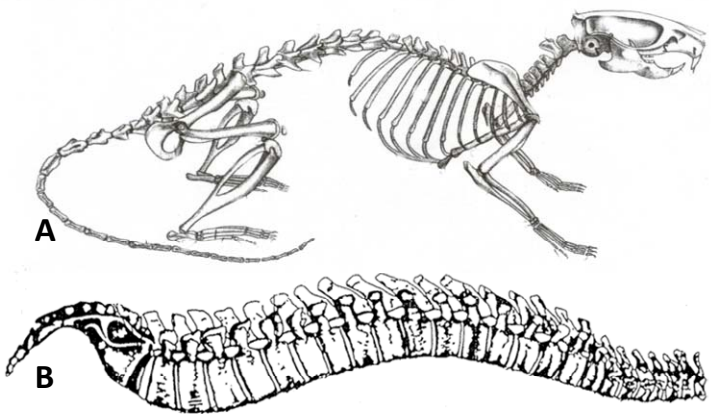

Figure 1.5: *Artistic renderings of the rat skeleton (A) and human spine (B). (Note: A was obtained from Atlas of Rat Anatomy and B from Grey's Anatomy [2]*

1.6.1 Micro-computed tomography (µCT)

Micro-computed tomography (µCT) is a technique which allows for high resolution imaging of musculo-skeletal tissues. Images can be obtained at resolutions as high as 5µm. In the studies presented here we used µCT imaging to evaluate changes in morphology at the rat lumbar vertebra (L4 & L5) and at the femoral metaphysis. Since

data is reported for isolated regions segmented by virtual cut-plane surfaces, it is important to note the importance of regular alignment when scanning each bone. To do this, a custom jig was designed so that the posterior grove of the spinal canal was aligned the vertical axis as shown in Figure 1.2. Therefore, virtual transverse slices were made using morphological landmarks placed at regular positions reducing potential variability due to irregular regions of interest (ROI).

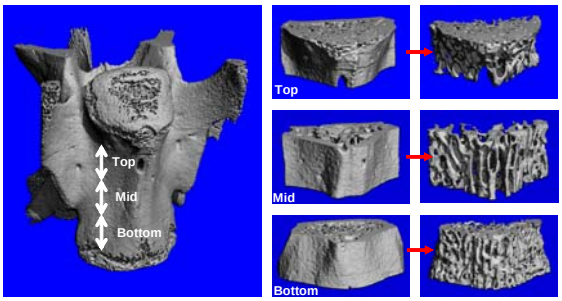

Figure 1.6: *µCT analysis of the lumbar vertebral body. Three consecutive regions of 1.5mm (100 slices) positioned at the center of the vertebral body were used for analysis of trabecular bone.*

1.6.2 Micro-finite element analysis (µFEA)

Micro-finite element analysis (µFEA) is a technique which uses high resolution three-dimensional images to perform "virtual" mechanical testing. The results obtained from µFEA include both global/apparent level measures, such as elastic modulus, and tissue level stress and strain distributions. Therefore, it may provide an improved understanding of bone quality, as it pertains to in vivo response to mechanical loading, over more indirect measures such as BVF, Tb.N., and Conn.D. It is a highly versatile technique, which allows one to perform a number of mechanical test simulations on a single specimen. This could potentially reduce the number of animals required to answer a particular research question.

Micro-finite element analysis has been adapted to the field of orthopedic biomechanics and has proven to be a powerful tool in the study of diseases and treatments affecting cancellous bone. At the millimeter length scale, cancellous bone is highly anisotropic and its response to mechanical loads is sensitive to changes in trabecular thickness, number and the overall connectedness of the specimen. It has been referred to as a "virtual biopsy" as it presents an alternative to the more invasive, iliac crest bone biopsy. It has become an important research tool for animal studies which investigate new diagnostic and therapeutic modalities. It has also been applied to address the effects of aging and pharmacologic treatments on bone at key skeletal sights such as the hip and spine in human models.

While this technique offers a valuable tool in the study of bone biomechanics, it has several limitations which should be considered in application and when interpreting data. First, there is a minimum physical size required of the model to produce accurate results. There are also minimum requirements for mesh resolution. It is widely accepted that the mean trabecular thickness be approximated by at least four times the image resolution. Lastly, as with all modeling studies, the accuracy of the results are only as

good as the quality of the input data. Therefore a reasonable approximation of the boundary and loading conditions should be considered.

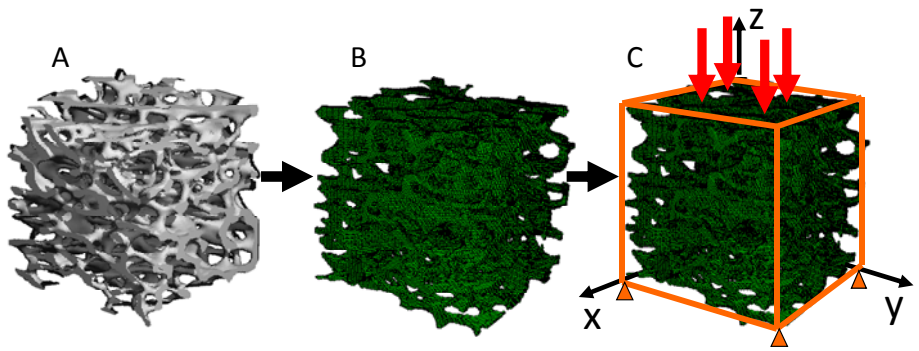

Figure 1.7: *Specimen-specific finite elements may be created using realistic geometries. (A) Bones are imaged using μCT and a region of interest is "virtually" isolated for analysis. (B) A hexahedral mesh is generated using the pixel-to-voxel technique. (C) Boundary and loading conditions are applied at virtual cut-plane surfaces. The model is then solved using a finite element solver such as ABAQUS.*

1.6.3 Nanoindentation (QSM and DMA)

Nanoindentation is an emerging technology that has recently found applications in musculoskeletal research. The principals behind nanoindentation evolved from traditional micro-indentation tests used to measure hardness, such as the Vickers and Knoop tests. Subsequently, development of this technique was driven by the demands of the microelectronics industry to investigate the performance of thin films and MEMS (Micro Electrical Mechanical System) devices. Although still a relatively new technique to the field, nanoindentation possesses several characteristics that make it particularly attractive for answering research questions related to musculoskeletal biomechanics.

First, nanoindentation uses a sharp indenter tip and highly sophisticated load sensing technology to probe mechanical properties at extremely small length scales. Depending on the type of material and indenter tip, mapping of material properties can be achieved at a resolution on the order of 10nm. This is often useful in studies addressing the spatial heterogeneity found within native and diseased tissues such as bone and cartilage [76, 77]. A second advantage of nanoindentation's high spatial resolution is that it allows for the characterization of material properties within various organizational structures such lamellar and interstitial bone [78-80] and superficial and deep zones in cartilage [81]. This can be useful when addressing the effects of disease or treatment as it provides a means of keying in on the mechanical response of tissues undergoing specific stages of the modeling or remodeling cycle. A third advantage of nanoindentation's high spatial resolution is that it can be used in concert with complimentary imaging modalities. For example, several researchers have combined nanoindentation studies with high-resolution atomic force microscopy (AFM) imaging to characterize the local topology of a specimen's surface before and after indentation [82-86]. This allows for greater understanding of local geometric effects present throughout the indentation process. Other researchers have used infrared microscopy to compliment the findings of nanoindentation studies in order to better understand the

underlying chemical composition associated with a sample's response to mechanical loading [87, 88]. Finally, the information obtained from nanoindentation studies can be used as inputs for powerful modeling and simulation tools, which address bone's macro-scale response to loading. One such example, known as "virtual biopsy", uses finite element (FE) analysis to approximate the response of cancellous bone to applied loads and has been established as an effective tool in predicting fatigue [89, 90].

Nanoindentation, is a relatively new tool to the field of musculoskeletal research. As a result, standards have yet to be defined for the instrumented indentation testing of biological materials such as bone and cartilage. In light of this fact, nanoindentation studies are highly sensitive to several key parameters such as sample preparation, loading protocol, indent location and sample storage [91]. Therefore, future studies should carefully consider these factors in the design of experiments and reporting of results. The focus of this chapter is to outline the key materials and methods required of a successful nanoindentation protocol and to highlight technical considerations relevant to the design of experiments and interpretation of results.

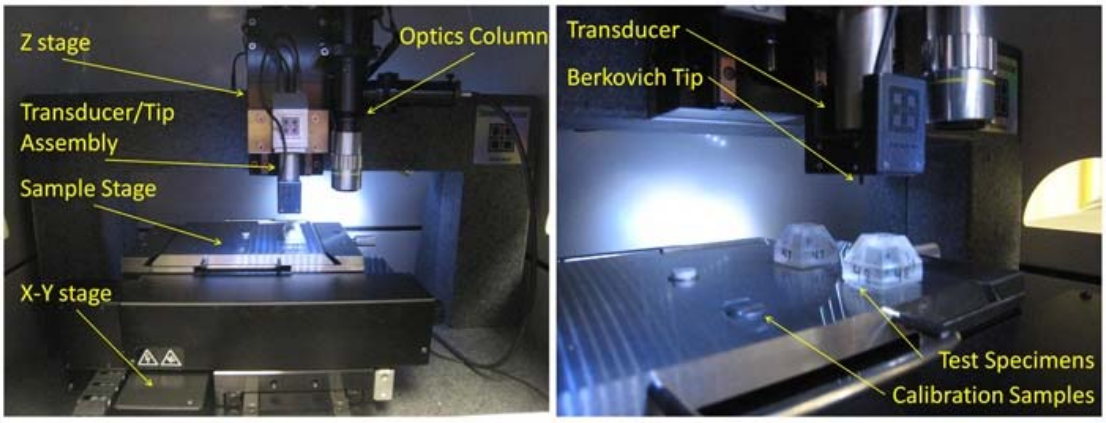

Figure 1.8: *Test components within the nanoindenter's acoustic enclosure in front (left) and oblique view (right).*

1.6.3.1 *Quasi-static nanoindentation*

Nanoindentation was performed by penetrating a relatively hard, indenter tip into the sample surface, and then withdrawing it from the sample. As the tip penetrates the sample surface, the material undergoes both elastic and plastic deformation. Upon withdrawal from the sample, the force/displacement relationships predominantly reflect the material's elastic response. It is for this reason that the unloading portion of the curve is used to evaluate elastic modulus and hardness. Thus, a curve was fit to the initial portion of the unloading curve using the segment between 95 and 20% of the maximum applied load with the following power law relationship.

$$P = \alpha(h - h_f)^m$$

In the above equation, P is the measured force, h is the indentation depth, h_f is the maximum penetration depth and α and m are power law fitting constants [92, 93].

Stiffness, S, was then calculated by taking the first derivative of the power law relation, P, with respect to depth (∂P/∂h) and evaluating at the maximum load, P_{max}.

Material hardness, H, was then calculated using the following formula.

$$H = \frac{P_{max}}{A(h_c)}$$

In the above equation $A(h_c)$ is the tip area function at the maximum contact depth [92, 93]. As the indenter penetrates the sample surface it is assumed that the sample surface "sinks in" resulting in a contact depth that is less than the maximum penetration depth, h_{max}. The maximum contact depth, h_c, is defined by the following equation.

$$h_c = h_{max} - 0.75\frac{P_{max}}{S}$$

The reduced modulus, E_r, which reflects the material properties of both the sample and the indenter, is determined using the following formula.

$$E_r = \frac{S\sqrt{\pi}}{2\sqrt{A_c}},$$

Here, A_c is the contact area evaluated at the contact depth, h_c [92, 93]. The elastic modulus for the sample, E_s, is then calculated using the following equation, where E_i and ν_i are the elastic modulus and Poisson's ratio of the indenter and ν_s is the Poisson's ratio of the sample [92, 93].

$$E_s = \frac{E_i \times E_r \times (1 - \nu_s^2)}{E_i + E_r \times (\nu_i^2 - 1)}$$

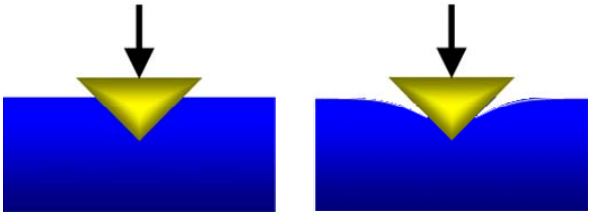

Figure 1.9: *Schematic representing the difference between an ideal "full contact" relationship between the indenter tip and the sample and the "sink-in" phenomena observed in the majority of samples experimentally.*

1.6.3.2 Dynamic nanoindentation

Dynamic indentation is performed by applying a quasistatic load to the indenter tip followed by the superposition of a small-amplitude, sinusoidal load. The dynamic load is characterized by a user-defined frequency (ω) and force (F_o). For materials in which viscous effects play a role, the resulting displacement will be out of phase from the applied dynamic load. This is primarily the result of damping mechanisms within the tissue. In bone, factors contributing to this response could include micro-porosities, collagen and water. Within our existing set-up, a loc-in amplifier is used to measure the amplitude (X_o) and phase shift (ϕ) between the applied dynamic force and the resulting dynamic displacement as seen in Figure 1.5.

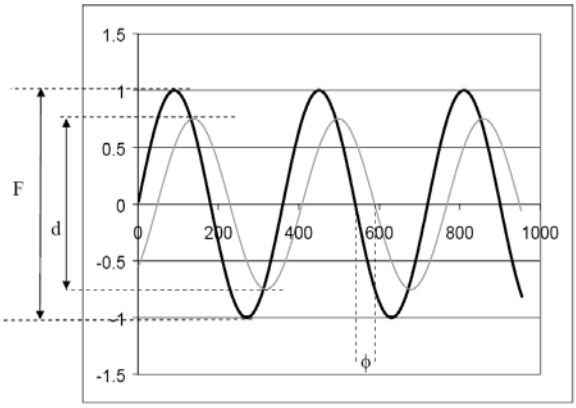

Figure 4: Dynamic Signals

Figure 1.10: *Graphical representation of the phase shift (φ) between the user-defined, applied dynamic force (F) and the resulting experimentally-measured, dynamic displacement (d). Inherent damping characteristics within specimen cause the two signals to be out of phase. (Note: This image modified from a hysitron technical communication.)*

The system consisting of the indenter tip and sample can then be modeled as a single degree of freedom, damped, forced harmonic oscillator. Stiffness (k) and damping (C) are then calculated using the solutions to differential equations describing the equation of motion $F_0 \sin(\omega t) = m\ddot{x} + C\dot{x} + kx$ and the displacement response $x = X\sin(\omega t - \phi)$. The solutions for k and C are described in the following two equations.

$$k = \frac{F_o}{X}\frac{1}{\sqrt{1+\tan^2\phi}} + m\omega^2 \qquad \text{and} \qquad C = \sqrt{\frac{\left(\frac{F_o}{X}\right)^2 \tan^2\phi}{1+\tan^2\phi}}\left(\frac{1}{\omega}\right)$$

Here, k and C represent the total stiffness and damping of the system consisting of the indenter tip and sample. We extract the stiffness and damping of the sample using the following relations, $k = k_i + k_s$ and $C = C_i + C_s$. The storage modulus (E') (a/k/a elastic modulus) and loss modulus (E'') (a/k/a viscous modulus) are defined using the following equations.

$$E' = \frac{k_s\sqrt{\pi}}{2\sqrt{A_c}} \qquad \text{and} \qquad E'' = \frac{\omega C_s\sqrt{\pi}}{2\sqrt{A_c}}$$

A_c is the contact area evaluated at the contact depth and h_c is the same as previously defined for quasi-static analysis. Storage modulus (E') describes the elastic recovery within the sample and is proportional to the fraction of the displacement signal which is in-phase with the applied dynamic force. Loss modulus (E'') however, captures the samples damping characteristics and is represented by the portion of the resulting dynamic signal, which is out of phase with the applied dynamic force. The relative contribution of both of these parameters is described by the loss tangent (tan δ) and represented by the following equation.

$$\tan\delta = \frac{E''}{E'} = \frac{k_s}{\omega C_s}$$

Chapter 2:

Specific Aims and Hypotheses

Osteoporosis is a disease characterized by decreased bone mass and progressive erosion of the microstructure. As a result, bone is at higher risk for developing chronic and traumatic fractures at key skeletal sites such as the hip, spine and wrist. Osteoporosis related fractures often result in a decreased quality of life, increasing one's susceptibility to prolonged disability and increased mortality [6, 94, 95]. Current therapies, including hormonal and pharmacologic approaches, are not site-specific and often incur adverse side effects. Therefore, it is necessary to develop complementary and alternative, site-specific interventions for the treatment of osteopenic bone loss and microstructural deterioration. Therapeutic ultrasound may offer a potential non-pharmacologic, site-specific intervention. It has been proposed that LIPUS acts as an alternating pressure wave, creating local pressure gradients within bone's micro porosities, which may result in the production of anabolic shear forces on cell membranes, changes in local solute concentrations or inducing local fluid flow exchange and interaction [96, 97].

Several observations indicate therapeutic ultrasound is a potential non-pharmacologic, site-specific intervention for treatment of osteopenic bone loss. First, the principle that bone is responsive to mechanical loading is widely accepted [14, 22]. One particular aspect of this observation is that bone and bone cells have been shown to be sensitive to bone fluid flow stimulus [98]. Second, in vitro studies have shown that low intensity pulsed ultrasound (LIPUS) enhances osteoblast proliferation and endochondral bone formation [31-34]. Third, in vivo studies have shown LIPUS to be anabolic to fresh fractures, enhancing endochondral bone formation, mineral density and mechanical strength [47-52]. However, for treatment of intact bone, the efficacy of therapeutic ultrasound remains unclear [58-63, 99]. In light of these findings, the goal of this dissertation is to explore the therapeutic potential of LIPUS for treatment of bone loss associated with estrogen deficient osteopenia.

The principal hypothesis is that non-invasive, therapeutic ultrasound improves bone quantity and quality under conditions of estrogen deficient osteopenia, and bone's adaptive response is sensitive to ultrasound signal parameters such as frequency, intensity and pulse duration.

This hypothesis will be tested in several specific aims. In the first and third specific aims, ultrasound signal parameters were investigated by addressing the roles of pulse duration and signal intensity in bone adaptation using high resolution μCT imaging and specimen specific micro finite element models. In the second and fourth specific aims, elastic and viscoelastic nanoscale material properties were be evaluated in response to ultrasound stimulus using quasi-static and dynamic nanoindentation. Finally, in the fifth specific aim, computational models were used to approximate ultrasound wave propagation in bone in an effort to better understand the mechanism by which geometry and ultrasound signal parameters interact and affect the tissue level signals that drive bone modeling and remodeling processes. The results of these specific aims will form the framework for the formation of future hypotheses which will seek to optimize the ultrasound signal and suggest additional applications for which therapeutic ultrasound may be beneficial.

Specific Aim 1: Characterize bone's <u>apparent level</u> response to therapeutic ultrasound under conditions of estrogen deficient osteopenia, quantifying the role of ultrasound <u>pulse duration</u>.

Hypothesis 1: LIPUS is anti-catabolic to bone and will mediate the progression of hormonally induced osteopenia in the rat lumbar vertebra. Further, bone's response is sensitive to pulse duration and cycle number.

- Apply a therapeutic ultrasound signals consisting of a center frequency of 0.5MHz, a pulse repetition frequency (PRF) of 1 kHz and spatial-averaged temporal-averaged intensities (I_{SATA}) of 0.1, 0.2 and 0.4 mW/cm^2 to the L4 and L5 lumbar vertebra using three different stimulus regimes including short (200μs), moderate (400μs) to long (800μs) duration pulses.
- Quantify cancellous bone quantity and morphology in the L4 and L5 lumbar vertebrae using μCT.
- Determine cancellous bone strength and load transmission characteristics using high resolution μCT based finite element models.

Specific Aim 2: Characterize bone's <u>tissue level</u> response to therapeutic ultrasound under conditions of estrogen deficient osteopenia, quantifying the role of ultrasound <u>pulse duration</u>.

Hypothesis 2: Bone's tissue level response to LIPUS intervention is sensitive to changes in ultrasound pulse duration

- Use ultrasound signals delivered in SA's 1 & 2
- Quantify tissue level mechanical properties using both quasi-static and dynamic nanoindentation.

Specific Aim 3: Determine bone's <u>apparent level</u> sensitivity to therapeutic ultrasound <u>signal intensity</u> under conditions of estrogen deficient bone loss.

Hypothesis 3: LIPUS is anti-catabolic to bone and will mediate the progression of hormonally induced osteopenia in the rat lumbar vertebra. Further, bone's response is sensitive to signal intensity.

- Apply a therapeutic ultrasound signals consisting of a center frequency of 1.5MHz, a pulse repetition frequency (PRF) of 1 kHz and a 200μs pulse duration. The spatial-averaged temporal-averaged intensity (I_{SATA}) will be evaluated at 5 mW/cm^2, 30 mW/cm^2 and 100 mW/cm^2.
- Quantify cancellous bone quantity and morphology in the L4 and L5 lumbar vertebrae using μCT.
- Determine cancellous bone strength and load transmission characteristics using high resolution μCT based finite element models.

Specific Aim 4: Characterize bone's tissue level response to therapeutic ultrasound under conditions of estrogen deficient osteopenia, quantifying the role of ultrasound signal intensity.

Hypothesis 4: Bone's tissue level response to LIPUS intervention is sensitive to ultrasound signal intensity.

- Use ultrasound signals delivered in specific aim 3
- Quantify tissue level mechanical properties using both quasi-static and dynamic nanoindentation.

Specific Aim 5: Quantify signal attenuation in the rat lumbar vertebra using experimental and computational approaches.

Hypothesis 5: µFE models of ultrasound wave propagation can help to explain the transmission of waves in the studies presented in SA's 1 & 2.

- Quantify the transmission of transdermally applied ultrasound energy into the vertebral body using an ex vivo model of the rat lumbar vertebra.
- Determine the effect of signal attenuation due to soft tissue and cortical bone using µCT-image-based finite difference techniques.

Chapter 3:

Therapeutic Ultrasound as a Mediator for Bone loss in an OVX Rat Model of Osteopenia: The Role of Ultrasound Pulse Duration

3.1 Abstract

Low intensity pulsed ultrasound (LIPUS) has been proposed as a potential therapeutic agent in the treatment of estrogen deficient osteopenia. This study quantifies the role of signal pulse duration in bone's response to LIPUS. Seventy-two, 16 week old Sprague-Dawley rats were divided into six groups; baseline control, age-matched control, OVX control, OVX + 200μs ultrasound (US), OVX + 400μs US and OVX + 800μs US. LIPUS was delivered transdermally at the L4/L5 vertebrae, using gel-coupled plane wave US transducers. The signal, characterized by 200μs, 400μs or 800μs pulses of 1.5 MHz sine waves repeating at 1 kHz with intensities of 0.1, 0.2 or 0.4mW/cm^2, was applied 20 min/day, 5 days/week for 4 weeks. OVX treatment reduced bone mass and compromised microstructure at 4 weeks post surgery. The introduction of LIPUS improved bone volume fraction and microstructure. There was no correlation between cycle number or intensity and the strength of bone's response. Significant changes were observed for both the shortest (200μs) and longest (800μs) pulse durations. This study suggests that LIPUS may provide an effective early intervention capable of mediating the changes to cancellous bone microstructure and mechanical robustness associated with estrogen deficient osteopenia.

Key Words: *Therapeutic Ultrasound, Bone Remodeling, Mechanotransduction, Low Intensity Ultrasound, Ovariectomy, MicroCT, Finite-Element Analysis*

3.2 Introduction

Osteoporosis represents a significant public health concern in aging populations [10]. Fractures resulting from osteoporosis are often associated with decreased long term mobility, an increased rate of mortality and an overall decreased quality of life [5, 6]. Osteoporosis is the result of an imbalance in the rates of bone resorption and bone formation. As a result, bone is less equipped to sustain physiologic mechanical forces, which leaves it increasingly susceptible to fractures [3, 95]. Pharmacologic treatments, including bisphosphonates, seek to address this imbalance by decreasing bone resorption rates which, over time leads to increased net bone volume [100, 101]. Suppression of bone resorption, however could result in the accumulation of micro cracks potentially compromising bone quality [102, 103]. Pharmacologic treatments and whole body vibrations affect the whole skeleton, yet chronic and traumatic fractures are specific to a few key skeletal sites including the hip, spine and wrist [10, 104-106]. Thus, there exists a need to develop new and complementary treatments to address the changes due to osteoporosis and the subsequent risk of fracture.

Low intensity pulsed ultrasound has been shown to be an effective treatment for the acceleration of fracture healing in animal models [48, 49, 64, 107, 108]. Furthermore, LIPUS has been shown to be effective in treating delayed and nonunion fractures in humans [43, 44, 109, 110] and was approved by the United Stated Food and Drug Administration (FDA) for the treatment of nonunion fractures[111]. Several in vitro studies also support the premise that LIPUS could drive anabolic effects in bone

cells [31-34]. Ultrasound was shown to be capable of increasing osteoblast proliferation and stimulating endochondral ossification in excised tissues [31-34].

Given the effectiveness of LUPUS in accelerating fracture healing and generating osteogenic effects in vitro, ultrasound may prove to be an effective treatment in other cases of altered bone remodeling such as hind limb unloading or ovariectomy. There is limited, conflicting evidence with respect to the effectiveness of LIPUS in treating in vivo, non-fracture related bone disease [58, 61]. It is also unclear what role ultrasound signal parameters such as pulse duration or duty cycle play in bone's response. Bone and bone cells have been shown to be sensitive to the ratio of on cycles to off cycles applied during low amplitude, high frequency vibrations in vitro [23] and in vivo [24, 25]. In addition, at ultrasound frequencies, membrane permeability may be associated with changes in duty cycle [37].

The goal of this study was to explore the therapeutic potential of LIPUS for treatment of bone loss associated with estrogen deficient osteopenia using high resolution μCT imaging and finite element models. **We hypothesized that ultrasound, acting as a mechanical wave in bone, delivers a dynamic mechanical signal capable of altering bone's modeling and remodeling processes. Furthermore, ultrasound pulse duration plays a role in bone's response by modulating bone loss and maintaining mechanical strength.**

3.3 Materials and Methods

3.3.1 Experimental Design

All surgical and therapeutic procedures were approved by the Institutional Animal Care and Use Committee (IACUC) at Stony Brook University (Stony Brook, NY). Eighty-four, 16-week-old virgin female, Sprague-Dawley rats (301 ± 7g) were obtained from Charles River Laboratories (Wilmington, MA) and subjected to either ovariectomy (OVX) or sham operation. Animals were allowed to recover for 3 days, after which they were randomly assigned to one of six groups: (1) baseline control, (2) sham control, (3) OVX control, (4) OVX + 200μs ultrasound stimulation (US), (5) OVX + 400μs US or (6) OVX + 800μs US. All animals were housed individually in standard cages at 24◦C and allowed free access to standard rodent chow and tap water. Body weight and food consumption were recorded at day zero and monitored bi-weekly throughout the study. Upon completion of the study, animals were euthanized via CO_2 asphyxiation.

3.3.2 US Treatment

Animals were anesthetized using isofluorane gas and therapeutic ultrasound was delivered transdermally over the posterior aspect of the L4 and L5 lumbar vertebra using a plane wave ultrasound transducer (Panametrics, Inc.) in series with an amplifier (Tegam, Inc.) and function generator (HP, Inc.). To maximize coupling of the transducer with the skin surface, fur was removed from the lumbar spine region and an ultrasonic coupling gel (Aquasonic, Inc.) was applied between the skin and ultrasound transducer. The system was configured to produce pulsed-wave ultrasound with 200, 400 or 800 μs bursts of 0.5 MHz sine waves repeating at 1 kHz. The spatial-averaged-temporal-

averaged intensity was calibrated at the center of the radiating area using a membrane hydrophone (Precision Acoustics, Ltd., UK) and found to be 0.1, 0.2 and 0.4 mW/cm^2 for the 200, 400 and 800μs pulse duration ultrasound signals respectively. The stimulus was applied 20 min/day, 5 days/week over 4 weeks. To minimize potential confounding effects due to isofluorane exposure, age-matched control and OVX control animals were simultaneously subjected to 20 minutes of isofluorane anesthesia per day, 5 days/week for 4 weeks. Upon completion of the study, animals were sacrificed via CO_2 asphyxiation and the L4 and L5 lumbar vertebra were removed, cleaned of soft tissue and stored in saline soaked gauze at -40◦C.

3.3.3 Micro-Computed Tomography

The L5 vertebra was imaged at 15μm isotropic resolution using μCT (μCT40, SCANCO) with energy (E) and intensity (I) equal to 55 kVp and 145 μA respectively. Cancellous bone was then manually segmented from a 1.5mm long axial region of interest (ROI) from the cranial third of the anterior vertebral body. Cancellous microstructure was then characterized using standardized techniques to determine bone volume fraction (BVF), structural model index (SMI), connectivity density (Conn.D.), trabecular number (Tb.N.), trabecular thickness (Tb.Th.) and trabecular spacing (Tb.Sp.).

3.3.4 Finite-Element Analysis

Specimen specific models were generated using three-dimensional image data from the cancellous ROI's addressed previously by μCT analysis. Voxel based finite element meshes were created using custom software based on the pixel-to-voxel technique, in which each pixel is represented by an eight-noded cuboid element. Disassociated regions in the model which did not intersect virtual-cut plane surfaces were removed to ensure convergence. Trabecular tissue was assumed to behave as a homogeneous, linear elastic isotropic solid (E=18GPa & ν=0.3) and full friction boundary conditions were assigned at the cranial and caudal surfaces. Trabecular samples were subjected to 0.5% compressive strain in the cranial-caudal direction and a nonlinear finite element solver (ABAQUS v6.4, Dassault Systemes Inc.) was used to determine apparent stress and mean compressive principal stress.

3.3.5 Data Analysis

All values are reported as mean ± standard deviation, unless noted otherwise. One-way analysis of variance (ANOVA) and Tukey's post-hoc test was used to detect differences between groups for body weight, food consumption, morphological indices (BVF, Conn.D., Tb.N., Tb.Th., and Tb.Sp) and mechanical strength parameters (E, $\overline{\sigma_3}$, 75th percentile of σ_3 , $\overline{\sigma_{von\ Mises}}$, $\overline{SED}$ and 75th percentile of SED). Significance was determined at p≤0.05 and p≤0.001. A one way repeated measures analysis of variance with Tukey's post-hoc was used to detect differences between treated groups for SMI. In addition, we also performed a two-way ANOVA with Tukey's multiple comparison test to detect paired differences among the different regions within the L4 and L5 vertebra and between the different treatment groups. Correlations were determined using

multiple linear regressions and Pearson's product moment correlation coefficient. All statistical analyses were performed using SigmaStat v3.5 (Systat Software, Inc., San Jose, CA, USA).

3.4 Results

3.4 1 Body Mass and Food Intake

At the beginning of the study, there were no significant differences in body mass among any of the six experimental groups. There was no significant difference in body mass for the age-matched controls after 28 days compared with day zero. Conversely, OVX and OVX + LIPUS treated groups experienced significant increases in body mass at 28 days compared to day zero. There were no differences in body mass among any of the OVX and OVX + LIPUS treated groups. Increased body weight was not associated with increased food consumption which remained constant for all groups throughout the study.

3.4.2 Estrogen Deficient Osteopenia Alters Trabecular Morphology and Mechanics

At 28 days post-surgery, OVX treatment was associated with substantial alterations in cancellous bone volume and morphology. OVX controls had 40% lower ($p<0.01$) BVF than age-matched controls. Tb.N. decreased 17% ($p<0.001$), Tb.Th. decreased 19% ($p<0.001$) and Tb.Sp. increased 24% ($p<0.001$). OVX was also associated with higher SMI (436%, $p<0.001$) compared to age-matched controls. No changes, however in Conn.D. were observed in OVX treated animals.

Bone's load bearing characteristics were also strongly affected by OVX. At the apparent level, Elastic Modulus was 51% lower ($p<0.001$) for OVX treated animals compared to age-matched controls. Changes were also observed in average tissue stresses. Mean *von* Mises stress was 24% higher ($p<0.001$) while the *von* Mises stress coefficient of variation was 21% higher ($p<0.001$). Additionally, the mean and 75th percentile of maximum principal stress was 23 and 45% lower respectively ($p<0.001$). Strain energy density (SED), an indicator of local tissue fatigue and failure, had lower mean and 75th percentile values (26% $p<0.001$ and 32% $p<0.001$) compared to age-matched controls.

3.4.3 Skeletal maturation does not alter morphology or load bearing characteristics

Comparisons between age-matched and baseline controls were used to address potential changes in bone microarchitecture due to rodent maturation over the course of the experiment. No significant differences were identified among any of the morphological or mechanical strength parameters examined in this study.

3.4.4 LIPUS intervention preserves cancellous microarchitecture

BVF was significantly higher for the 200μs (25%, $p=0.018$) and 800μs (33%, $p<0.001$) treated groups compared to OVX controls. While there were no differences observed between US treated groups, BVF was not significantly higher than OVX controls for the 400μs treated group (15%, $p=0.447$). LIPUS however, did not

completely restore BVF to that of estrogen-intact animals. When compared with age-matched controls, BVF was significantly lower for the 200 (-24%, p<0.001), 400 (-31%, p<0.001) and 800μs (-19%, p<0.001) US treated groups.

Tb.Th. was significantly higher for the 200 (10%, p=0.049), 400 (11%, 0.03) and 800μs (14%, p<0.001) US treated groups compared to OVX controls. However, Tb.Th. was significantly lower in each of the US treated groups compared to age-matched controls (10%, 10% and -8%, P<0.001). There were no significant differences in Tb.N. or Tb.Sp. for any of the US treated groups compared with OVX controls. Tb.N. and Tb.Sp. were, however, significantly different compared to age-matched controls.

SMI was significantly lower for the 200μs (47%, p=0.02) and 800μs (-60%, p<0.001) US treated groups compared to OVX controls, indicating a shift towards a more plate-like structure for the US treated groups. There was a non-significant decrease (-30%, p=0.313) in SMI for the 400μs US treated group. In addition, SMI was significantly larger for each of the US treated groups compared with age-matched controls. Finally, there were no differences in Conn.D. between US treated groups and OVX controls, or between US treated groups and age-matched controls.

3.4.5 LIPUS intervention improves cancellous bone's structural integrity

Micro-finite element simulations approximate bone's ability to sustain and distribute mechanical strains, lending insight into how bone may perform in vivo under baseline and extreme physiologic conditions. LIPUS stimulation increased BVF 34% (p=0.273) and 35% (p=0.256) for the 200μs and 400μs signals relative to OVX controls and was significantly higher (58%, p<0.001) for the 800μs group. However, compared to age-matched controls, the 200μs, 400μs and 800μs groups were 34%(p<0.001), 34%(p<0.001) and 23%(p=0.002) lower respectively.

At the tissue level, LIPUS increased mean *von* Mises stress 11% (p=0.204), 14% (p0.068) and 18% (P<0.001) relative to OVX controls for the 200, 400 and 800μs groups respectively. Compared to age matched controls, mean *von* Mises Stress was lower (-10%, p=0.047) for the 200us treated group. However, there were no differences in mean *von* Mises stress between age-matched controls and the 400us and 800us treated groups. In addition, the COV of *von* Mises stress was significantly reduced for the 800μs (-15%, p<0.001) US treated group. There were no differences in the COV of *von* Mises stress between age-matched controls and any of the LIPUS treated groups. These relationships are also represented by frequency histogram plots (Figure 3.7). Each curve represents an average plot of *von* Mises stress for all animals in an individual experimental group. The curve peak indicates the median *von* Mises stress value while the shape of the curve describes the distribution of critical stresses throughout the tissue. When compared to age-matched controls, OVX controls showed a sharp decrease in median stress and a more narrow distribution of peak stresses throughout the tissue.

The maximum principle compressive stress ($ó_3$) for volume elements throughout the tissue was then described by average values as well as measures indicating the 25th and 75th percentiles. There were no significant increases in mean (13%, p=0.181), 25th percentile (12%, p=0.231) or 75th percentile (37%, p=0.184) of $ó_3$ for the 200μs US

treated group compared to OVX controls. Groups treated with the 400µs US signal had 16% (p=0.062), 15% (p=0.040) and 38% (p=0.164) higher ó$_3$ compared to OVX controls. The 800µs US signal treated groups had 21% (p<0.001), 19% (p<0.001) and 57% (p<0.001) higher ó$_3$ relative to OVX controls. Compared to age-matched controls, the 200us treated group had lower mean (-13%, p=0.019), 25th percentile (-11%, p=0.036) and 75th percentile (-25%, p=0.026) values. The 400us treated group had a significantly lower 75th percentile ó3, and no significant differences in mean (-11%, p=0.068) and 25th percentile (-8%, p=0.217) values. There were no significant differences in mean (-7%, p=0.272), 25th percentile (-5%, p=0.506) or 75th percentile (-14%, p=0.228) ó$_3$ for the 800µs treated group compared to age matched controls.

SED was reported at the mean, 25th and 75th percentile values for volume elements within the tissue. Mean and 75th percentile SED was significantly higher (19%, p<0.05 and 28%, p<0.05) in the 400µs treated group compared to OVX controls. And the 800µs treated group had higher mean (24%, p<0.001), 25th percentile (87%, p=0.006) and 75th percentile (35%, p<0.001) values. Compared to age-matched controls, the 200µs treated group had lower mean (-15%, p=0.010), 25th percentile (-32%, p=0.054) and 75th percentile (-19%, p=0.025) values. However there were no significant differences in mean, 25th percentile or 75th percentile SED for the 400µs or 800µs treated group compared to age-matched controls.

3.5 Discussion

The findings presented here showed that LIPUS intervention was able to partially mediate changes to bone associated with ovariectomy. The results show that LUPUS reduced the bone loss by decreasing trabecular thinning. Changes to SMI as a result of OVX were significantly reduced in experimental groups treated with short and long duration pulses. The changes to bone morphology were also associated with improved mechanical performance and resistance to applied strains. At the whole bone level, changes in apparent modulus due to OVX were minimized in groups treated with ultrasound. Thus, when exposed to comparable strain levels, groups treated with ultrasound could support higher load magnitudes. At the tissue level, average principle compressive stresses remained unaffected by LIPUS intervention. However, peak 75th percentile principle compressive stresses were significantly higher in LIPUS treated groups compared to untreated controls. In addition, stress distribution profiles were preserved to more closely represent those of the hormonally intact age-matched counterparts. The presence of higher peak stresses as well as an increased trabecular thickness suggests that LIPUS treated groups may be at reduced risk for local tissue failure at critical sites. While caution must be used in interpolating these results to humans, the results of this study suggest that LUPUS may serve as an effective complimentary countermeasure in the treatment of estrogen deficient bone loss.

We found that there was a decrease in median *von* Mises stress and a more narrow distribution of peak stressed in the OVX groups compared to age-matched controls. This suggests that not only did the maximum sustainable load for the OVX group decrease, but that the peak stresses were distributed over a smaller fraction of the tissue. Combined with a significant decrease in BVF, these results suggest that there

is an increased likelihood of critical stresses occurring across eroded tissue, potentially resulting in tissue yielding and failure. When compared to OVX and age-matched controls, the 800μs US treated group most closely approximated that of the age-matched control, preserving not only peak loads, but the characteristic load distribution.

We also observed significant improvements in BVF and apparent level Elastic Modulus with the shortest (200μs) and longest (800μs) pulse durations, but not with pulse durations of 400μs. Subsequently, bone's response was not linearly correlated with either cycle number or spatial-averaged temporal-averaged intensity. This suggests that mechanisms involving the cumulative effect of mechanical strains delivered at ultrasound frequencies are not the exclusive driving factor in bone's response to US treatment. In addition, mechanisms involving the periodicity of applied loading, including bone fluid flow, could play a role in regulating bone's response. One other possibility could be that bone senses ultrasound signals as a cumulative burst of energy occurring at the pulse repetition rate (1 kHz in this study).

The potential for ultrasound to generate anabolic effects in the cases of fracture healing and soft tissue damage have led several groups to suggest possible mechanisms. First, ultrasound may act to generate an electric field [112], which could then drive an osteogenic adaptation [113]. A second potential mechanism could involve thermal heating [114-116]. However, given the maximum range of intensities addressed in this study, it is unlikely that heating plays a role in bone's response. Ultrasound may also be capable of inducing stable cavitation [117-119]; however, given the intensities used in our study, this is highly unlikely. Acoustic streaming may also plays a role in bone's response, particularly at lower frequencies [120]. Ultrasound behaves as a mechanical wave in bone; therefore, it may be possible to generate local pressure gradients within bone's microporosities [96, 97]. Several recent studies have suggested that fluid movement within these structures could generate the mechanical signals associated with an increased osteogenic response [27, 29].

Our findings do not support those of Warden et al. who found that LIPUS was ineffective in preserving bone mineral density (BMD) and BVF in OVX rats [61]. A second study addressed the effect of ultrasound in preserving bone loss due to disuse [60]. In this study a 125mW/cm^2 US was ineffective in preserving BMD and BVF in rats following sciatic nervectomy [121]. Similarly, Spadaro et al., found no differences in BMD at the femur/tibia between treated and untreated young growing four week old rats [59]. There are several factors which could contribute to these differences including animal age, the targeted skeletal site and the differences in the response measures cited in both studies.

Our findings, in part, support those of Carvalho et al., who found that a 30mW/cm^2 ultrasound signal was capable of reducing bone loss and increasing bone formation rates in OVX rats [62]. Interestingly, our study noted significant improvements in BVF at spatial-averaged temporal-averaged intensities two orders of magnitude smaller than those used in this study. One possible difference could be that this study used ultrasound frequencies of 1.5 MHz, while ours used a signal of 0.5MHz. Due to a longer wavelength, ultrasound signals of 0.5 MHz could more easily penetrate the cortical shell and intermediate soft tissue compared to the 1.5MHz signal [122]. Our

study also supports the findings of Ari et al. who showed that LIPUS was capable improving BMD in bedridden patients [63]. While significant, these findings should be viewed with caution due to the small sample size (n=5) used in the study.

3.6 Limitations

Several limitations should be considered when interpreting the results of this study. First, we do not know precisely how the ultrasound wave propagates through the skin, fat, muscle and bone to act at the cancellous region addressed in this study. Ongoing studies in our lab will continue to develop computer models, which simulate acoustic wave propagation through realistic tissue geometries. Second, we have examined only a short window of time in the course of OVX related bone loss in the rat. Further studies would benefit from the use of in vivo imaging and image registration software to monitor the changes in bone morphology.

3.7 Conclusions

In summary, we have shown that LIPUS is capable of partially mitigating the adverse changes to bone induced by estrogen deficient osteopenia. Furthermore we showed that while bone's response was not linearly related to cycle number or SATA intensity, pulse duration was an important factor. In addition, the mechanisms by which US acts to deliver an anabolic signal in bone remain elusive, indicating the need for further in vitro and computer simulation studies. This suggests that US technology could be capable of integrating prophylaxis, treatment and diagnostic applications.

3.8 Figures and Tables

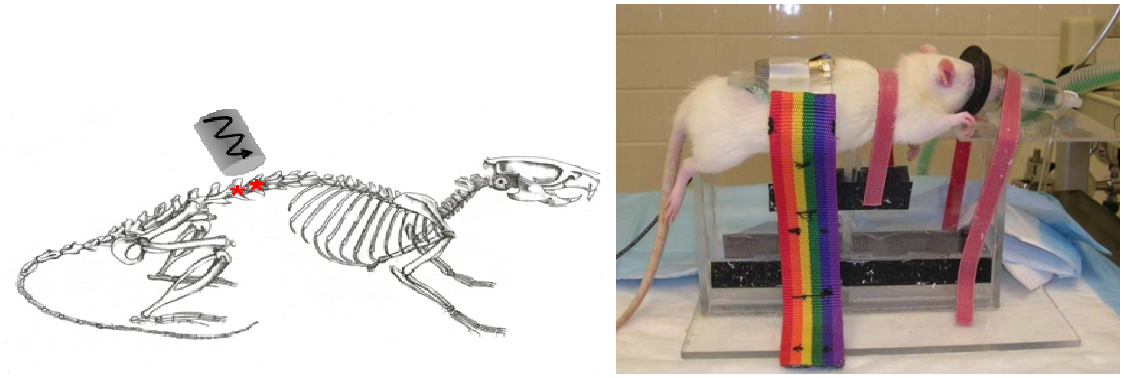

Figure 3.1: *(Left) Ultrasonic treatment was applied transdermally to the L4 and L4 vertebral bodies. The schematic to the left depicts the animal's position in sterna recumbancy and the direction of the applied ultrasound signal. (Right) An ultrasonic stimulator and transducer used to deliver the ultrasonic dynamic mechanical signal.*

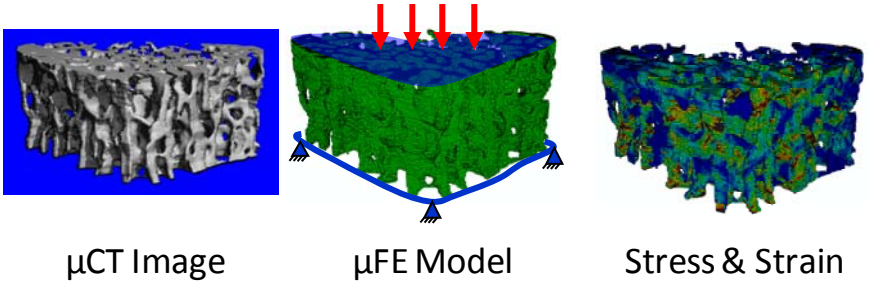

Figure 3.2: *µCT derived Image data was used to generate three-dimensional, specimen-specific finite element models. Each model was then loaded to 0.5% strain and solved to derive both global and tissue level stresses and strains.*

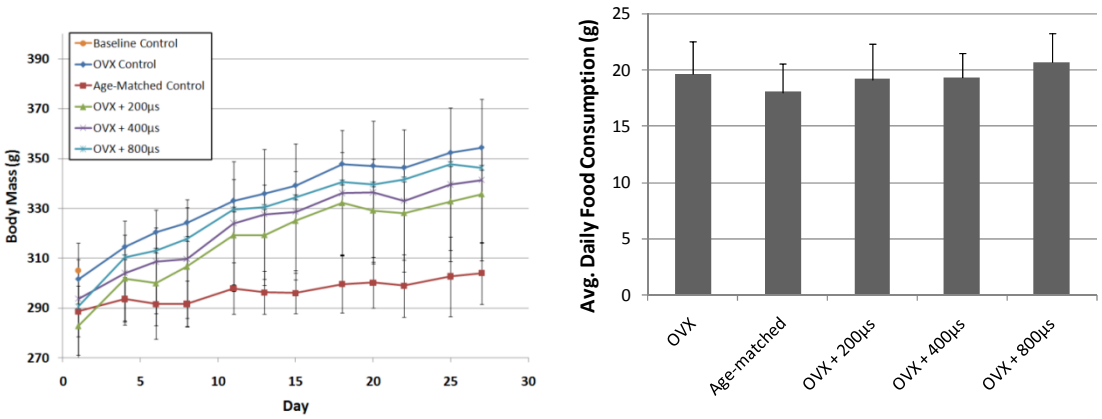

Figure 3.3: *(Left) Body mass in grams for experimental and control groups throughout the 28 day experiment. (Right) Average daily food consumption for experimental and control groups over the course of the 28 day experiment.*

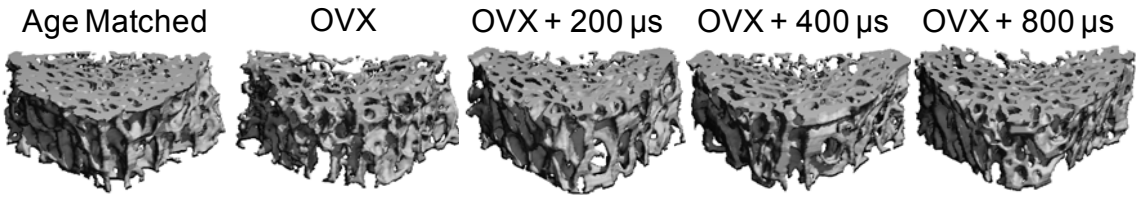

Figure 3.4: *Representative µCT images for experimental and control groups.*

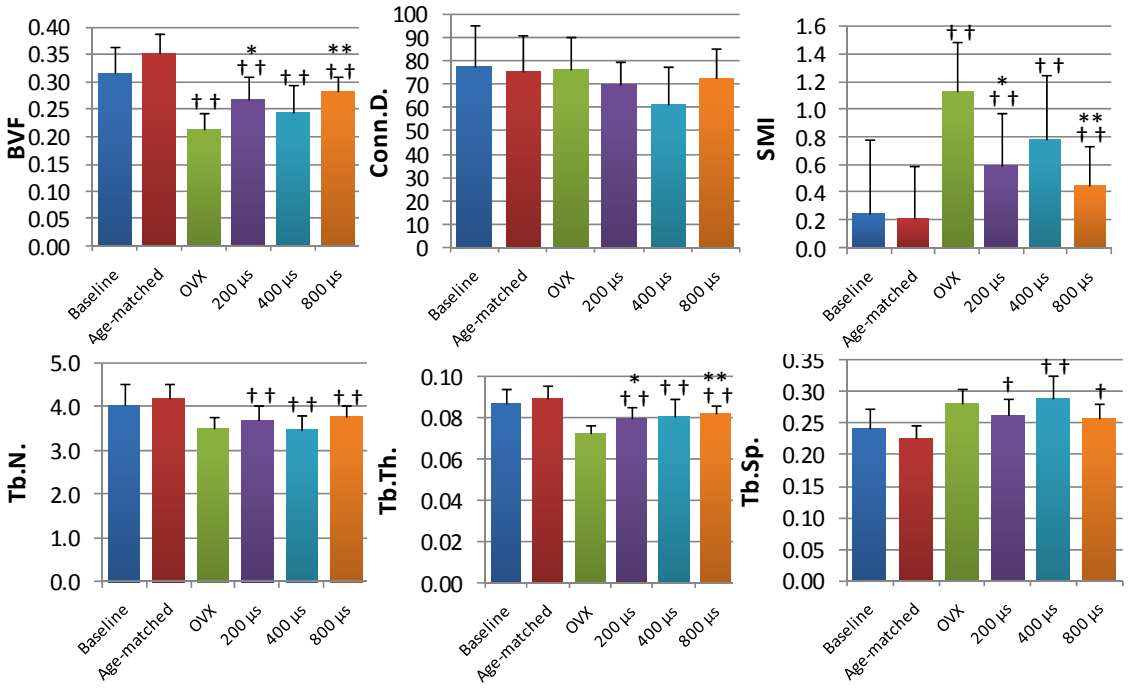

Figure 3.5: *Mean values of microstructural parameters for experimental and control groups. Values are reported as mean ± SD. (Note: † = p<0.05 vs. Age-matched Control, † † = p<0.001 vs. Age-matched Control * = p<0.05 vs. OVX Control, ** = p<0.002 vs. OVX Control.)*

	BVF	Conn.D.	SMI	Tb.N.	Tb.Th.	Tb.Sp.
OVX vs. Age-matched	-40% **	1%	436% **	-17% **	-19% **	24% **
OVX + 200µs PD US vs. OVX	25% *	-9%	-47% *	5%	10% *	-7%
OVX + 400µs PD US vs. OVX	15%	-19%	-30%	-1%	11%	2%
OVX + 800µs PD US vs. OVX	33% **	-5%	-60% **	8%	14% **	-9%
OVX + 200µs PD US vs. Age-matched	-24% **	-8%	185% **	-12% **	-10% **	16% *
OVX + 400µs PD US vs. Age-matched	-31% **	-19%	273% **	-18% **	-10% **	27% **
OVX + 800µs PD US vs. Age-matched	-19% **	-4%	115% **	-10% **	-8% **	13% *

Table 3.1: *Percent change in trabecular microstructure parameters for the L5 vertebral body. Values are reported as mean ± SD. (Note: † = p<0.05 vs. Age-matched Control, † † = p<0.001 vs. Age-matched Control * = p<0.05 vs. OVX Control, ** = p<0.002 vs. OVX Control.)*

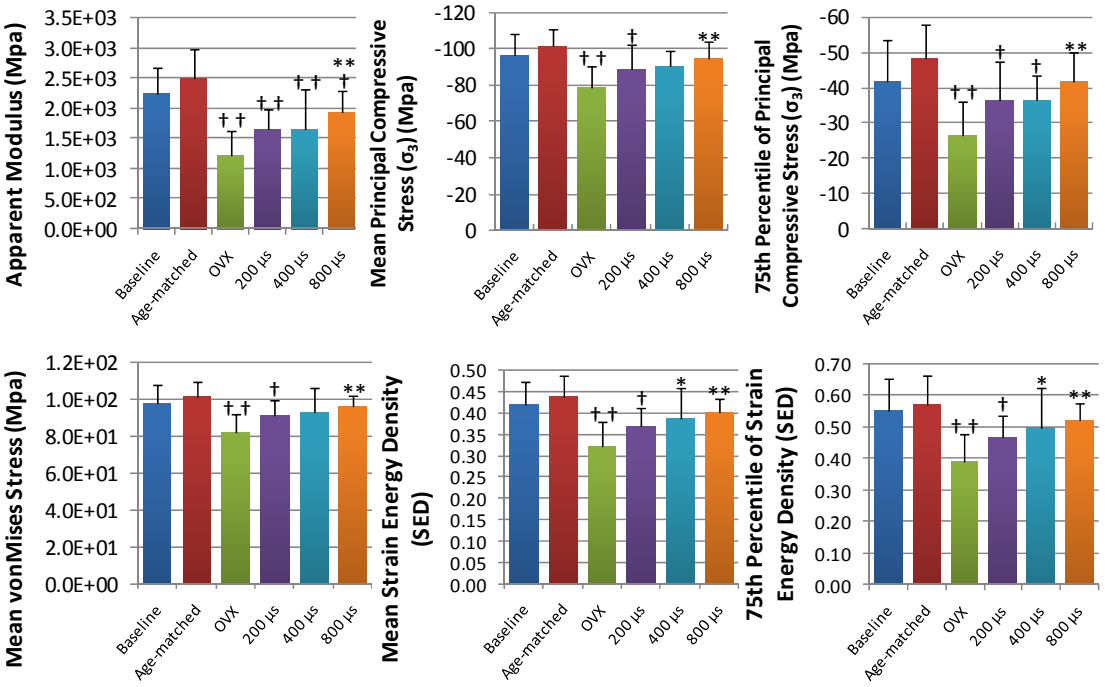

Figure 3.6: *Mean values of strength parameters for experimental and control groups. Values are reported as mean ± SD. (Note: † = p<0.05 vs. Age-matched Control, † † = p<0.001 vs. Age-matched Control * = p<0.05 vs. OVX Control, ** = p<0.002 vs. OVX Control.)*

	$E_{Apparent}$	$\overline{\sigma_{von\ Mises}}$	$\overline{\sigma_3}$	σ_3 75th %	$\overline{SED}$	SED75th %
OVX vs. Age-matched	-51% **	-19% **	-23% **	σ_3 75th %	-26% **	-32% **
OVX + 200µs PD US vs. OVX	34%	11%	13%	-45% **	15%	20%
OVX + 400µs PD US vs. OVX	35%	14% *(P=0.062)*	16% *(p=0.062)*	37%	19% *	28% *
OVX + 800µs PD US vs. OVX	58% **	18% **	21% **	38%	24% **	35% **
OVX + 200µs PD US vs. Age-matched	-34% **	-10% *	-13% *	57% **	-15% *	-19% *
OVX + 400µs PD US vs. Age-matched	-34% **	-8%	-11%	-25% *	-12%	-13%
OVX + 800µs PD US vs. Age-matched	-23% *	-5%	-7%	-24% *	-8%	-9%

Table 3.2: *Percent change in trabecular mechanical strength parameters for the superior third of the L5 vertebral body.*

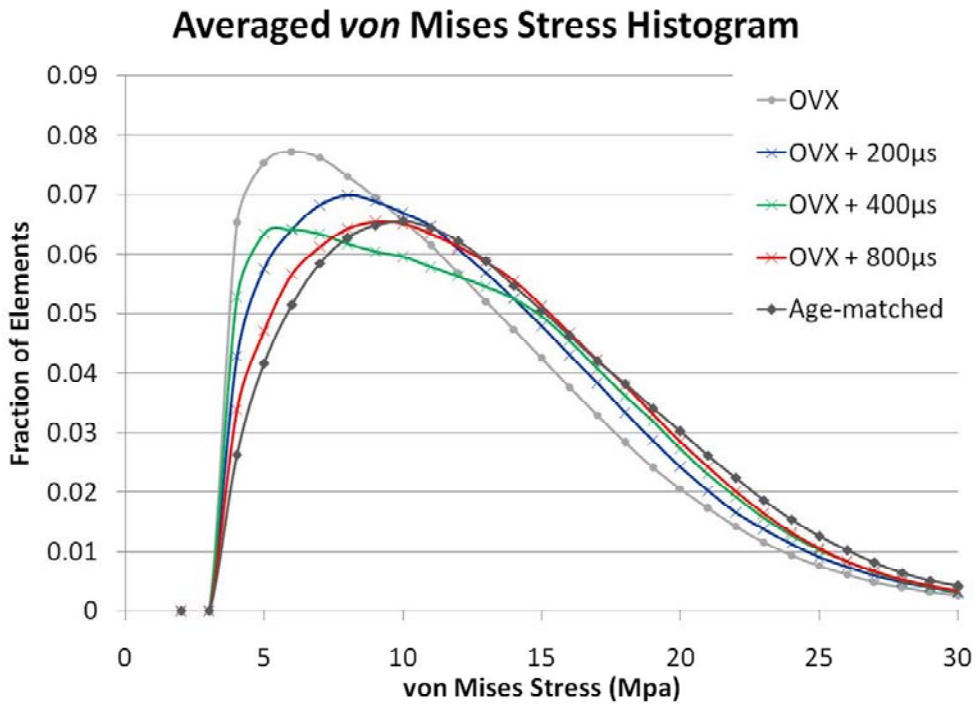

Figure 3.7: *von Mises stress histograms for experimental control groups. Each curve represents an average of curves normalized to the total number of elements in a group.*

Chapter 4:

Quantification of bone's tissue level response to low frequency pulsed ultrasound: The role of pulse duration

4.1 Abstract

Low intensity pulsed ultrasound (LIPUS) has been proposed as a potential therapeutic agent in the treatment of estrogen deficient osteopenia. This study addresses bone's tissue level response to LUPUS treatment using elastic and viscoelastic nanoindentation techniques. Seventy-two, 16 week old Sprague-Dawley rats were divided into six groups; baseline control, age-matched control, OVX control, OVX + 200μs ultrasound (US), OVX + 400μs US and OVX + 800μs US. LIPUS was delivered transdermally at the L4/L5 vertebrae, using gel-coupled plane wave US transducers. The signal, characterized by 200μs, 400μs or 800μs pulses of 1.5 MHz sine waves repeating at 1 kHz with intensities of 0.1, 0.2 or 0.4mW/cm^2, was applied 20 min/day, 5 days/week for 4 weeks. OVX treatment decreased Elastic Modulus (-19%, $p<0.05$) and Hardness (-16%, $p<0.05$) and increased loss tangent (tan δ) in trabecular bone compared to age-matched controls at 4 weeks post surgery. LIPUS treatment had no effect on bone's elastic material properties. Loss tangent, however was significantly increased in the trabecular region by 32% ($p<0.001$), 34% ($p<0.001$) and 26% ($p<0.001$) in the 200μs, 400μs and 800μs ultrasound treated groups. A similar response in elastic and viscoelastic material properties was observed in the anterior and posterior cortices of the vertebral body.

Key Words: *Therapeutic Ultrasound, Bone Remodeling, Mechanotransduction, Low Intensity Ultrasound, Ovariectomy, Nanoindentation, Elastic Material Properties, Viscoelastic Material Properties*

4.2 Introduction

Osteoporosis related fractures present a significant challenge to the clinical and orthopedic research communities [10], as they are often associated with increased mortality and decreased quality of life [5, 6]. Osteoporosis results in a number of changes to bone at both the apparent and tissue level which lead to altered mechanical performance. At the apparent level, the relationship between bone mass and mechanical performance is well understood [123, 124]. At the tissue level, imbalances in bone's remodeling processes result in compromised tissue mineralization, increased porosity and decreased tissue organization. From a mechanics perspective, fracture risk can be described in terms of compromised bone volume and microstructure as well as decreased structural integrity in response to static and dynamically applied loads [125]. Therefore, effective treatments should address preservation of bone's structural integrity at both the millimeter and sub-micron length scales.

Low intensity pulsed ultrasound (LIPUS) has been shown to be anabolic in vitro [33] and in vivo in the case of fracture repair [47, 48]. In a previous study we reported that therapeutic ultrasound (US) was capable of minimizing loss of bone volume and mechanical strength in an ovariectomy (OVX) rat model and that bone's response was sensitive to ultrasound pulse duration [126]. This study showed that using a center frequency of 0.5 MHz and a pulse repetition frequency (PRF) of 1 kHz, both short

(200μm) and long (800μs) pulse durations were capable of partially mediating changes to BVF and apparent level Elastic Modulus due to OVX.

The effects of ultrasound in bone microarchitecture and mechanical strength suggest that ultrasound may play a role in bone's remodeling process [126]. This altered bone remodeling could cause changes in tissue mineralization, porosity and organization which, could result in changes to bone's tissue level material properties [81, 127-129]. It is thought that bone's elastic material properties reflect the local mineral components and the viscoelastic material properties are strongly influenced by the collagen content [127, 130-132]. Changes to bone mineralization levels and to the relative mechanical contributions' of mineral and collagen could alter both the elastic and viscoelastic components of bone's material properties. Thus, it is important to consider both elastic and viscoelastic material characteristic when evaluating bone's overall performance.

The goal of this study was to determine the role of therapeutic ultrasound pulse duration in modulating changes to bone's nanoscale elastic and viscoelastic material properties associated with estrogen deficient osteopenia. **We hypothesize that high frequency dynamic mechanical signals delivered via ultrasound play a role in regulating bone's remodeling processes, affecting local porosity and mineralization. Subsequently, therapeutic US may be capable of mediating changes to bone's nanoscale elastic and viscoelastic material properties which result from estrogen deficient osteopenia.**

4.3 Methods

4.3.1 Experimental Design

All surgical and therapeutic procedures were approved by Stony Brook University's Institutional Animal Care and Use Committee (IACUC). The experimental design described here reflects that, which was described previously in Chapter 3 of this dissertation. Virgin, 16 week old Sprague-Dawley rats (301 ± 7g) were divided into six groups; baseline control (n=11), sham operated age-matched control (n=21), OVX control (n=20) (OVX), OVX + 200μs ultrasound stimulation (n=9) (US), OVX + 400μs US (n=9) and OVX + 800μs US (n=17). Animals were housed individually, subjected to 12 hour light/dark cycles and allowed free access to standard rodent chow and water. Body mass and food consumption were monitored bi-weekly throughout the study.

4.3.2 Therapeutic ultrasound stimulation

Under isofluorane anesthesia, therapeutic ultrasound was delivered transdermally over the posterior aspect of lumbar vertebra L4 and L5 using a gel-coupled plane wave ultrasound transducer (Panametrics, Inc.) in series with an amplifier (Tegam, Inc.) and function generator (HP, Inc.). The system was configured to produce pulsed-wave ultrasound with 200, 400 or 800 μs bursts of 0.5 MHz sine waves repeating at 1 kHz PRF. Spatial-averaged-temporal-averaged intensity (I_{SATA}=0.1, 0.2 and 0.4 mW/cm^2 respectively) was calibrated using a membrane hydrophone. The stimulus was applied 20 min/day, 5 days/week over 4 weeks.

4.3.3 Sample preparation

Following sacrifice via CO_2 asphyxiation, the L5 vertebra was cleaned, wrapped in saline soaked gauze, sealed in aluminum foil and stored at -40◦C. Samples were allowed one freeze-thaw cycle. A 1.5mm thick transverse slice was removed from the center of the vertebra using a water irrigated diamond wafer saw. Specimens were then dehydrated for 24 hours in 100% Ethanol, embedded in a low viscosity epoxy resin (EpoThin™, Buehler, Inc.) and allowed to cure under negative pressure in a vacuum chamber. Samples were then polished to a final surface roughness of 0.05µm and re-hydrated for 24 hours in physiologic solution (10x PBS) immediately prior to testing. A total of ten indents were made in each sample: three indents were placed at 25%, 50% and 75% of the cortical thickness at both the anterior and posterior cortices and four indents were placed in each of the four quadrants of the anterior cancellous space.

4.3.4 Nanoindentation

Nano-mechanical testing was performed using a triboscanner (Hysitron Inc., Minneapolis, MN) equipped with a nanoDMA module. A quasi-static indent was made at each location, followed by a dynamic indent, which was offset by a distance of three microns. The system optics was calibrated periodically throughout the study using a standard alumina reference sample. Quasi-static and dynamic calibration indents were also performed in fused quarts and polycarbonate reference samples. In the polycarbonate sample, the quasi-static and dynamic loading protocol was the same as was used for the bone samples. Fused quartz samples were indented using a quasistatic load of 10,000 µN and a dynamic load of 100 µN, so that a contact depth could be achieved similar to that of the tests in bone and polycarbonate.

Quasi-static indentation was performed using a loading/unloading rate of 50µN/s to a peak load of 200µN with a hold period of 10s. Elastic Modulus (E) and hardness (H) were then calculated from the initial portion of the unloading curve using the method of Oliver and Pharr[93].

Dynamic indentation was performed by applying a quasistatic load of 200µN, followed by a 90s hold period. Then a 20µN sinusoidal load was superimposed onto the 200µN quasistatic load and frequency was ramped between 20 and 200Hz sampling at 40 equally distributed frequencies. The phase shift between the input load and measured displacement was then used to calculate the material's viscoelastic properties including Storage Modulus (E') and Loss Modulus (E'') and loss tangent (tan δ) using the method of Loubet et al.[133].

4.3.5 Data Analysis

All values are reported as mean ± standard deviation unless otherwise noted. One way ANOVA and Tukey's post-hoc tests were used to detect paired differences between groups for E, H, E', E'', tan δ and slope (m). Significance was defined at $p<0.05$ (*) and $p<0.001$ (**). Correlations were determined using multiple linear regressions and Pearson's product moment correlation coefficient. All statistical analyses were performed using SigmaStat v3.5 (Systat Software, Inc., San Jose, CA, USA).

4.4 Results

4.4.1 Elastic and viscoelastic material properties vary spatially in the lumbar vertebra

Indents made in the anterior and posterior cortices were placed at locations 25%, 50% and 75% of the cortical thickness. Neither Elastic Modulus, nor Hardness was found to be dependent on the relative position within the cortex.

Elastic Modulus did not depend of the position within the vertebral body. Similarly, Storage Modulus was not dependent on indent position. Conversely, Loss modulus was shown to be significantly higher in the trabecular region compared to indents made in the anterior and posterior cortices.

4.4.2 OVX Alters Bone's Elastic and Viscoelastic Material Properties

OVX treatment significantly decreased elastic modulus in the anterior cortex (-20%, $p<0.05$), posterior cortex (-25%, $p<0.05$) and trabecular regions (-19%, $p<0.05$) compared to Age-matched controls. Similarly, Hardness decreased in the anterior cortex (-19%, $p<0.05$), posterior cortex (-15%, $p<0.05$) and trabecular region (-16%, $p<0.05$).

Bone's 20Hz viscoelastic material properties were also altered after 28 days of estrogen deficiency. In the anterior cortex, Loss Modulus decreased (-10%, $p<0.05$), Storage Modulus decreased (-28%, $p<0.05$) and loss tangent was significantly increased (19%, $P<0.001$) compared to age-matched controls. In the posterior cortex, Loss Modulus decreased (-11%, $p<0.05$), Storage Modulus decreased (-34%, $p<0.05$) and loss tangent was significantly increased (28%, $P<0.001$) compared to age-matched controls. In the trabecular region, Loss Modulus decreased (-15%, $p<0.05$), Storage Modulus decreased (-27%, $p<0.05$) and loss tangent was significantly increased (16%, $P<0.001$) compared to age-matched controls.

4.4.3 Elastic and Viscoelastic Material Properties are not altered by animal aging

There were no significant differences in Elastic Modulus at the anterior cortex between baseline and age-matched groups. Similarly no differences were found between baseline and age-matched groups in the posterior cortex or trabecular region.

4.4.4 Elastic Material Properties are Unltered by LIPUS Intervention

In the anterior cortex, there were no significant differences in Elastic Modulus between OVX controls and the 200μs ($p>0.05$), 400μs ($p>0.05$), or 800μs ($p>0.05$) US treated groups. Similarly, there were no differences in Hardness between OVX controls and 200μs ($p>0.05$), 400μs ($p>0.05$), or 800μs ($p>0.05$) US treated groups. In the posterior cortex, there were no significant differences in Elastic Modulus between OVX controls and the 200μs ($p>0.05$), 400μs ($p>0.05$), or 800μs ($p>0.05$) US treated groups. No differences were found in hardness between OVX and 200μs ($p>0.05$), 400μs ($p>0.05$), or 800μs ($p>0.05$) US treated groups. And, within the trabecular region, there were no significant differences in Elastic Modulus between OVX controls and the 200μs ($p>0.05$), 400μs ($p>0.05$), or 800μs ($p>0.05$) US treated groups or in hardness between

OVX and 200μs (p>0.05), 400μs (p>0.05), or 800μs (p>0.05) US treated groups. Lastly, Elastic Modulus and Hardness were significantly lower in all positions and for all treatment groups compared to age matched controls.

No significant differences were found between US treated groups for either Elastic Modulus or Hardness at any of the spatial position. In addition, Elastic Modulus and Hardness showed no correlation to cycle number or signal intensity.

4.4.5 LIPUS Intervention Alters Bone's Viscoelastic Material Properties

We first considered bone's viscoelastic response at a superimposed dynamic load of 20 Hz. At the Anterior cortex, no significant differences in Storage Modulus were found in between OVX controls and groups treated with 200μs, 400μs or 800μs US pulse duration. Compared with age-matched controls, Storage Modulus was significantly lower in the 200 μs (-33%, P<0.05), 400μs (-30%, P<0.05), and 800μs (-21%, P<0.05), US treated groups. Loss Modulus however was significantly increased in the 200 μs (24%, P<0.05), 400μs (27%, P<0.05), and 800μs (36%, P<0.05), US treated groups. Loss tangent (tan δ), which represents the ratio between Loss Modulus and Storage Modulus increased 34% (p<0.001), 31% (p<0.001) and 25% (p<0.001) for the 200μs, 400μs and 800μs US treated groups respectively.

At the Posterior cortex, no significant differences in Storage Modulus were found in between OVX controls and groups treated with 200μs, 400μs or 800μs US pulse duration. Compared with age-matched controls, Storage Modulus was significantly lower in the 200 μs (-41%, P<0.05), 400μs (-28%, P<0.05), and 800μs (-32%, P<0.05), US treated groups. Loss Modulus however was significantly increased in the 200 μs (20%, P<0.05), 400μs (33%, P<0.05), and 800μs (35%, P<0.05), US treated groups. Loss tangent (tan δ) increased 34% (p<0.001), 22% (p<0.001) and 32% (p<0.001) for the 200μs, 400μs and 800μs US treated groups respectively.

Within the trabecular region, no significant differences in Storage Modulus were found in between OVX controls and groups treated with 200μs, 400μs or 800μs US pulse duration. Compared with age-matched controls, Storage Modulus was significantly lower in the 200 μs (-34%, P<0.05), 400μs (-32%, P<0.05), and 800μs (-28%, P<0.05), US treated groups. Loss Modulus however was significantly increased in the 200 μs (19%, P<0.05), 400μs (24%, P<0.05), and 800μs (24%, P<0.05), US treated groups. Loss tangent (tan δ) increased 32% (p<0.001), 34% (p<0.001) and 26% (p<0.001) for the 200μs, 400μs and 800μs US treated groups respectively.

There were no significant differences in Storage Modulus, Loss Modulus or Loss Tangent for among any of the US treated groups at the anterior cortex, posterior cortex or trabecular regions. In addition, there were no significant correlations or trends between E', E'', or tanδ and intensity or cycle number.

4.4.6 Frequency Sensitivity Remains Unaltered by Changes in US Pulse Duration

We found increases in the slope of OVX treated groups compared to age-matched controls at the anterior cortex (150%, P<0.05), posterior cortex (228%, P<0.05) and within the trabecular region (106%, P/<0.05). When compared to OVX controls, US

treated groups showed no significant differences in slope at any of the positions within the vertebral body.

4.5 Discussion

In this study we examined bone's tissue level response to OVX and LIPUS intervention using signals of varying US pulse duration. We first considered the sensitivity of material properties to position within the vertebral body. It has been shown that bone's elastic material properties vary across the cortical thickness of the tibial mid-diaphysis [88], however, we did not observe differences across the cortical thickness of the anterior and posterior cortices. This may be due the fact indents made closest to the endosteal and periosoteal surfaces were not close enough to the actual surface, but rather positioned away from the rapidly remodeling surfaces. We found no differences in elastic Modulus or Hardness between the anterior and posterior regions as was noted by Hengsberger et al [130]. Several factors could have contributed to this discrepancy including different tissue hydration levels and the maximum indentation load/contact depth to which the samples were tested.

In this study we noted significant changes in bone's tissue level elastic and viscoelastic material properties as a result of ovariectomy. It has been shown that during the first four weeks following OVX, rats experience a decrease in bone volume fraction (BVF) and compromised microstructural measures of bone quality [68-70]. These changes are likely the result of an imbalance in bone's remodeling processes, including increased bone resorbtion and decreased bone formation[68]. We noted significant decreases in elastic modulus, storage modulus and hardness, which could be the result of decreased local mineral quality [81, 127-130, 134]. We also noted a decrease in Loss Modulus, which could suggest an alteration in tissue level organization or an increased role of collagen due to reduced mineral content [127, 135, 136].

The introduction of the low intensity, 0.5 MHz signals did not affect bone's elastic response as noted by Elastic Modulus (E), Hardness (H) and Storage Modulus (E'). Since bone's static material properties primarily reflect the amount and quality of bone mineral content[127], this could indicate that the increased bone resoption characteristic of OVX groups left bone less equipped to withstand peak load magnitudes. Conversely, US intervention had a significant effect on bone's tissue level viscous damping characteristics, as noted by an increase in loss modulus (E''). These changes could indicate that while the ultrasound signal did not drive tissue mineralization, changes in E'' could be the result of a remodeling driven increase in porosity or in the case of less bone mineral, an increased relative contribution of collagen content.

The sensitivity of loss tangent to changes in frequency was also considered. The slope of each line represents the sensitivity of each group to changes in loading frequency. Thus, larger slopes could indicate a greater range of damping responses within the tested frequency range. In this study we found that OVX groups and LIPUS treated groups had a significantly higher slope (>100%, $p<0.05$) compared to age-matched groups, indicating that there would be greater variability in bone's damping characteristics, particularly at lower frequencies (<100Hz). This frequency range is

particularly relevant because it encompasses that of postural muscle attachments and their subsequent mechanical strain signals within this range [137-139]. It could therefore suggest that these groups experienced an altered state of mechanical loading with different loading frequencies, which could lead to the transmission of different remodeling signals. Thus, these groups may not only be responding differently to external mechanical signals, but rather could be subjected to fundamentally different signals due to the inherent mechanical properties.

In our previous study [126], trabecular bone volume and microarchitecture were partially preserved as a result of LIPUS intervention. Here, we noted significant improvements in bone volume fraction (BVF) and apparent level elastic modulus for the shortest pulse (200μs) and longest pulse (800μs) US treated groups. Together, these results indicate that while LIPUS was capable of minimizing changes to trabecular microarchitecture, changes at the sub-micron length scale resulted in bone matrix that was increasingly compliant and better equipped to dissipate dynamically applied loads.

The precise mechanisms by which ultrasound affects bone remodeling are unclear given the current body of research and the data presented here. However, we know that in bone, ultrasound behaves as a mechanical wave. As a result, it may be capable of generating gradients in pressure within bone's micro-porosities sufficient to produce fluid-flow generated anabolic signals. It is unlikely that thermal effects are involved in mediating bone remodeling. The intensities used here in this study are far below those required to induce a temperature change greater than 1◦C, the upper limit established for ultrasound safety by the FDA.

4.6 Limitations

Several limitations should be considered when interpreting the results of this study. First, our measurements of material properties were made in a direction orthogonal to that of the propagating ultrasound wave. Measurements were made in the axial direction to reflect bone's response in the predominant physiologic direction; however, this difference could result in measurements which do not fully capture bone's response to ultrasound signals. A second limitation involves our use of axial loading techniques to measure material properties in trabecular bone. Several studies have shown that bone's material properties vary with loading direction [140, 141], thus slight misalignments in sample orientation could alter results. Trabecular bone's inherent morphology makes it difficult to align indents to the local (Lagrangian) trabecular orientation. In our study we attempted to place indents at or near the intersection of several trabecular "rods", i.e. within trabecular "plates" in order to minimize these potentially confounding factors.

4.7 Conclusions

In conclusion, we found that OVX decreased elastic modulus and tan δ. And, that while LIPUS intervention had no effect on preserving bone's tissue level elastic material properties, tan δ showed significant improvements following four weeks of treatment. These tissue level observations are in line with what one may expect if

therapeutic ultrasound played a partial role in regulating bone's modeling and remodeling processes.

4.8 Figures and Tables

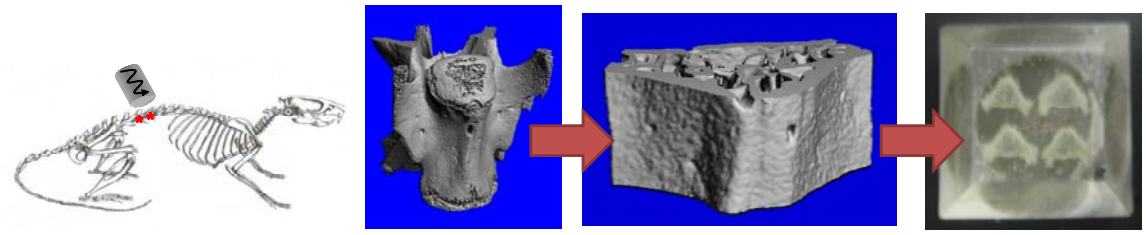

Figure 4.1: *An approximately 2mm transverse slice(center) was removed from the center of the L5 vertebra (left) using a water irrigated wafer saw. The samples were dehydrated for 24 hrs in 100% ethanol and embedded in a weakly exothermic epoxy resin (Epothin™, Buhler Inc.). Each sample was then polished to a final surface roughness of 0.05µm (right).*

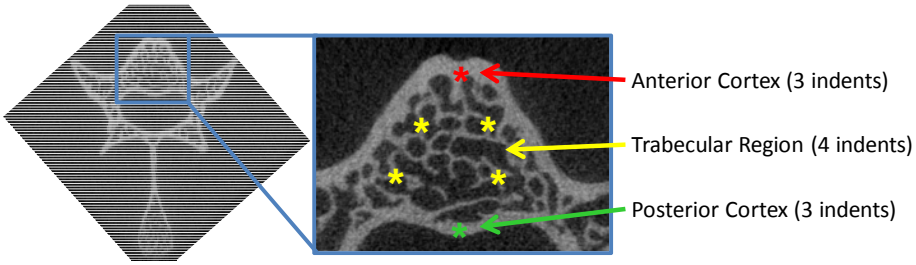

Figure 4.2: *Indentation was performed perpendicular to the transverse plane and therefore primarily reflects the material properties in the predominant physiologic direction. A total of 10 indents were made in each vertebral sample. Three indents were made across the thickness of the anterior cortex, placed at 25, 50 and 75% of the total thickness. Three indents were also made across the thickness of the posterior cortex and placed at 25, 50 and 75% of the total thickness. Four indents were made on individual trabeculae and distributed within each of the four quadrants. Whenever possible, Indents were placed near the intersection of trabecular structures and therefore are more likely to be axially oriented trabeculae.*

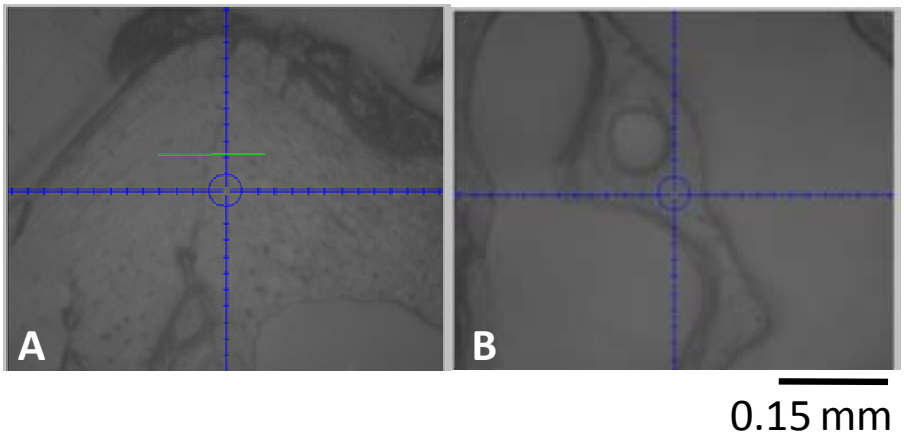

Figure 4.3: *Images of representative indent locations in the anterior cortex (A), posterior cortex (B) and trabecular bone (C & D) as seen through the nanoindenter system optics.*

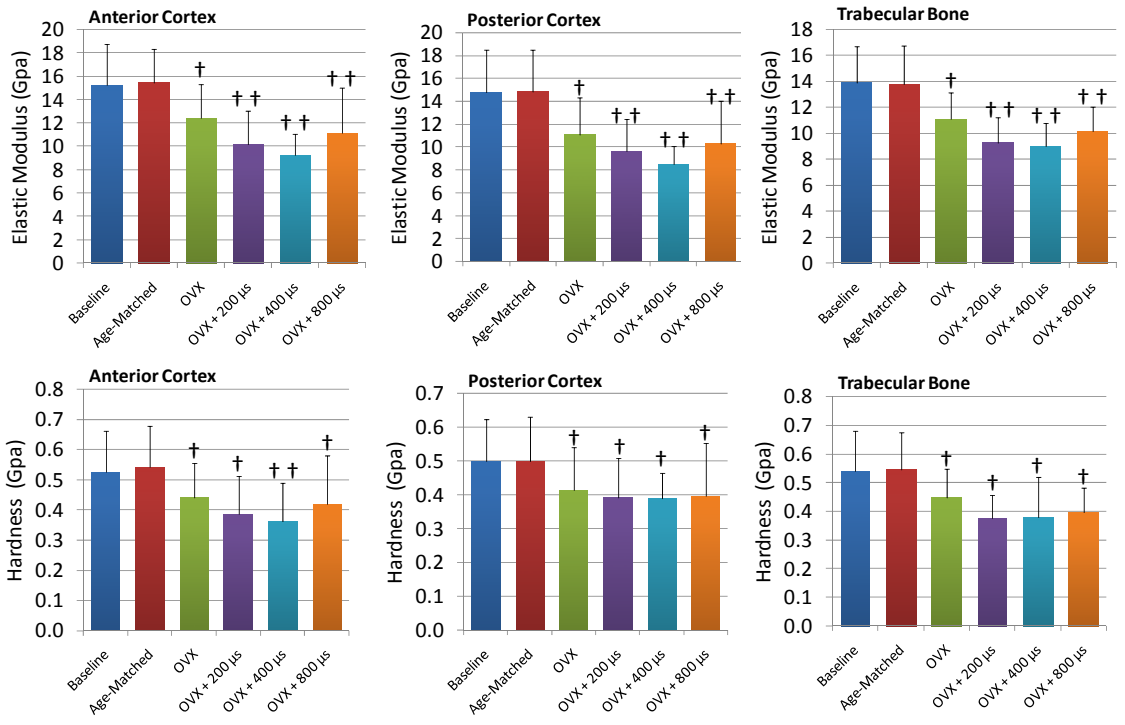

Figure 4.4: *Elastic Modulus and Hardness for the anterior cortex, posterior cortex and trabecular regions. († = p<0.05 vs. age-matched, †† = p<0.001 vs. age-matched, *=p<0.05 vs. OVX, and **=p<0.001 vs. OVX)*

	Elastic Modulus (E)		
	Anterior	**Posterior**	**Trabecular**
OVX vs. Age-matched	-20% †	-25% †	-19% †
OVX + 200μs US vs. OVX	-18%	-13%	-16%
OVX + 400μs US vs. OVX	-26%	-23%	-19%
OVX + 800μs US vs. OVX	-11%	-7%	-9%
OVX + 200μs US vs. Age-matched	-34% ††	-35% ††	-33% ††
OVX + 400μs US vs. Age-matched	-40% ††	-43% ††	-35% ††
OVX + 800μs US vs. Age-matched	-28% ††	-31% ††	-26% ††

Table 4.1: *Percent change in Elastic Modulus (E) for experimental and control groups. Values reflect changes between OVX and age-matched groups, between experimental groups and OVX controls and between experimental groups and age-matched controls. (Note: statistical significance is reported at p<0.05, p<0.01 and p<0.001.)*

	Hardness (H)		
	Anterior	**Posterior**	**Trabecular**
OVX vs. Age-matched	-19% †	-15%†	-16% †
OVX + 200μs US vs. OVX	-12%	-8%	-17%
OVX + 400μs US vs. OVX	-18%	-9%	-17%
OVX + 800μs US vs. OVX	-5%	-7%	-13%
OVX + 200μs US vs. Age-matched	-29% †	-22% †	-31% †
OVX + 400μs US vs. Age-matched	-34% ††	-22% †	-30% †
OVX + 800μs US vs. Age-matched	-23% †	21% †	-27% †

Table 4.2: *Percent change in Hardness (H) for experimental and control groups. Values reflect changes between OVX and age-matched groups, between experimental groups and OVX controls and between experimental groups and age-matched controls. (Note: statistical significance is reported at p<0.05, p<0.01 and p<0.001.)*

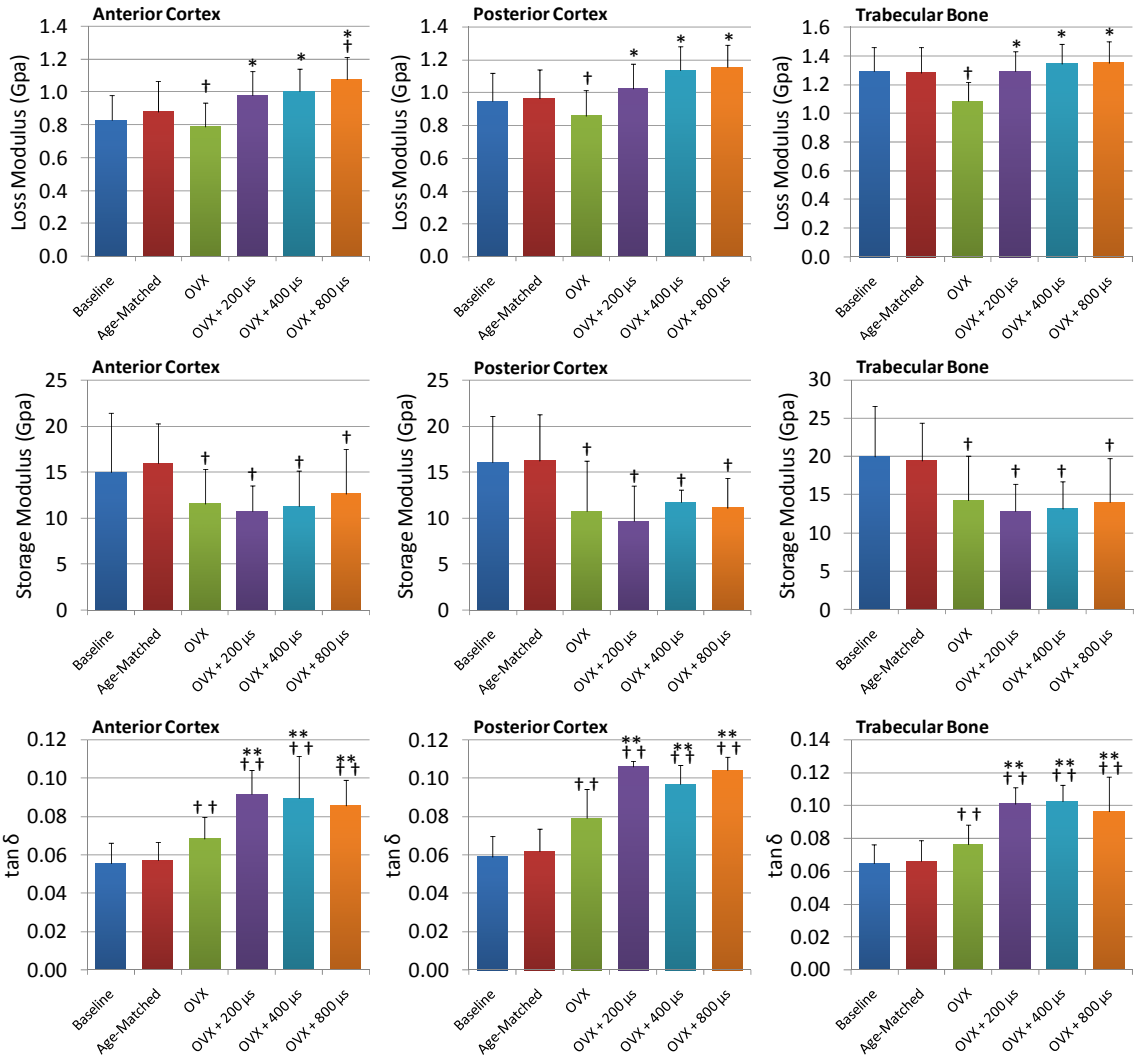

Figure 4.5: *Mean viscoelastic material properties under 20Hz dynamic loading. Loss Modulus (E''), Storage Modulus (E') and loss tangent (tan δ) are reported for indents in the anterior cortex, posterior cortex and trabecular regions. († = p<0.05 vs. age-matched and *=p<0.05 vs. OVX)*

Slope of tan δ (m)	Anterior	Posterior	Trabecular
OVX vs. Age-matched	150% †	228% †	106%
OVX + 200μs US vs. OVX	-21%	-19%	-36%
OVX + 400μs US vs. OVX	-1%	-10%	-22%
OVX + 800μs US vs. OVX	48%	73%	26%
OVX + 200μs US vs. Age-matched	97% †	167%	32%
OVX + 400μs US vs. Age-matched	147% †	194% †	61%
OVX + 800μs US vs. Age-matched	269% †	466% †	159%

Table 4.3: *Percent change in slope of tan δ curves. Changes are reported at the anterior cortex, posterior cortex and within the trabecular bone. (Note: statistical significance is reported at p<0.05, p<0.01 and p<0.001.)*

	Anterior		
	E''	**E'**	**tan δ**
OVX vs. Age-matched	-10% †	-28% †	19% ††
OVX + 200μs US vs. OVX	24% *	-7%	34% **
OVX + 400μs US vs. OVX	27% *	-3%	31% **
OVX + 800μs US vs. OVX	36% *	9%	25% **
OVX + 200μs US vs. Age-matched	12%	-33% †	60% ††
OVX + 400μs US vs. Age-matched	14%	-30% †	57% ††
OVX + 800μs US vs. Age-matched	22% †	-21% †	50% ††

Table 4.4: *Percent change in Storage Modulus (E'), Loss Modulus (E'') and Loss Tangent (tan δ). Changes are reported at the anterior cortex. (Note: statistical significance is reported at p<0.05, p<0.01 and p<0.001.)*

	Posterior		
	E''	**E'**	**tan δ**
OVX vs. Age-matched	-11% †	-34% †	28% ††
OVX + 200μs US vs. OVX	20% *	-11%	34% **
OVX + 400μs US vs. OVX	33% *	9%	22% **
OVX + 800μs US vs. OVX	35% *	3%	32% **
OVX + 200μs US vs. Age-matched	7%	-41% †	71% ††
OVX + 400μs US vs. Age-matched	18%	-28% †	56% ††
OVX + 800μs US vs. Age-matched	20%	-32% †	68% ††

Table 4.5: *Percent change in Storage Modulus (E'), Loss Modulus (E'') and Loss Tangent (tan δ). Changes are reported at the posterior cortex. (Note: statistical significance is reported at p<0.05, p<0.01 and p<0.001.)*

	Trabecular		
	E''	**E'**	**tan δ**
OVX vs. Age-matched	-15% †	-27% †	16% ††
OVX + 200μs US vs. OVX	19% *	-10%	32% **
OVX + 400μs US vs. OVX	24% *	-8%	34% **
OVX + 800μs US vs. OVX	24% *	-2%	26% **
OVX + 200μs US vs. Age-matched	1%	-34% †	53% ††
OVX + 400μs US vs. Age-matched	5%	-32% †	55% ††
OVX + 800μs US vs. Age-matched	5%	-28% †	46% ††

Table 4.6: *Percent change in Storage Modulus (E'), Loss Modulus (E'') and Loss Tangent (tan δ). Changes are reported at trabecular bone. (Note: statistical significance is reported at p<0.05, p<0.01 and p<0.001.)*

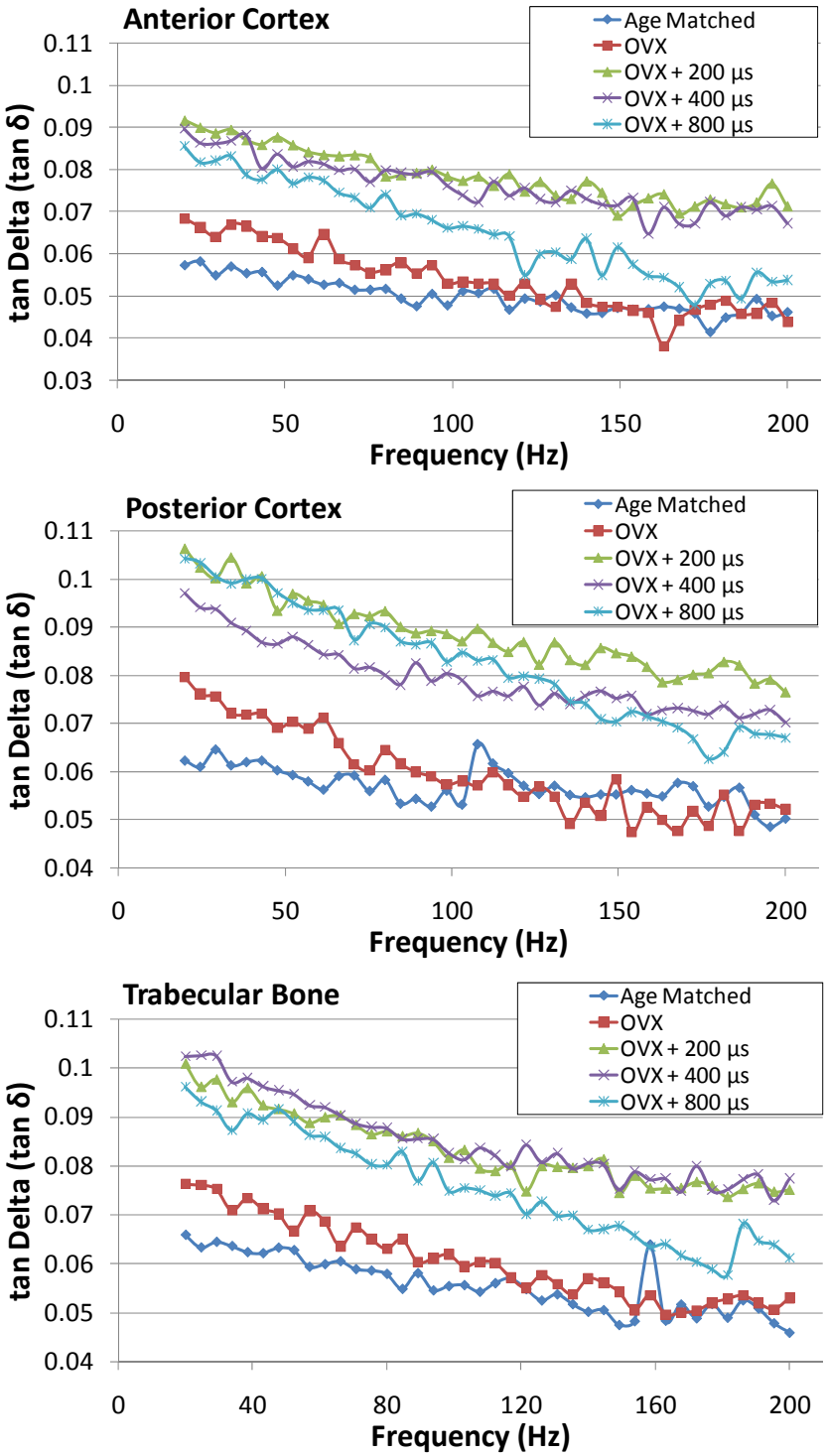

Figure 4.6: *Average Loss modulus (E'') values as a function of frequency for experimental and control groups. Each plot represents data from the anterior cortex, posterior cortex and trabecular regions.*

Chapter 5:

The Role of Ultrasound Signal Intensity on Osteopenic Bone Loss

5.1 Abstract

This study tests the hypothesis that an ultrasound generated dynamic mechanical signal can attenuate bone loss in an estrogen deficient model of osteopenia. Eighty-four, sixteen week old Sprague-Dawley rats were divided into six groups: baseline control, age-matched control, ovariectomy (OVX) OVX control, OVX + 5 mW/cm^2 ultrasound (US), OVX + 30 mW/cm^2 US and OVX + 100 mW/cm^2 US. Low intensity pulsed ultrasound (LIPUS) was delivered transdermally at the L4/L5 vertebrae, using gel-coupled plane wave US transducers. The signal, characterized by 200μs pulses of 1.5 MHz sine waves repeating at 1 kHz with intensities of 5, 30 or 100mW/cm^2, was applied 20 min/day, 5 days/week for 4 weeks. OVX treatment reduced bone volume fraction 40% and compromised microstructure at 4 weeks post surgery. LIPUS treatment, however, significantly increased BVF 33% compared to OVX controls for the 100mW/cm^2 treated group. Additionally, SMI, and Tb.N showed significant improvements compared with OVX for the 100mW/cm^2 treated group and Tb.Th was significantly improved in the 30 and 100mW/cm^2 treated groups. Interestingly, the 100mW/cm^2 treated group showed a significant improvement over the 5mW/cm^2 treated group in terms of BVF, SMI and Tb.N. Improvements in bone's microstructural characteristics with 100mW/cm^2 US treatment translated into improved load bearing characteristics, including a significant, 42% increase in apparent level Elastic Modulus compared to OVX controls. Mean principal compressive stress demonstrated a non-significant increasing trend for the 100mW/cm^2 treated group; however, significant differences were observed for the same group among peak principal compressive stresses associated with the 75th percentile. This study also suggests that there exists a minimum intensity threshold below which LIPUS in less effective at maintaining bone's microstructural and mechanical characteristics.

Key Words: *Therapeutic Ultrasound, Bone Remodeling, Mechanotransduction, Low Intensity Ultrasound, Ovariectomy, MicroCT, Finite-Element Analysis*

5.2 Introduction

Osteoporosis is a disease characterized by decreased bone mass and progressive erosion of the microstructure. As a result, key skeletal sites such as the hip, spine and wrist are at increased risk for developing chronic and traumatic fractures. Current treatments include hormonal, pharmachologic and mechanical strain interventions. Hormonal and pharmachologic interventions are often associated with adverse side effects and target the skeleton as a whole, as opposed to specifically targeting skeletal sites at increased risk for failure. Mechanical strain interventions, however, are noninvasive and have demonstrated promising results. In vitro studies have shown low-magnitude, high-frequency vibrations to be anabolic in both human[142] and animal models [12]. In addition, whole bone accelerations have been shown to be anabolic to bone [143, 144]. A contributing mechanism by which low-magnitude mechanical stimulations act, could involve bone fluid flow. A recent study has shown that in the

absence of mechanical strain, intramedulary bone fluid flow can drive bone remodeling [98, 145].

It has been suggested that in bone, ultrasound behaves as a mechanical wave, generating local pressure gradients. This may result in the production of anabolic shear forces on cell membranes or changes in local solute concentrations [96, 97]. These gradients could drive local fluid flow, potentially resulting in an anabolic signal. Therefore, low intensity pulsed ultrasound (LIPUS) may offer a noninvasive method for delivery of high frequency, low amplitude and large cycle number, dynamic mechanical signals.

In vitro studies have shown that LIPUS is capable of increasing osteoblast proliferation and stimulating endochondral ossification in excised tissues [31-34]. It has also been shown that ultrasound signal intensity plays an important role in modulating the response of osteoblasts in vitro [35, 36]. Harle et al also showed that alkaline phosphatase expression was linked to ultrasound signal intensity [38]. In vivo studies have also shown that LIPUS accelerated fracture healing in both animal [48, 49, 64, 107, 108] and human models [43, 44, 109, 110]. In addition, Yang et al, showed that bone's response to ultrasound during fracture healing was sensitive to ultrasound signal intensity [64]. Thus, it is likely that ultrasound may be an effective treatment in other cases of altered bone remodeling. However, there is limited, conflicting evidence with respect to the effectiveness of LIPUS in treating in vivo, non-fracture related bone diseases [58, 61], particularly in conditions associated with chronic bone loss. It is also unclear what role ultrasound signal parameters such as signal intensity play in bone's response.

Our objective was to explore the therapeutic potential of LIPUS for treatment of bone loss associated with estrogen deficient osteopenia using high resolution three-dimensional imaging and computational structural analysis techniques. **This study tests the hypothesis that an ultrasound generated dynamic mechanical signal can mediate bone loss and preserve mechanical strength in an estrogen deficient model of osteopenia.** To this end, we have completed a study in which we tested the effectiveness of various US signal intensities in preserving bone's micro architecture and mechanical integrity using high resolution imaging and computer modeling techniques.

5.3 Methods

5.3.1 Experimental Design

All surgical and therapeutic procedures were approved by the Institutional Animal Care and Use Committee (IACUC) at Stony Brook University. Sixteen week old, virgin female, Sprague-Dawley rats (304 ± 9g) were obtained from Charles River Laboratories (Wilmington, MA) and subjected to either ovariectomy (OVX) or sham operation. Animals were allowed to recover for 3 days, after which they were randomly assigned to one of six groups: (1) baseline control (n=18), (2) age-matched (sham-operated) control (n=21), (3) OVX control(n=20), (4) OVX + 5 mW/cm^2 ultrasound stimulation (US) (n=8), (5) OVX + 30 mW/cm^2 US (n=8) and (6) OVX + 100 mW/cm^2 US (n=8). All animals were housed individually in standard cages at 24◦C and allowed free

access to standard rodent chow and tap water. Body weight and food consumption were recorded at day zero and monitored bi-weekly throughout the study. Upon completion of the study, animals were euthanized via CO_2 asphyxiation.

5.3.2 US Treatment

Under isofluorane anesthesia, animals were positioned in sternal recumbency on a custom platform and therapeutic ultrasound was delivered transdermally over the posterior aspect of lumbar vertebra L4 and L5 using a 1 inch diameter disk plane wave ultrasound transducer (manufactured by Piezo Technologies,mounted on an Ultrasonic Instrument delivered by Juvent Medical Inc) . To maximize coupling of the transducer with the skin surface, fur was removed from the lumbar spine region and an ultrasonic coupling gel (Aquasonic, Inc.) was applied between the skin and ultrasound transducer. The signal was characterized by 200μs pulses of 1.5 MHz sine waves with a PRF (Pulse Repetition Rate) of 1 kHz and spatial-averaged temporal-averaged intensity (I_{SATA}) equal to 5, 30 or 100 mW/cm^2. Treatment was applied 20 min/day, 5 days/week for 4 weeks. Ultrasound signals were calibrated at the beginning, midpoint and end of the study using a membrane hydrophone (Precision Acoustics, Ltd., UK). The stimulus was applied 20 minutes/day, 5 days/week for 4 weeks. To minimize potential confounding effects due to isofluorane exposure, age-matched control and OVX control animals were simultaneously subjected to 20 minutes of isofluorane anesthesia per day, 5 days/week for 4 weeks. Upon completion of the study, animals were sacrificed via CO_2 asphyxiation and the L5 lumbar vertebra and left femur were removed, cleaned of soft tissue and stored in saline soaked gauze at -40◦C.

5.3.3 Microcomputed tomography

The L5 vertebra and left femur were imaged at 15μm isotropic resolution using μCT (μCT40, SCANCO) with energy (E) and intensity (I) equal to 55 kVp and 145 μA respectively. Cancellous bone was then manually segmented from a 1.5mm long axial ROI from the cranial third of the anterior vertebral body and a 1.5mm long region of the femoral metaphysis. Representative μCT images for experimental and control groups are shown in Figure 1 for the L5 vertebra and femoral metaphysis. Cancellous microstructure was then characterized using standardized techniques to determine bone volume fraction (BVF), structural model index (SMI), connectivity density (Conn.D.), trabecular number (Tb.N.), trabecular thickness (Tb.Th.) and trabecular spacing (Tb.Sp.).

5.3.4 Finite Element Analysis

Three-dimensional image data from each ROI was used to generate specimen specific finite-element models, which were then used to evaluate the load bearing capabilities for each sample. Voxel based finite element meshes were created using custom software based on the pixel-to-voxel technique, in which each pixel is represented by an eight-noded cuboid element. Disassociated regions of the model, which did not intersect virtual-cut plane surfaces, were removed to ensure convergence. Trabecular tissue was assumed to behave as a homogenous, linear elastic

isotropic solid (E=18GPa & ν=0.3) and full friction boundary conditions were assigned at the superior and inferior surfaces. Trabecular samples were subjected to 0.5% compressive strain in the cranio-caudal direction and a commercial, nonlinear finite element solver (ABAQUS v6.4, Dassault Systemes, Inc., Providence, RI) was used to solve for apparent and tissue level stresses and strains.

5.3.5 Data Analysis

All values are reported as mean ± standard deviation, unless noted otherwise. One-way analysis of variance (ANOVA) and Tukey's post-hoc test was used to detect differences between groups for body weight, food consumption, morphological indices (BVF, Conn.D., Tb.N., Tb.Th., and Tb.Sp) and mechanical strength parameters (E, $\overline{\sigma_3}$, 75th percentile of σ_3 , $\overline{\sigma_{von\ Mises}}$, $\overline{SED}$ and 75th percentile of SED). Significance was determined at p≤0.05 and p≤0.001. A one way repeated measures analysis of variance with Tukey's post-hoc was used to detect differences between treated groups for SMI. In addition, we also performed a two-way ANOVA with Tukey's multiple comparison test to detect paired differences among the different regions within the L4 and L5 vertebra and between the different treatment groups. Correlations were determined using multiple linear regressions and Pearson's product moment correlation coefficient. All statistical analyses were performed using SigmaStat v3.5 (Systat Software, Inc., San Jose, CA, USA).

5.4 Results

5.4.1 Body Mass and Food Intake

At day zero, there were no significant differences in body mass among any of the experimental groups. Body mass for age-matched controls did not vary significantly from baseline throughout the duration of the 28 day study. Body mass for OVX and OVX + LIPUS treated groups, however increased significantly throughout the study (17%, P<0.001) compared to age-matched controls. No differences in body mass were observed among OVX control and OVX + LIPUS treated groups. Increased body weight was not associated with increased food consumption, which remained constant for all groups throughout the study.

5.4.2 OVX effects on bone microarchitecture and mechanical integrity

At 28 days post-surgery, OVX treatment was associated with substantial alterations in cancellous bone volume and morphology (Table 1 and Figure 3). OVX controls had 40% lower (p<0.01) BVF than Age-matched controls. Tb.N. decreased 17% (p<0.001), Tb.Th. decreased 19% (p<0.001) and Tb.Sp. increased 24% (p<0.001). OVX was also associated with higher SMI (436%, p<0.001) compared to age-matched controls. No changes, however, in Conn.D. were observed in OVX treated animals.

Bone's load bearing characteristics were also strongly affected by OVX (Table 2 and Figure 4). At the apparent level, Elastic Modulus was 51% lower (p<0.001) for OVX treated animals compared to age matched controls. Changes were also observed in average tissue stresses. Mean *von* Mises stress was 24% higher (p<0.001) while the *von*

Mises stress coefficient of variation was 21% higher ($p<0.001$). Additionally, the mean and 75th percentile of maximum principal stress was 23 and 45% lower respectively ($p<0.001$). Strain energy density, an indicator of local tissue fatigue and failure, had lower mean and 75th percentile values (26% $p<0.001$ and 32% $p<0.001$) compared to age-matched controls.

5.4.3 Effect of age on microarchitecture and mechanical integrity

Comparisons between age-matched and baseline controls were used to address potential changes in bone microarchitecture due to rodent maturation over the course of the experiment. No significant differences were identified among any of the morphological or mechanical strength parameters examined in this study.

5.4.4 Effects of therapeutic ultrasound treatment on microarchitecture

The effects of therapeutic ultrasound on bone microarchitecture from the L5 vertebra are shown in Table 1 and Figure 3. BVF was positively correlated (R^2=0.96) with ultrasound signal intensity, and was significantly higher (33%, $p<0.001$) in the 100mW/cm^2 US treated group compared to OVX controls. In addition, BVF was also 23% higher in the 100mW/cm^2 treated group compared to that of the 5mW/cm^2 treated group. However, when compared with age-matched controls, BVF was significantly lower in all US treated groups. Similarly, SMI was 48% lower ($p<0.001$) in the 100mW/cm^2 US treated group compared to OVX controls, and was negatively correlated (R^2= 0.99) to intensity. When compared to age matched controls, SMI was significantly higher in each of the US treated groups. There was no difference in Conn.D. between OVX and age-matched controls, and no differences between US treated groups and either OVX or age-matched controls.

Tb.Th. was significantly higher in the 30mW/cm^2 and 100mW/cm^2 treated groups compared to OVX controls (11%, $p<0.05$ and 13%, $p<0.001$) and had strong correlation to signal intensity (R^2 = 0.71). Compared to Age-matched controls, Tb.Th. was significantly lower in each of the US treated groups. Tb.N. was positively correlated to signal intensity (R^2 = 0.97) and was significantly higher (12%, $p<0.05$) in the 100mW/cm^2 treated group. Compared with age matched controls, Tb.N. was significantly lower for the 5 and 30mW/cm^2 signals (-15%, $P<0.001$ and -11%, $p<0.05$), however there was no significant difference in Tb.N. between age-matched controls and the 100mW/cm^2 treated group. Tb.Sp. also showed a strong negative correlation with signal intensity (R^2 = 0.94) and was significantly lower (-14%, $P<0.001$) for the 100mW/cm^2 treated group compared to OVX controls. Compared with age matched controls, Tb.Sp. was significantly higher for the 5 and 30mW/cm^2 signals (21%, $P<0.001$ and 15%, $p<0.05$), however there was no significant difference in Tb.N. between age-matched controls and the 100mW/cm^2 treated group.

5.4.5 Effects of therapeutic ultrasound treatment on mechanical integrity

The effects of therapeutic ultrasound on bone's mechanical integrity at the L5 vertebra are shown in Table 2 and Figure 4. Similar trends were also observed in bone's response to mechanical strain. At the apparent level, Elastic Modulus was positively

correlated with US signal intensity (R^2 = 0.95), and was significantly higher for the 100mW/cm^2 US treated groups (42%, $p<0.05$) compared to OVX controls. However, compared to age-matched controls, each of the US treated groups had a significantly lower Elastic Modulus. Mean *von* Mises stress and the coefficient of variation of *von* Mises stress were strongly correlated with ultrasound signal intensity (R^2 = 0.99 and R^2 = 0.99), but were not significantly different compared to OVX controls. When compared to age-matched controls, both mean *von* Mises stress and the coefficient of variation of *von* Mises stress were significantly different for the 5 and 30mW/cm^2 US treated groups, however, there were no significant differences between age-matched controls and 100mW/cm^2 US treated groups.

Positive correlations were also observed between mean maximum principal stress and the 75th percentile of maximum principal stress and US signal intensity (R^2 = 0.99 and R^2 = 0.99). While there were no significant differences between mean maximum principal stress and OVX controls, the 75th percentile of maximum principal stress was significantly higher in the 100mW/cm^2 US treated groups and OVX controls. Both mean maximum principal stress and the 75th percentile of maximum principal stress were significantly different compared with age-matched controls.

Lastly, we considered strain energy distributions in US treated groups compared to OVX and age-matched controls. Both average and 75th percentile of strain energy densities were well correlated with US signal intensity, but were not significantly different compared to OVX controls. When compared with age-matched controls, the 5 and 30mW/cm^2 US treated groups were significantly different, but there were no differences between the 100mW/cm^2 US treated group and age-matched controls.

5.4.6 Bone Morphology at a Non-stimulated Skeletal Site

Following four weeks of OVX, animals had 66% ($P<0.001$) lower BVF at the femoral metaphysis compared to age matched controls. In addition, Conn.D. decreased 66% ($P<0.001$), SMI decreased 407% ($P<0.001$), Tb.N. decreased 52% ($P<0.001$), Tb. Th. decreased 28% ($P<0.001$) and Tb.Sp. increased 123% ($P<0.001$) (Figure 5). However, there were no significant differences between any of the US treated groups when compared with OVX controls (Figure 5).

5.5 Discussion

In this study, LIPUS was proposed as a therapeutic intervention for treatment of bone loss based on its effectiveness in previous in vitro and in vivo fracture related studies as well as its potential as an anabolic high frequency mechanical signal. Our data indicate that dynamic mechanical signals, delivered using low intensity pulsed ultrasound, were able to partially mitigate detrimental changes to bone morphology and mechanical robustness induced by estrogen deficient osteopenia. Furthermore, we have also shown that bone's response is strongly correlated with ultrasound signal intensity. Here, at 28 days post-OVX, vertebral trabecular bone had lower BVF, decreased Tb.Th. and Tb.N. and increased Tb.Sp. Apparent modulus as well as tissue level stress and strains were also compromised. US treatment, however, was in part capable of mitigating the effects, as was shown by significant improvements over OVX

controls and in some cases returning values to a level similar to that of the age-matched controls. In addition, adaptations were not observed at a remote skeletal site, indicating that bone's response to US was site specific.

This study addresses the effects of three different spatial-averaged temporal-averaged ultrasound signal intensities: 5mW/cm^2, 30mW/cm^2 and 100mW/cm^2. These signals represent the low, moderate and higher ranges of what is typically considered low-intensity ultrasound. Ultrasound signals have been shown to be highly effective in stimulating delayed and nonunion fractures in animal models at 11mW/cm^2 [146], 30mW/cm^2 [107, 108] and 100mW/cm^2 [64]. Finally, one concern for the development of any medical ultrasound device is that of thermal heating. At very high intensities, > 1000mW/cm^2, it is possible to generate changes in local tissue temperature > 1◦C, which would exceed established safety limits [147]. Several studies have shown that intensities as high as 50mW/cm^2 did not induce changes in temperature > 1◦C [53, 148]. Thus, the 100mW/cm^2 signals used in this study are below intensities known to induce thermal heating and are believed to be safe for treatment in humans and animals.

To our knowledge, this study is the first to investigate the role of LIPUS in an OVX animal model of osteopenia using high resolution response measures, including three-dimensional μCT imaging and finite element simulation techniques. While caution must be used in extrapolating these results to humans, the results of this study suggest that LIPUS may serve as an effective intervention or a complimentary treatment for estrogen deficient bone loss.

The effectiveness of LIPUS in treating delayed and nonunion fractures has been widely established in controlled studies involving both human [43, 44, 109, 110] and animal models [48, 49, 64, 107, 108]. However, this application presents a unique environment dominated by acute inflammation and altered bone geometry. Subsequently, there is conflicting evidence regarding the use of therapeutic US in intact bone. Our findings partially support those of Carvalho et al., who used a 30mW/cm^2 ultrasound signal, and found that four weeks of US treatment reduced bone loss and increased bone formation rates [62]. While our study did not find significant improvements in BVF with 30mW/cm^2 US intervention, we observed a significant improvement with 100mW/cm^2 as well as a trend toward bone preservation with the 30mW/cm^2 US signal. Our study also supports the findings of Ari et al, who showed that LIPUS was capable improving BMD in bedridden patients [63]. While significant, the findings of Arai et al. should be viewed with caution due to the small sample size (n=5) used in their study.

Our findings are in discord with a previous study by Warden et al., which found that LIPUS was ineffective in preserving bone mineral density (BMD) and BVF [61]. In contrast, our study noted significant improvements in cancellous bone microstructure and subsequent improvements in structural integrity. Possible explanations for the discrepancy may include the age of the animals, the targeted skeletal site and the differences in measurement techniques. Ultrasound has also been tested in other animal models of bone remodeling. Yang et al found that a 125mW/cm^2 US was ineffective in preserving BMD and BVF in rats following sciatic nervectomy [121].

Similarly, Spadaro et al, found no differences in BMD at the femur/tibia between treated and untreaded four week old rats [59].

While the precise mechanism by which LIPUS acts in bone remains unclear, several possibilities have been suggested. First, ultrasound may act to generate an electric field, which could then drive an osteogenic adaptation [113]. While we did not specifically address this issue in our study, an in vitro study has shown that ultrasound could generate an electric field in the range believed to be anabolic to bone tissue [112]. A second potential mechanism could involve thermal heating. However, given the maximum range of intensities addressed in this study, it is unlikely that heating plays a role in bone's response [114, 115]. Ultrasound has also been shown to induce stable cavitation [149], however, given the intensities used in our study, this is highly unlikely. Lastly, it has been suggested that acoustic streaming may play a role in bone's response. Because ultrasound behaves as a mechanical wave in bone, it may be possible to generate local pressure gradients within bone's microporosities[96, 97]. Several recent studies have suggested that fluid movement within these structures could generate the mechanical signals associated with an increased osteogenic response [27, 29].

It is important to recognize that ultrasound signal attenuation likely plays an important role in the delivery of US energy. It has been estimated that, ignoring attenuation, an US signal with a spatial-averaged temporal-averaged intensity of 30mW/cm^2 exerts a spatial-averaged temporal-averaged force in the vicinity of 2mg/cm^2. This force is far below physiologic loads or high frequency strain signals, which have been shown to be anabolic. This suggests that acoustic radiation force plays an insignificant role in bone's response to the LIPUS signals addressed in this study.

5.6 Limitations

Several limitations should be considered when interpreting the results of this study. First, we do not know precisely how the ultrasound wave propagates through skin, fat, muscle and bone to act at the cancellous region addressed in this study. Given our current technologies, it would be extremely difficult to gain reliable in vivo measurements of signal transmission. However, we have conducted ex vivo measurements using a hydrophone, which suggest that approximately 30% of the initial ultrasound signal penetrates through the skin, muscle and cortical shell. Furthermore, ongoing studies in our lab will continue to develop computer models which simulate acoustic wave propagation through realistic tissue geometries. Such studies will help to explain the local environment during ultrasound stimulation.

5.7 Conclusions

In summary, we have shown that LIPUS is capable of partially mitigating adverse changes to bone induced by estrogen deficient osteopenia and that bone's response is sensitive to US signal intensity. To date, there is conflicting evidence for US as a treatment in intact bone; therefore, future studies will need to address the effects of US signal parameters (frequency, pulse duration, intensity and modulation). In addition, the mechanisms by which US acts to deliver an anabolic signal in bone remain elusive,

indicating the need for further in vitro and computer simulation studies. It is interesting to note that recent developments in qualitative ultrasound (QUS) technology have shown that BUA is sensitive not only to bone quantity, but to measures of bone quality as well. This suggests that US technology could be capable of integrating prophylaxis, treatment and diagnostic applications.

5.8 Figures and Tables

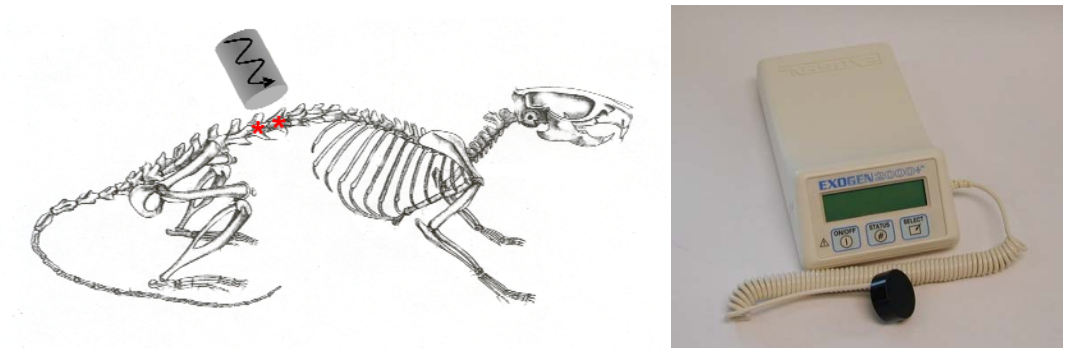

Figure 5.1: *(Left) Ultrasonic treatment was applied transdermally to the L4 and L4 vertebral bodies. The schematic to the left depicts the animal's position in sternal recumbancy and the direction of the applied ultrasound signal. (Right) An ultrasonic stimulator and transducer used to deliver the ultrasonic dynamic mechanical signal.*

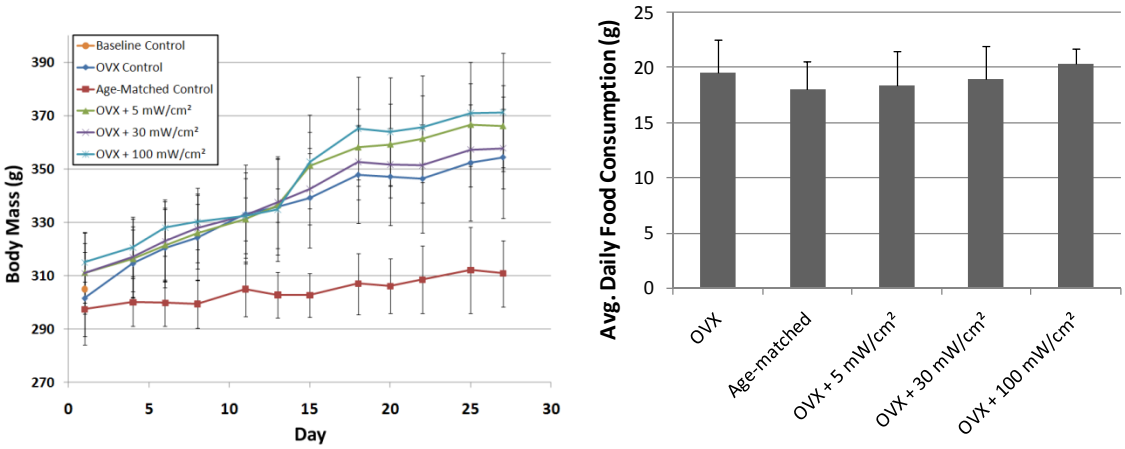

Figure 5.2: *(Left) Body mass (mean ± SD) throughout the 28 day experiment. (Right) Average daily food consumption throughout the 28 day experiment. * = significant difference between OVX treated and age-matched controls.*

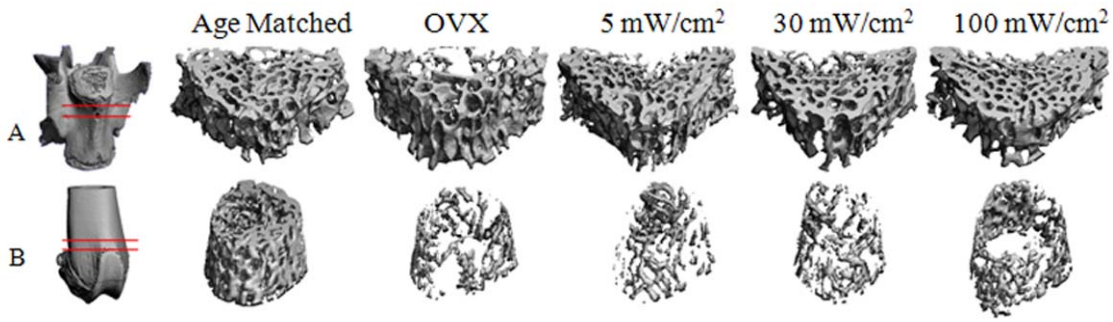

Figure 5.3: *Representative µCT images of cancellous bone in the L5 vertebra (A) and distal femoral metaphysis (B) for experimental and control groups.*

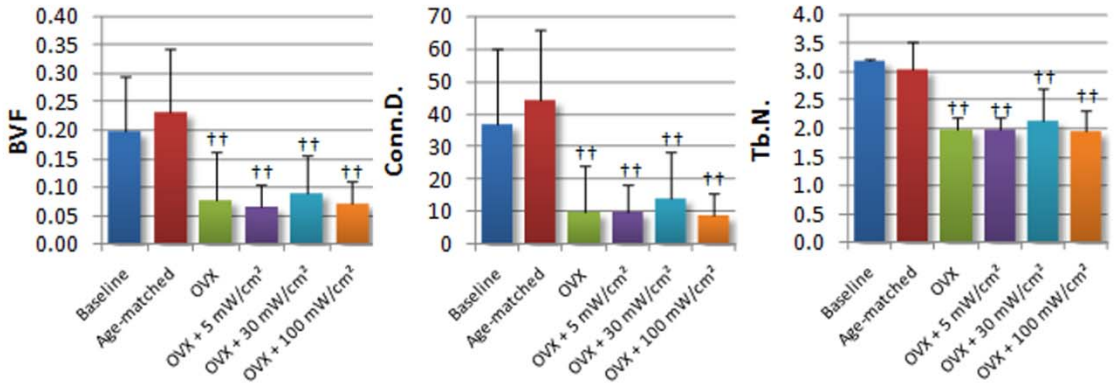

Figure 5.4: *Mean values of microstructural parameters at the femoral metaphysis for experimental and control groups. Values are reported as mean ± SD. (Note: † = p<0.05 vs. Age-matched Control, † † = p<0.001 vs. Age-matched Control)*

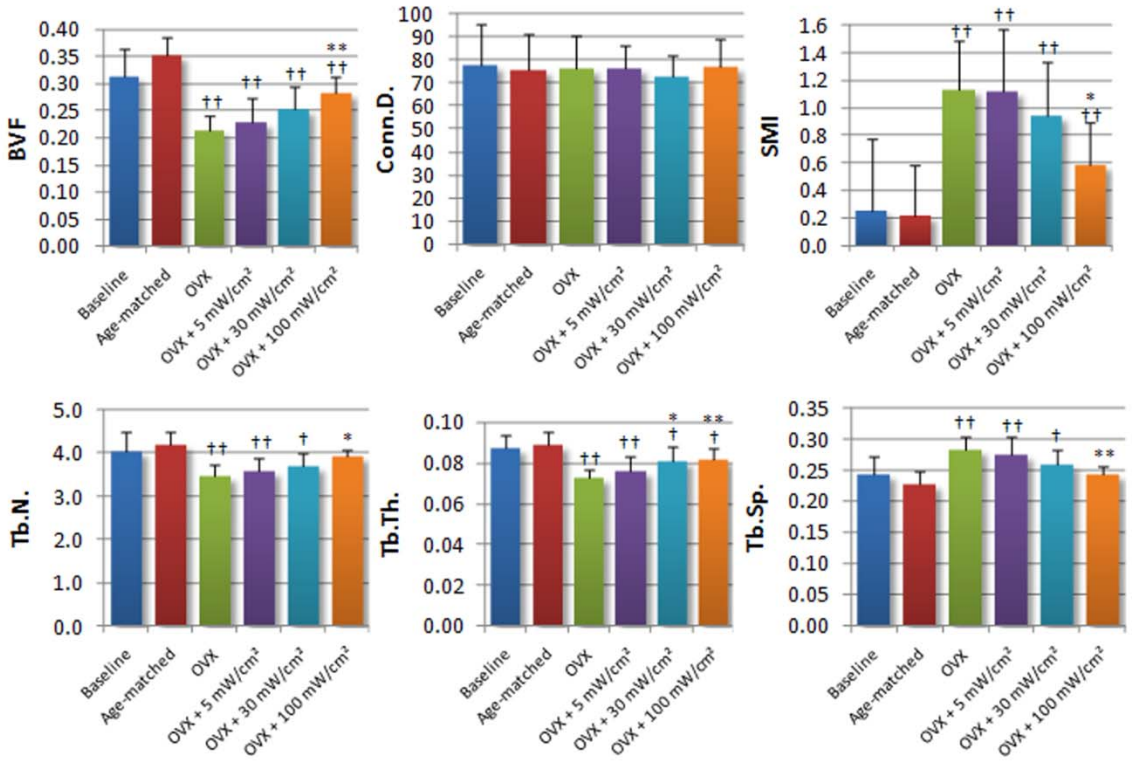

Figure 5.5: *Mean values of microstructural parameters for experimental and control groups. Values are reported as mean ± SD. (Note: † = p<0.05 vs. Age-matched Control, † † = p<0.001 vs. Age-matched Control * = p<0.05 vs. OVX Control, ** = p<0.002 vs. OVX Control .)*

	BVF	Conn.D	SMI	Tb.N.	Tb.Th.	Tb.Sp.
OVX vs. Age-matched	-40% **	1%	436% **	-17% **	-19% **	24% **
OVX + 5 mW/cm^2 vs. OVX	8%	-1%	-1%	3%	5%	-2%
OVX + 30 mW/cm^2 vs. OVX	19%	-4%	-17%	7%	11% *	-8%
OVX + 100 mW/cm^2 vs. OVX	33% **	1%	-48% *	12% *	13% **	-14% **
OVX + 5 mW/cm^2 vs. Age-matched	-35% **	1%	432% **	-15% **	-14% **	21% **
OVX + 30 mW/cm^2 vs. Age-matched	-28% **	-3%	347% **	-11% *	-10% *	15% *
OVX + 100 mW/cm^2 vs. Age-matched	-20% **	3%	177% **	-7%	-8% *	7%

Table 5.1: *Percent change in trabecular microstructure parameters for the superior third of the L5 vertebral body.*

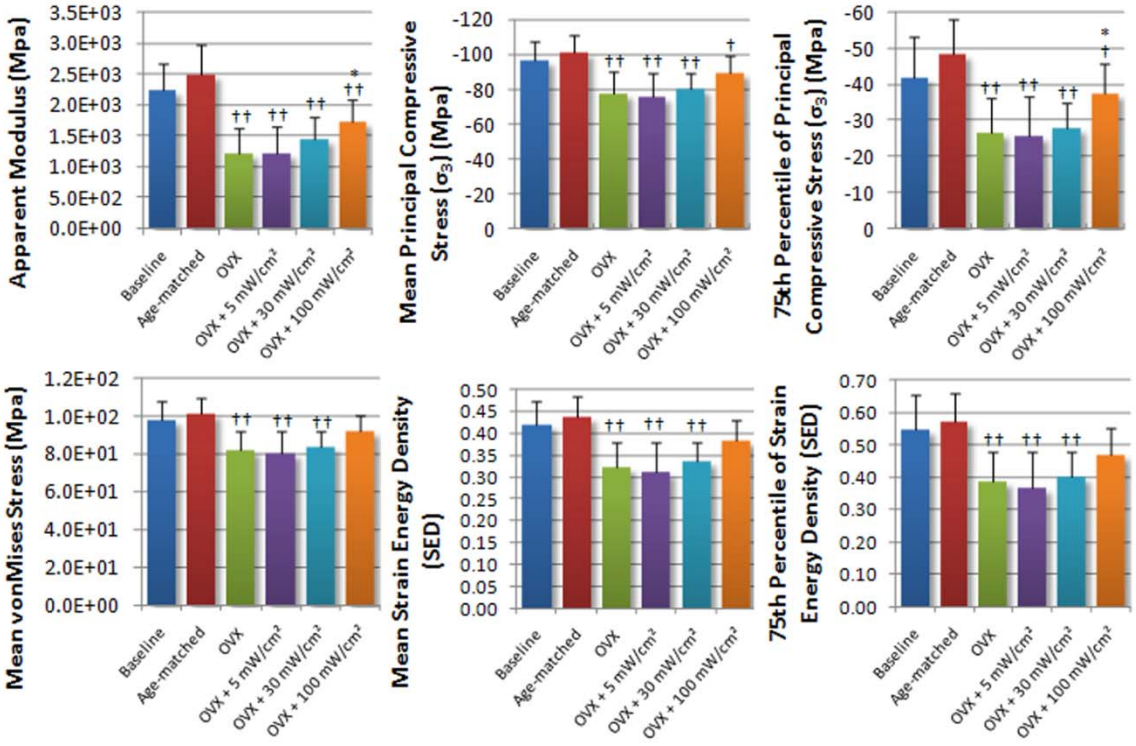

Figure 5.6: *Mean values of strength parameters for experimental and control groups. Values are reported as mean ± SD. (Note: † = p<0.05 vs. Age-matched Control, † † = p<0.001 vs. Age-matched Control * = p<0.05 vs. OVX Control, ** = p<0.002 vs. OVX Control .)*

	$E_{Apparent}$	$\overline{\sigma_{von\ Mises}}$	$\overline{\sigma_3}$	σ_3 75th %	$\overline{SED}$	SED75th %
OVX vs. Age-matched	-51% **	-19% **	-23% **	-45% **	-26% **	-32% **
OVX + 5 mW/cm^2 vs. OVX	-1%	-2%	-3%	-2%	-3%	-5%
OVX + 30 mW/cm^2 vs. OVX	18%	3%	3%	6%	4%	3%
OVX + 100 mW/cm^2 vs. OVX	42% *	13%	15%	41% *	18%	21%
OVX + 5 mW/cm^2 vs. Age-matched	-52% **	-21% **	-25% **	-46% **	-29% **	-36% **
OVX + 30 mW/cm^2 vs. Age-matched	-42% **	-18% **	-21% **	-42% **	-23% **	-30% **
OVX + 100 mW/cm^2 vs. Age-matched	-31% **	-9%	-11% *	-22% *	-13%	-18%

Table 5.2: *Percent change in trabecular mechanical strength parameters for the superior third of the L5 vertebral body.*

Chapter 6:

Quantification of Bone's Tissue Level Response to Low Frequency Pulsed Ultrasound: The Role of US Signal Intensity

6.1 Abstract

Low intensity pulsed ultrasound (LIPUS) has been shown to attenuate bone loss in an estrogen deficient model of osteopenia. This study tests the hypothesis that ultrasound mediated changes in bone remodeling alter bone's elastic and viscoelastic tissue level mechanical properties. Eighty-four, sixteen week old Sprague-Dawley rats were divided into six groups: baseline control, age-matched control, ovariectomy (OVX) OVX control, OVX + 5 mW/cm^2 ultrasound (US), OVX + 30 mW/cm^2 US and OVX + 100 mW/cm^2 US. Low intensity pulsed ultrasound (LIPUS) was delivered transdermally at the L4/L5 vertebrae, using gel-coupled plane wave US transducers. The signal, characterized by 200μs pulses of 1.5 MHz sine waves repeating at 1 kHz with intensities of 5, 30 or 100mW/cm^2, was applied 20 min/day, 5 days/week for 4 weeks. OVX treatment decreased Elastic Modulus (-19%) and Hardness (-16%) and increased loss tangent (tan δ) in trabecular bone compared to age-matched controls at 4 weeks post surgery. LIPUS treatment increased Elastic Modulus (21%, $p<0.05$) and Hardness (25%, $p<0.05$) for 100mW/cm^2 US treated groups in the trabecular region compared to OVX controls. In the posterior cortex LIPUS treatment increased Elastic Modulus (20%, $p<0.05$) and Hardness (28%, $p<0.05$) for 100mW/cm^2 US treated groups compared to OVX controls. In the anterior cortex there was no significant difference between US treated groups and OVX controls. Loss tangent, was significantly reduced in the posterior cortex for groups treated with 30mW/cm2 US signals (-12%, $p<0.001$) and 100mW/cm^2 US signals (-17%, $p<0.001$) and in the trabecular region for the group treated with 100mW/cm^2 US (-30%, $p<0.001$). In the trabecular region there were no significant differences in loss tangent between LIPUS treated groups and OVX controls.

Key Words: *Therapeutic Ultrasound, Bone Remodeling, Mechanotransduction, Low Intensity Ultrasound, Ovariectomy, Nanoindentation, Elastic Material Properties, Viscoelastic Material Properties*

6.2 Introduction

High frequency, low amplitude mechanical signals have been proven effective in mediating bone loss and improving mechanical strength in both human [150, 151] and animal models [152-154]. It has been shown that given a sufficiently high frequency signal (~20Hz), bone may be sensitive to mechanical strain signals as low as 20με [12]. Ultrasound, which behaves as an alternating pressure wave in bone, may offer an effective, non-invasive technology for delivery of anabolic signals.

In vitro studies have shown that LIPUS is capable of increasing osteoblast proliferation and stimulating endochondral ossification in excised tissues [31-34]. It has also been shown that ultrasound signal intensity plays an important role in modulating the response of osteoblasts in vitro [35, 36]. In vivo studies have also shown that LIPUS accelerated fracture healing in both animal [48, 49, 64, 107, 108] and human models [43, 44, 109, 110]. In addition, Yang et al, showed that bone's response to ultrasound during fracture healing was sensitive to ultrasound signal intensity [64]. Thus, it is likely that ultrasound may be an effective treatment in other cases of altered bone

remodeling. However, there is limited, conflicting evidence with respect to the effectiveness of LIPUS in treating in vivo, non-fracture related bone diseases [58, 61], particularly in conditions associated with chronic bone loss. It is also unclear what role ultrasound signal parameters such as signal intensity play in bone's response. In a previous study, we showed that ultrasound signals similar to those currently used in a clinical setting for fracture healing were effective in mediating decreases in bone volume and mechanical strength at the millimeter length-scale in response to estrogen deficient osteopenia [155]. Furthermore, these signals were shown to be site specific, modulating only changes to bone morphology at the targeted skeletal site.

Due to bone's inherent viscoelasticity and the dynamic nature of the applied ultrasound signals, it is particularly important to consider both elastic and viscous components of bone's adaptive response to applied loads. Recently, developments in nanomechanical testing hardware have enabled measurement of viscoelastic material properties at the nanometer length scale using a dynamic mechanical analysis (DMA) approach. DMA techniques have been widely used at the bulk tissue level [156] and recently have been adapted to measurements at the nanoscale for polymers [157] and bone tissue [158, 159].

In light of these findings, the goal of this study was to determine the role of therapeutic ultrasound signal intensity in modulating changes in bone's nanoscale elastic and viscoelastic material properties associated with estrogen deficient osteopenia. **We hypothesize that bone is sensitive to dynamic mechanical signals delivered via ultrasound and that bone's tissue level nano-scale material properties, particularly viscoelastic properties, are sensitive to ultrasound signal intensity.**

6.3 Methods

6.3.1 Experimental Design

Seventy-six, 16 week old Sprague-Dawley rats (307 ± 11g) were divided into six groups; baseline control(n=11), age-matched control(n=21), OVX control(n=20), OVX + 5 mW/cm^2 ultrasound stimulation(n=8) (US), OVX + 30 mW/cm^2 US(n=8) and OVX + 100 mW/cm^2 US(n=8). All surgical and therapeutic procedures were approved by Stony Brook University's Institutional Animal Care and Use Committee (IACUC).

6.3.2 Therapeutic Ultrasound Stimulation

Animals were anesthetized using isofluorane gas and therapeutic ultrasound was delivered transdermally at the L4/L5 vertebrae, using gel-coupled plane wave US transducers (Exogen, Inc.). The signal, characterized by 200μs pulses of 1.5 MHz sine waves repeating at 1 kHz with intensities of 5, 30 or 100mW/cm^2, was applied 20 min/day, 5 days/week for 4 weeks.

6.3.3 Sample Preparation

Following sacrifice via CO_2 asphyxiation, the L5 vertebra was removed, cleaned of soft tissue and stored at -40◦C. A 1.5mm thick slice was isolated from the L5 vertebra and dehydrated for 24 hours in 100% ethanol, embedded in an epoxy resin (EpoThin,

Buehler, Inc.) and allowed to cure under negative pressure in a vacuum chamber. Samples were then polished using abrasive papers and diamond particle suspensions ending in a final particle size of 0.05µm. Prior to nanomechanical testing, each sample was re-hydrated for 24 hours in physiologic solution (10x PBS). Three indents were placed in both the anterior and posterior cortices and four indents were evenly distributed throughout the trabecular region.

6.3.4 Nanoindentation

Nano-mechanical testing was performed using a triboscanner (Hysitron Inc., Minneapolis, MN) equipped with a nanoDMA module. A quasi-static indent was made at each location, followed by a dynamic indent, which was offset by a distance of three microns. Quasi-static indentation was performed using a loading/unloading rate of 50µN/s to a peak load of 200µN with a hold period of 10s. Bone's elastic material properties including Elastic Modulus (E) and Hardness (H) were then calculated from the unloading curve using the method of Oliver and Pharr [93]. Dynamic Mechanical Analysis (DMA) nanoindentation was performed by applying a quasi-static load of 200µN, followed by a 90s hold period. Then a 20µN sinusoidal load was superimposed onto the 200µN quasi-static load and frequency was ramped between 20 and 200Hz sampling at 40 equally distributed frequencies. Viscoelastic material properties including Storage (E') and Loss (E'') modulus and loss tangent (tan δ) were calculated using the method of Loubet et al. [133].

6.3.5 Data Analysis

All values are reported as mean ± standard deviation unless otherwise noted. One way ANOVA and Tukey's post-hoc tests were used to detect paired differences between groups for E, H, E', E'', tan δ and slope (m). Significance was defined at $p<0.05$ (*) and $p<0.001$ (**). Correlations were determined using multiple linear regressions and Pearson's product moment correlation coefficient. All statistical analyses were performed using SigmaStat v3.5 (Systat Software, Inc., San Jose, CA, USA).

6.4 Results

6.4.1 Elastic and viscoelastic material properties vary spatially in the lumbar vertebra

Indents made in the anterior and posterior cortices were placed at locations 25%, 50% and 75% of the cortical thickness. Neither Elastic Modulus, nor Hardness was found to be dependent on the relative position within the cortex.

Elastic Modulus did not depend of the position within the vertebral body. Similarly, Storage Modulus was not dependent on indent position. Conversely, Loss modulus was shown to be significantly higher in the trabecular region compared to indents made in the anterior and posterior cortices.

6.4.2 OVX alters bone's elastic and viscoelastic material properties

OVX treatment significantly decreased Elastic Modulus in the anterior cortex (-20%, $p<0.05$), posterior cortex (-25%, $p<0.05$) and trabecular regions (-19%, $p<0.05$)

compared to age-matched controls. Similarly, Hardness decreased in the anterior cortex (-19%, $p<0.05$), posterior cortex (-15%, $p<0.05$) and trabecular region (-16%, $p<0.05$).

Bone's 20Hz viscoelastic material properties were also altered after 28 days of estrogen deficiency. In the anterior cortex, Loss Modulus decreased (-10%, $p<0.05$), Storage Modulus decreased (-28%, $p<0.05$) and loss tangent was significantly increased (19%, $P<0.001$) compared to age-matched controls. In the posterior cortex, Loss Modulus decreased (-11%, $p<0.05$), Storage Modulus decreased (-34%, $p<0.05$) and loss tangent was significantly increased (28%, $P<0.001$) compared to age-matched controls. In the trabecular region, Loss Modulus decreased (-15%, $p<0.05$), Storage Modulus decreased (-27%, $p<0.05$) and loss tangent was significantly increased (16%, $P<0.001$) compared to age-matched controls.

6.4.3 Elastic and viscoelastic material properties are not altered by animal aging

There were no significant differences in Elastic Modulus at the anterior cortex between baseline and age-matched groups. Similarly no differences were found between baseline and age-matched groups in the posterior cortex or trabecular region.

6.4.4 Elastic material properties are enhanced with LIPUS intervention

In the anterior cortex, both Elastic Modulus ($r^2 = 0.72$) and Hardness ($r^2 = 0.74$) were linearly correlated with US signal intensity. However, there were no significant differences in Elastic Modulus or Hardness between OVX controls and the 5mW/cm^2 ($p>0.05$), 30mW/cm^2 ($p>0.05$), or 100mW/cm^2 ($p>0.05$) US treated groups. When compared to age-matched controls significant differences were only identified for the 5 mW/cm^2 US treated group.

In the posterior cortex, both Elastic Modulus ($r^2 = 0.88$) and Hardness ($r^2 = 0.75$) were linearly correlated with US signal intensity. Elastic Modulus was 20% ($p<0.05$) higher in the 100mW/cm^2 US treated group compared to OVX controls. Similarly, Hardness was 28% ($p<0.05$) higher in the 100mW/cm^2 US treated group compared to OVX controls. When compared to age-matched controls, Elastic Modulus and Hardness were significantly lower in the 5 mW/cm^2 US treated group.

In the trabecular region, both Elastic Modulus ($r^2 = 0.87$) and Hardness ($r^2 = 0.94$) were linearly correlated with US signal intensity. Elastic Modulus was 21% ($p<0.05$) higher in the 100mW/cm^2 US treated group compared to OVX controls. Similarly, Hardness was 25% ($p<0.05$) higher in the 100mW/cm^2 US treated group compared to OVX controls. Elastic Modulus and Hardness were significantly lower in the 5 mW/cm^2 US treated group compared to age matched controls.

Lastly, while Elastic Modulus and Hardness were found to be linearly correlated with signal intensity, no significant differences were identified between US treated groups for either Elastic Modulus or Hardness in the anterior, posterior or trabecular regions.

6.4.5 LIPUS intervention alters bone's viscoelastic material properties

Viscoelastic material properties were sampled at 40 equally distributed frequencies ranging from 20 to 200Hz. Here, we report bone's response at a superimposed dynamic load of 20 Hz. At the anterior cortex, Storage Modulus was correlated with signal intensity (r^2 = 0.93). There were no significant differences in Storage Modulus between groups treated with LIPUS and OVX controls. When compared to age-matched controls, the 5mW/cm^2 US treated group was 27% ($p<0.001$) lower; however, there were no significant differences between the 5mW/cm^2 and 100mW/cm^2 US treated groups. Loss Modulus was also correlated (r^2 = 0.8962) with US signal intensity. Compared to OVX controls, Loss Modulus was increased 16% ($p<0.001$), 15% ($p<0.001$) and 29% ($p<0.001$) higher in the 5, 30 and 100mW/cm^2 US treated groups. There were no significant differences in Loss Modulus between any of the experimental groups compared to age-matched controls. The loss tangent, which represents the ration between Loss Modulus and Storage Modulus, was weakly correlated with signal intensity (r^2 = 0.54). Loss tangent was significantly higher in the 5mW/cm^2 US treated group compared to both age-matched controls (15%, $p<0.001$) and OVX controls (37%, $p<0.001$).

At the posterior cortex, Storage Modulus was correlated with signal intensity (r^2 = 0.97). Storage Modulus was 61% ($p<0.001$) higher in the 100mW/cm^2 US treated group compared to OVX controls. Compared to age-matched controls, Storage Modulus was 28% ($p<0.001$) and 24% ($p<0.05$) lower in the 5mW/cm^2 and 30 mW/cm^2 US treated groups. Loss Modulus was weakly correlated (r^2 = 0.53) with US signal intensity. In addition, Loss Modulus was increased 10% ($p<0.001$) and 13% ($p<0.001$) in the 5 and 100mW/cm^2 US treated groups. There were no significant differences in Loss Modulus between any of the experimental groups compared to age-matched controls. The loss tangent was well correlated with signal intensity (r^2 = 0.98). Loss tangent was significantly lower in the 100mW/cm^2 US treated group compared to OVX controls (-30%, $p<0.001$). When compared to age-matched controls, loss tangent was significantly higher in the 5 and 30mW/cm2 US treated but no differences were identified between age-matched and the 100mW/cm2 US treated groups.

At the trabecular regions, Storage Modulus was correlated with signal intensity (r^2 = 0.76). Storage Modulus was 33% ($p<0.001$) and 44% ($p<0.001$) higher in the 30mW/cm^2 and 100mW/cm^2 US treated group compared to OVX controls. Compared to age-matched controls, Storage Modulus was 22% ($p<0.001$) lower in the 5mW/cm^2 US treated group. Loss Modulus was correlated (r^2 = 0.87) with US signal intensity. When Loss modulus was increased 17% ($p<0.001$) and 20% ($p<0.001$) in the 5 and 100mW/cm^2 US treated groups, there were no significant differences in Loss Modulus between any of the experimental groups compared to age-matched controls. The loss tangent was moderately correlated with signal intensity (r^2 = 0.6807). Loss tangent was significantly lower in the 30 and 100mW/cm^2 US treated groups compared to OVX controls (-12%, $p<0.001$ and -17%, $p<0.001$). When compared to age-matched controls, loss tangent was significantly higher in the 5mW/cm2 US treated group (22%, $p<0.001$) but no differences were identified between the age-matched and either the 30 or the 100mW/cm2 US treated groups.

6.4.6 Frequency sensitivity remains unaltered by changes in US signal intensity

We found increases in the slope of OVX treated groups compared to the age-matched controls at the anterior cortex (150%, $P<0.05$), posterior cortex (228%, $P<0.05$) and within the trabecular region (106%, $P<0.05$). When compared to OVX controls, groups treated with 100mW/cm^2 US had lower slopes in the anterior (-62% $p<0.05$), posterior (-66% $p<0.05$) and trabecular regions (-60% $p<0.05$).

6.5 Discussion

In this study, we considered bone's tissue level response to both statically and dynamically applied loads using quasi-static and dynamic nanoindentation approaches. It is thought that Elastic Modulus and Storage Modulus reflect the mechanical contribution of bone's mineral content while Loss Modulus reflects collagen and water content [81, 127-129]. Altered bone remodeling could affect local tissue composition by altering the degree and components of bone mineral. In addition, bone remodeling due to changes in sex steroid levels or dynamic mechanical stimuli could affect local porosity or the organization of mineral and collagen components [130]. We found that OVX groups experienced significant reductions in both Storage Modulus and Loss Modulus when compared to age-matched controls. US treatment significantly increased Elastic Modulus, Storage Modulus and Hardness in the posterior and trabecular regions. Loss Modulus was reduced with OVX and was moderately increased in all US treated groups, with good correlations to signal intensity at the anterior and trabecular regions.

We did not observe significant differences across the cortical thickness of the anterior and posterior cortices as was noted in previous studies [88]. This may be due to the fact that indents made at the endosteal and periosoteal regions were not positioned close enough to the rapidly remodeling surfaces. In addition, we did not find baseline significant differences in Elastic Modulus or Hardness between the anterior and posterior regions as was noted by Hengsberger et al. [130]. Several factors may contribute to this difference, including different material preparation techniques affecting tissue hydration levels and the maximum indentation load/contact depth to which the samples were tested.

In this study we noted significant changes in bone's tissue level elastic and viscoelastic material properties as a result of ovariectomy. It has been shown that during the first four weeks following OVX, rats experience a decrease in bone volume fraction (BVF) and compromised microstructural measures of bone quality [68-70]. These changes are likely the result of an imbalance in bone's remodeling processes, which could include increased bone resorption and decreased bone formation. We noted significant decreases in Elastic Modulus, Storage Modulus and Hardness, which could be the result of decreased local mineral quality. We also noted a decrease in Loss Modulus, indicating that the material was less capable of dissipating dynamically applied loads. This could suggest that bone was less organized, reducing the relative contribution of load-damping collagen.

There was a strong positive correlation between elastic modulus and signal intensity and a negative correlation between loss tangent and intensity. In both cases

groups treated with 100mW/cm^2 exhibited elastic and viscoelastic material behavior similar to the age-matched controls. Bone's static material properties are strongly influenced by mineralization levels [127], thus an increase in local elastic modulus and hardness could be an indication of altered bone remodeling in the presence of LIPUS.

We did not identify a significant improvement in elastic material properties at the anterior cortex compared to OVX controls. Although Elastic Modulus and Hardness were both correlated with signal intensity, the results were not significantly different when compared to age-matched controls. This may be the result of signal attenuation as the ultrasound wave propagates through the vertebra [122]. Thus, the ultrasound signal delivered to the anterior portion of the vertebral body could be lower in amplitude than ultrasound signals delivered to the posterior cortex and trabecular region.

Bone's tissue level viscous damping characteristics were also influenced by the introduction of a low intensity pulsed ultrasound. Loss tangent is a measure of the ratio of energy lost to energy stored [160] and describes the materials viscoelastic behavior. An increase in loss tangent may be an indication of improved resistance to fatigue and fracture, because energy would be dissipated through viscous damping and not by tissue yielding or the creation of new crack surfaces [161]. We found that while OVX groups had reduced elastic modulus compared to age-matched controls, they experienced an increase in loss tangent. This could suggest that bone microstructure is inherently optimized to resist fracture in the early stages of altered bone remodeling associated with aging and disease. However, this was not the case for sheep after three years of OVX. Les et al., found that at the whole bone level, sheep subjected to OVX had decreased loss tangent [162]. While there are marked differences between the two studies (including species, age, time of OVX, material property length scale), this could indicate that viscoelastic mechanical properties vary over the time course of OVX.

The increase in loss tangent with OVX and subsequent decrease with increasing US intensity may also be affected by local tissue porosity. In addition to collagen content, bone's viscoelastic material properties have been shown to be highly sensitive to hydration levels at the whole bone [163-165] and tissue levels [83, 135]. The formation of resorption cavities in OVX groups could result in increased tissue porosity and subsequently, increased hydration levels. As a result, bone would be more viscoelastic and have a higher loss tangent. LIPUS, however, has been shown to mediate overall loss of bone volume [126], possibly by minimizing the imbalance in resorption and modeling associated with OVX. The reduction in tissue level porosity would then decrease the hydration levels resulting in a less viscoelastic material and a lower loss tangent.

In a previous study we reported that application of the same non-invasive, transdermal ultrasound signal showed increased bone volume fraction and trabecular thickness with increased US signal intensity [155]. Together, these findings support the hypothesis that LIPUS plays a role in bone's remodeling processes. This may indicate that bone's viscoelastic damping characteristics play an important role in bone's adaptive response to both estrogen deficient osteopenia and therapeutic ultrasound intervention.

6.6 Limitations

Several limitations should be considered when interpreting the results of this study. First, our measurements of material properties were made in a direction orthogonal to that of the propagating ultrasound wave. Measurements were made in the axial direction to reflect bone's response in the predominant physiologic direction; however, this difference could result in measurements which do not fully capture bone's response to ultrasound signals. A second limitation involves our use of axial loading techniques to measure material properties in trabecular bone. Several studies have shown that bone's material properties vary with loading direction [140, 141], thus slight misalignments in sample orientation could alter results. Trabecular bone's inherent morphology makes it difficult to align indents to the local (Lagrangian) trabecular orientation. In our study we attempted to place indents at or near the intersection of several trabecular "rods", i.e. within trabecular "plates" in order to minimize these potentially confounding factors.

6.7 Conclusions

In conclusion, the results presented here support the hypothesis that low intensity ultrasound, acting as a mechanical wave in bone, alters bone's remodeling processes. These changes to modeling and remodeling affect bone's tissue level mechanical characteristics, possibly by changing the amount and organization of bone's mineral and organic components. The results of this study further emphasize inclusion of viscoelastic materials characterization in orthopaedic biomechanics research.

6.8 Figures and Tables

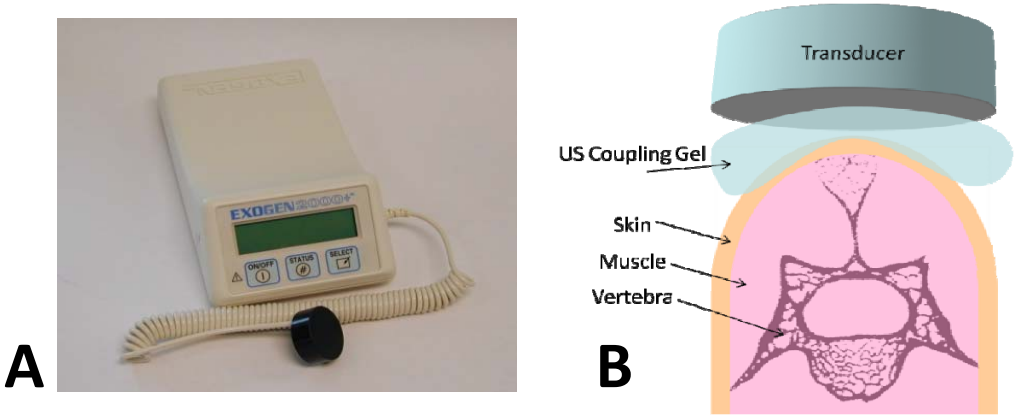

Figure 6.1: *(A) Ultrasound transducer (Piezo Technologies) and ultrasonic instrument delivered by Juvent Medical Inc. (B) Schematic depicting the path of US signal transmission by US coupling gel and through skin and soft tissue.*

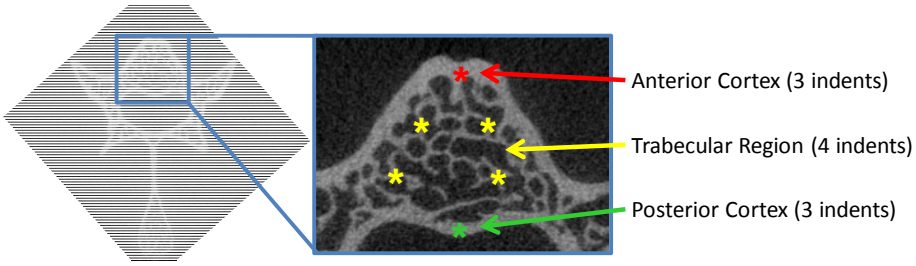

Figure 6.5: *Indentation was performed perpendicular to the transverse plane and therefore primarily reflects the material properties in the predominant physiologic direction. A total of 10 indents were made in each vertebral sample. Three indents were made across the thickness of the anterior cortex, placed at 25, 50 and 75% of the total thickness. Three indents were also made across the thickness of the posterior cortex and placed at 25, 50 and 75% of the total thickness. Four indents were made on individual trabeculae and distributed within each of the four quadrants. Whenever possible, Indents were placed near the intersection of trabecular structures and therefore are more likely to be axially oriented trabeculae.*

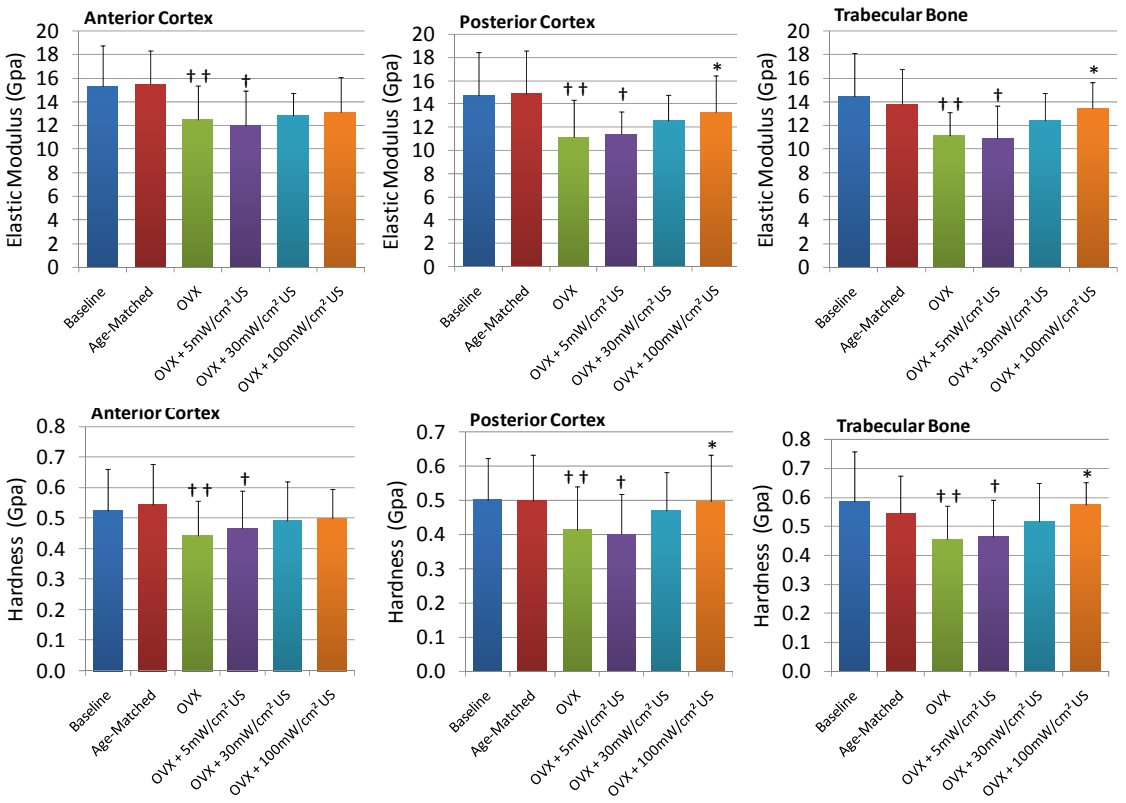

Figure 6.6: *Elastic Modulus and Hardness for the anterior cortex, posterior cortex and trabecular regions. († = p<0.05 vs. age-matched and *=p<0.05 vs. OVX)*

	Elastic Modulus (E)		
Elastic Modulus	Anterior	Posterior	Trabecular
OVX vs. Age-matched	-20% ††	-25% ††	-19% ††
OVX + 5 mW/cm^2 vs. OVX	-4%	3%	-2%
OVX + 30mW/cm^2 vs. OVX	3%	13%	12%
OVX + 100mW/cm^2 vs. OVX	8%	20% *	21% *
OVX + 5 mW/cm^2 vs. Age-matched	-22% †	-23% †	-21% †
OVX + 30mW/cm^2 vs. Age-matched	-17%	-15%	-10%
OVX + 100mW/cm^2 vs. Age-matched	-14%	-10%	-2%

Table 6.1: *Percent change in Elastic Modulus (E) for experimental and control groups. Values reflect changes between OVX and age-matched groups, between experimental groups and OVX controls and between experimental groups and age-matched controls. (Note: statistical significance is reported at p<0.05, p<0.01 and p<0.001.)*

	Hardness (H)		
Elastic Modulus	Anterior	Posterior	Trabecular
OVX vs. Age-matched	-19% ††	-15% ††	-16% ††
OVX + 5 mW/cm^2 vs. OVX	6%	-4%	2%
OVX + 30mW/cm^2 vs. OVX	11%	12%	13%
OVX + 100mW/cm^2 vs. OVX	19%	28% *	25% *
OVX + 5 mW/cm^2 vs. Age-matched	-14% †	-18% †	-15% †
OVX + 30mW/cm^2 vs. Age-matched	-10%	-4%	-5%
OVX + 100mW/cm^2 vs. Age-matched	-4%	9%	5%

Table 6.2: *Percent change in Hardness (H) for experimental and control groups. Values reflect changes between OVX and age-matched groups, between experimental groups and OVX controls and between experimental groups and age-matched controls. (Note: statistical significance is reported at p<0.05, p<0.01 and p<0.001.)*

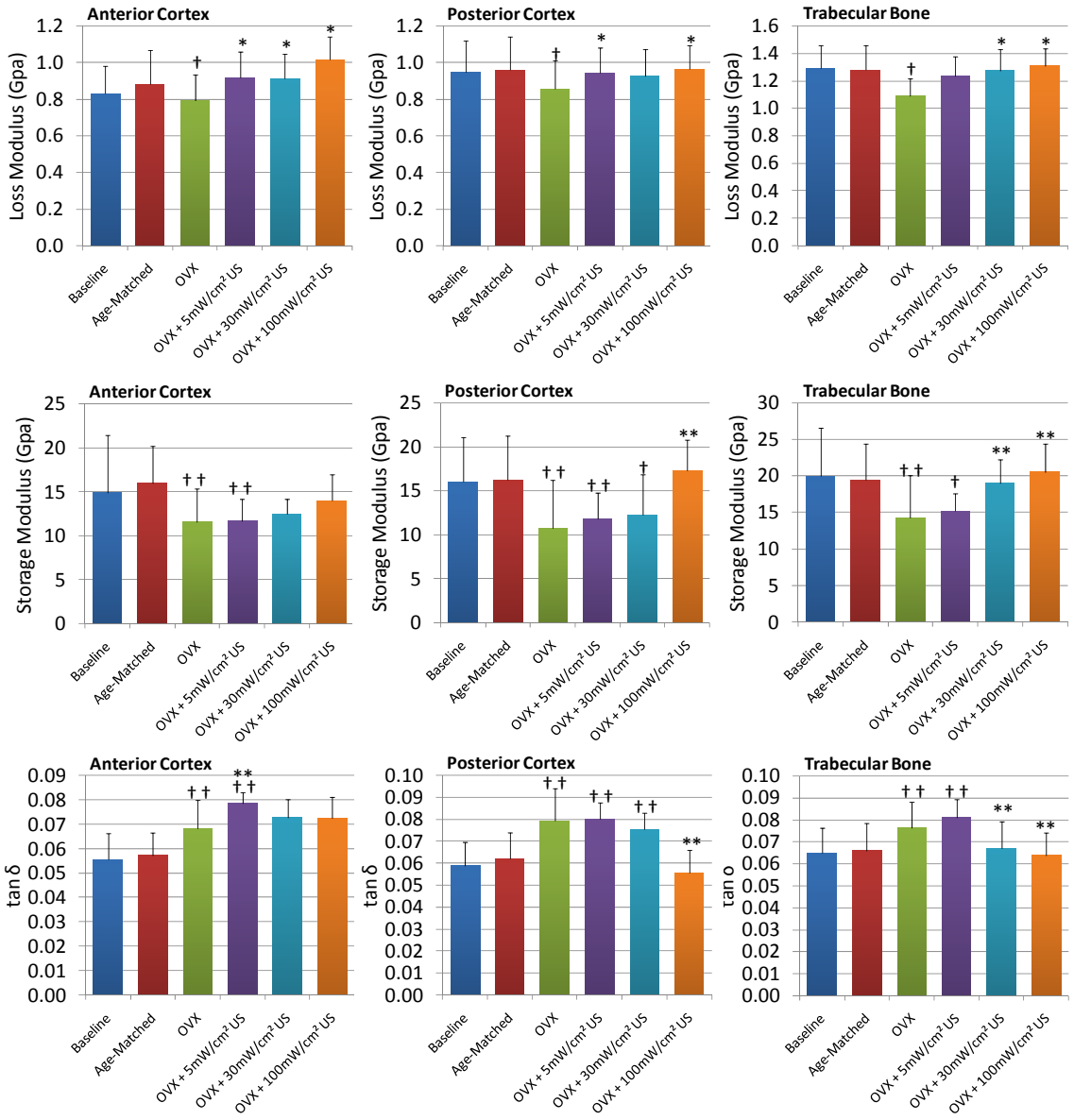

Figure 6.7: *Mean viscoelastic material properties under 20Hz dynamic loading. Loss Modulus (E''), Storage Modulus (E') and loss tangent (tan δ) are reported for indents in the anterior cortex, posterior cortex and trabecular regions. († = p<0.05 vs. age-matched and *=p<0.05 vs. OVX)*

Slope of tan δ (m)	Anterior	Posterior	Trabecular
OVX vs. Age-matched	150% †	228% †	106% †
OVX + 5 mW/cm^2 vs. OVX	-28%	-28%	-23%
OVX + 30mW/cm^2 vs. OVX	-30%	-29%	-32%
OVX + 100mW/cm^2 vs. OVX	-62% *	-66% *	-60% *
OVX + 5 mW/cm^2 vs. Age-matched	80% ††	135% ††	58% ††
OVX + 30mW/cm^2 vs. Age-matched	75%	132% ††	40% ††
OVX + 100mW/cm^2 vs. Age-matched	-5%	13%	-17%

Table 6.3: *Percent change in slope of tan δ curves. Changes are reported at the anterior cortex, posterior cortex and within the trabecular bone. (Note: statistical significance is reported at p<0.05, p<0.01 and p<0.001.)*

	Anterior		
	E''	E'	tan δ
OVX vs. Age-matched	-10% †	-28% ††	19% ††
OVX + 5 mW/cm^2 vs. OVX	16% *	1%	15% **
OVX + 30mW/cm^2 vs. OVX	15% *	8%	7%
OVX + 100mW/cm^2 vs. OVX	29% *	21%	6%
OVX + 5 mW/cm^2 vs. Age-matched	4%	-27% ††	37% ††
OVX + 30mW/cm^2 vs. Age-matched	3%	-22%	28%
OVX + 100mW/cm^2 vs. Age-matched	15%	-12%	27%

Table 6.4: *Percent change in Storage Modulus (E'), Loss Modulus (E'') and loss tangent (tan δ). Changes are reported at the anterior cortex. (Note: statistical significance is reported at p<0.05, p<0.01 and p<0.001.)*

	Posterior		
	E''	E'	tan δ
OVX vs. Age-matched	-11% †	-34% ††	27% ††
OVX + 5 mW/cm^2 vs. OVX	10% *	9%	1%
OVX + 30mW/cm^2 vs. OVX	8%	14%	-5%
OVX + 100mW/cm^2 vs. OVX	13% *	61% **	-30% **
OVX + 5 mW/cm^2 vs. Age-matched	-2%	-28%††	29% ††
OVX + 30mW/cm^2 vs. Age-matched	-4%	-24%†	21% ††
OVX + 100mW/cm^2 vs. Age-matched	0%	7%	-11%

Table 6.5: *Percent change in Storage Modulus (E'), Loss Modulus (E'') and loss tangent (tan δ). Changes are reported at the posterior cortex.. (Note: statistical significance is reported at p<0.05, p<0.01 and p<0.001.)*

	Trabecular		
	E''	E'	tan δ
OVX vs. Age-matched	-15% †	-27% ††	16% ††
OVX + 5 mW/cm^2 vs. OVX	13%	6%	5%
OVX + 30mW/cm^2 vs. OVX	17% *	33% **	-12% **
OVX + 100mW/cm^2 vs. OVX	20% *	44% **	-17% **
OVX + 5 mW/cm^2 vs. Age-matched	-4%	-22% †	22% ††
OVX + 30mW/cm^2 vs. Age-matched	0%	-2%	2%
OVX + 100mW/cm^2 vs. Age-matched	2%	6%	-4%

Table 6.6: *Percent change in Storage Modulus (E'), Loss Modulus (E'') and loss tangent (tan δ). Changes are reported in trabecular bone. (Note: statistical significance is reported at p<0.05, p<0.01 and p<0.001.)*

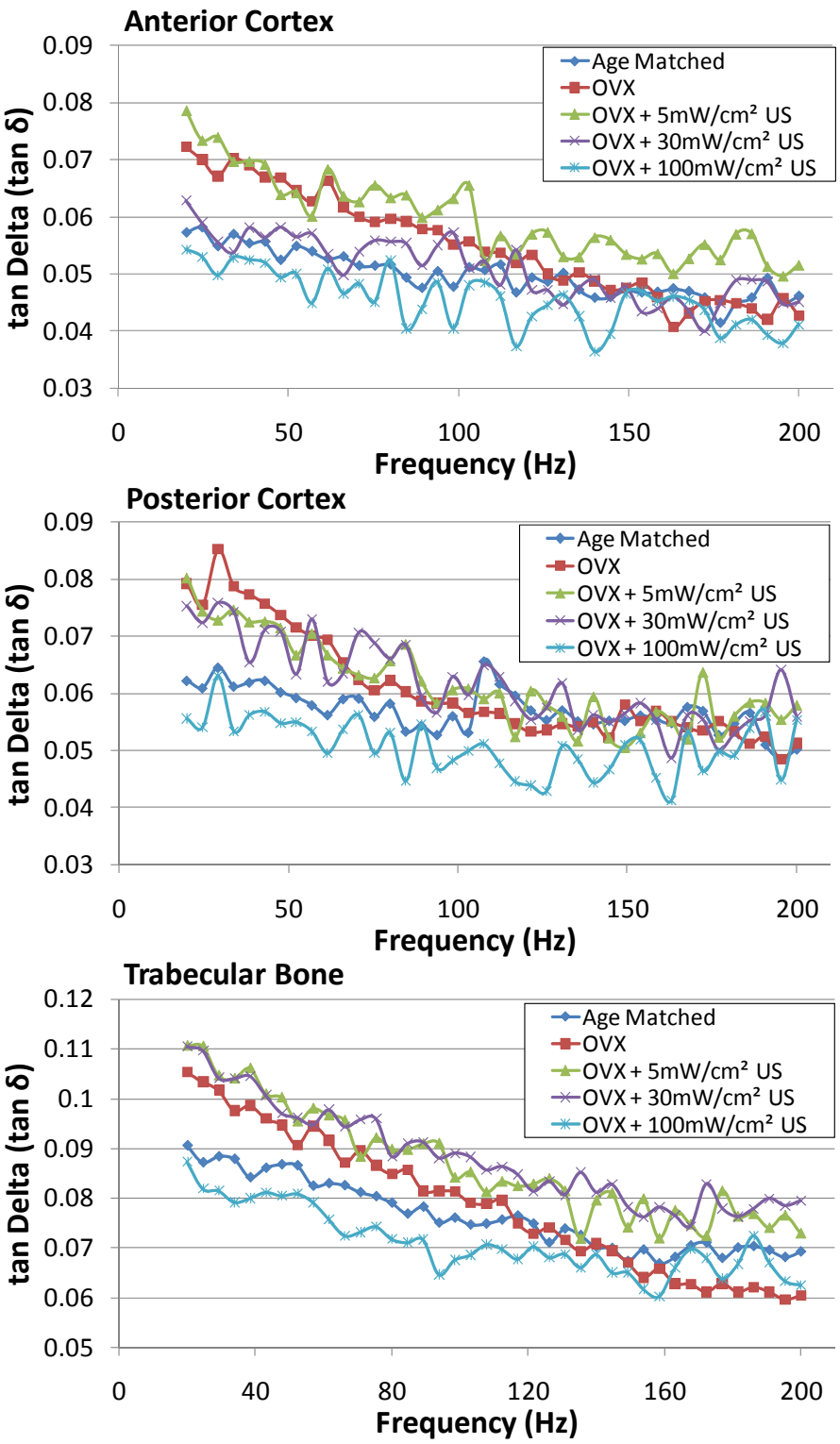

Figure 6.8: *Average tan δ values as a function of frequency for experimental and control groups. Each plot represents data from the anterior cortex, posterior cortex and trabecular regions.*

Chapter 7:

Experimental and computational approaches to ultrasound wave propagation in bone

7.1 Abstract

A critical issue related to the development of therapeutic ultrasound technology for use in a clinical setting is that of energy attenuation due to soft tissues (skin, fat, muscle, etc.) and bone. The principal objective of this study was to describe the spatial variation in ultrasound signals delivered to the vertebral body using input frequencies of 0.5 MHz and 1.5 MHz. We first experimentally measured US wave transmission into the anterior portion of the vertebral body using an ex-vivo rat model. Second, we used finite difference time domain (FDTD) models to simulate ultrasound wave propagation in a three-dimensional model using realistic bone geometries based on μCT images. Using experimental techniques and a 0.5MHZ transducer, we found that 30% of the ultrasound signal was transmitted through the skin and into anterior portion of the vertebral body. The results of our simulation experiments showed that a 0.5MHz signal could deliver 45% of the signal to the anterior region. A 1.5MHz signal however was capable of transmitting only 10% of the signal to this region. We also showed that signals delivered to bone tissue with 0.5MHz had less spatial variability at distances away from the source compared to 1.5MHz signals. These results may partially explain why we observed an anti-catabolic response in bone at both at low intensities (0.1mW/cm^2) with 0.5MHz and at high intensities (>30mW/cm^2) with 1.5MHz.

Key Words: *Therapeutic Ultrasound,* Finite Difference Time Domain (FDTD) Simulations, Ultrasound Signal Attenuation, L*ow Intensity Ultrasound,*

7.2 Introduction

One critical issue related to the development of therapeutic ultrasound technology for use in a clinical setting is that of energy attenuation due to soft tissues (skin, fat, muscle, etc.) and bone [166, 167]. As ultrasound propagates through soft tissue and bone, a portion of the signal is reflected at the bone surface. As a result, the signal delivered to the targeted skeletal site may be quite different from that of the source. It has been shown that ultrasound signal attenuation scales linearly with signal frequency [168-170]. In addition, Warden et al., showed that in long bones, up to 40% of the ultrasound signal is reflected at the bone surface and of the remaining energy, 80% is attenuated within the first millimeter of propagation [171]. Several confounding factors could affect our estimation of signal attenuation in bony structures including frequency, tissue composition, signal intensity and surface geometry. Given the nonlinear geometry, in particular the nonlinear shape of the cortical shell, of the rat lumbar spine, it is extremely difficult to predict attenuation within various structures using analytic models.

A number of computational models have been applied to simulate ultrasound wave propagation in bone. Biot theory simulates acoustic wave propagation in a porous medium [172, 173] and has been used to study the interactions between ultrasound and bone [174, 175]. Finite difference time domain approaches (FDTD) have also been used to study ultrasound wave propagation in trabecular bone using realistic bone architectures imaged using μCT [176-180]. Recently, commercially available FDTD

software (Wave3000®, Cyberlogic, Inc.) has been used to simulate ultrasound wave propagation in three-dimensional systems [179]. The use of FDTD techniques with high resolution imaging modalities such as μCT could prove to be a powerful tool in understanding how changes in bone geometry due to aging, disease and treatment interact with ultrasound waves and in the development of targeted new treatments.

The principal objective of this study was to describe the spatial variation in ultrasound signals delivered to the vertebral body using input frequencies of 0.5MHz and 1.5MHz. **We hypothesized that the interaction between ultrasound and the highly nonlinear geometry of the lumbar vertebra would result in inhomogeneous attenuation and distribution of the ultrasound signal which are sensitive to ultrasound frequency**. This aim was addressed in two experiments. First, we experimentally measured US wave transmission into the anterior portion of the vertebral body using an ex-vivo rat model. Second, we used FDTD models to simulate ultrasound wave propagation in a three-dimensional model using realistic bone geometries based on μCT images.

7.3 Methods

7.3.1 Experiment #1: Experimental measurement of ultrasound signal attenuation

Three female Sprague Dawley rats (310g ± 7) were obtained from the department of laboratory animal research (DLAR) at Stony Brook University and sacrificed via CO_2 asphyxiation. A 0.5MHz ultrasound transducer was placed on the skin over the posterior aspect of the lumbar vertebra. A small hole (d = ~1.5mm) was drilled into the anterior portion of the vertebral body and a small amount of trabecular bone was removed from the intracortical space. A membrane hydrophone was then placed within the intracortical space and acoustic shielding foam was placed around the hole to minimize the effects of wave transmission around the vertebral body. The entire system was then submerged in a vacuumed water bath. A single ultrasound pulse waveform with a center frequency of 0.5MHz was then delivered to the system. The transmitted signal was then measured using a membrane hydrophone. We then calculated the percent of peak-to-peak signal amplitude transmitted through the tissue and received at the hydrophone.

7.3.2 Experiment #2: Simulation of US wave propagation

MicroCT imaging

An L5 lumbar vertebra from a 140 day old Sprague Dawley rat was removed and scanned using μCT at 32μm resolution. The 3D scanned image was then segmented and re-sampled to an isotropic image resolution of 96μm. The 3D image data was then used to generate a realistic geometry in Matlab® (MATLAB, The Math Works, Inc.) for simulating acoustic wave propagation in the lumbar vertebra.

Acoustic wave modeling

Simulation of acoustic wave propagation in the time domain was then performed using a commercially available finite difference time domain (FDTD) solver

(Wave3000®, Cyberlogic, Inc.). The software calculates a solution to the three-dimensional wave equation using finite difference techniques.

$$\rho \frac{\partial^2 w}{\partial^2 t} = \left[\mu + \eta \frac{\partial}{\partial t} \right] \nabla^2 w + \left[\lambda + \mu + \varphi \frac{\partial}{\partial t} + \frac{\eta}{3} \frac{\partial}{\partial t} \right] \nabla (\nabla \bullet w)$$

Here, ρ is the material density [kg/m^3], λ and μ are the first and second Lame constants [N/m^2], η and ϕ are the shear and bulk viscosities [N-s/m^2], t is time (s) and w is a three-dimensional vector describing displacement. In addition, ∇ is the gradient operator, ∇● is the divergence operator and ∂ is the partial difference operator.

The vertebral body was simulated within a 15mm x 15mm x 15mm volume of water at 25◦C. Material properties were defined using values available in the pre-defined software library and listed in Table 7.1. Infinite boundary conditions were placed on all six sides of the model and a plane wave ultrasonic source was placed on the posterior side of the vertebra and configured to produce 10μs bursts of either 1.5 MHz or 0.5MHz sine waves. The simulated source transducer is sufficiently large relative to the size of the vertebra to deliver a signal which approximated that of the in vivo conditions described in chapters 3 thru 6. Several receivers were then placed throughout the model and waveforms for the longitudinal waves were collected at each increment in the simulation. The receiver positions are shown in Figure 7.1 and in each case were placed within a region occupied by bone. We then calculated the percentage of signal lost as the wave propagated through the system (Table 7.1). A grayscale mapping of the ultrasound wave was recorded throughout the simulation and periodic snapshots at three transverse planes and one sagittal plane are shown in Figure 7.3.

	Cortical Bone	***Water***
Density (kg/m^3)	1850	1000
Velocity (m/s)	2900	1497
λ (MPa) First Lamé constant	9306	2241
μ (MPa) Second Lamé constant	3127	0
α (dB/cm) Attenuation coefficient	2.03	6.82 x 10^{-4}

Table 7.1: *Material property definitions for components used in computational ultrasound simulation.*

7.4 Results

7.4.1 Experimental measurement of ultrasound signal attenuation

The results of our experimental study showed that 30% (± 11%) of the ultrasound signal penetrated the intracortical vertebral space and was received by the membrane hydrophone.

7.4.2 Simulation of US Wave Propagation

The transmitted ultrasound signals were recorded at five key locations throughout the vertebral body, which are shown graphically in Figure 7.2. The amplitudes reported in Figures 7.4 and 7.5 are normalized to an ultrasound input signal with peak-to-peak amplitude of two. Thus, a detected peak-to-peak response of one would indicate that 50% of the delivered signal amplitude was lost due to reflection and attenuation.

7.4.2.1 Lower ultrasound intensity improves signal penetration

The maximum peak-to-peak signal was recorded at five key locations for stimulation at 0.5 MHz and 1.5MHz. In each case, ultrasound pulse duration was delivered for 3μs. Peak-to-peak amplitudes were consistently larger for the 0.5 MHz signal compared to the 1.5 MHz signal. We found that for 0.5MHz signals, the percent of signal penetration was between 45 and 69% of the original amplitude. With 1.5MHz the percent of signal penetration was reduced to between 10 and 42% of the original amplitude. Percent differences in peak-to-peak amplitude are shown in Table 2.

7.4.2.2 Ultrasound signal amplitude varies spatially

For ultrasound stimulation at 0.5 MHz, peak-to-peak amplitude was larger in the posterior process compared to the more anterior measurement locations. For ultrasound simulation at 1.5 MHz, peak-to-peak amplitude was highest in the posterior process and decreased with increasing distance away from the source transducer. In particular, there was 57% reduction in signal amplitude between positions C and E with the 1.5MHz signal, but only a 17% reduction between the same positions with 0.5MHz.

	A	***B***	***C***	***D***	***E***
0.5 MHz	69%	47%	54%	59%	45%
1.5 MHz	42%	28%	23%	13%	10%

Table 7.2: *The percent of maximum peak-to-peak ultrasound signal amplitude transmitted to each of the receiver locations specified in Figure 7.2. Values are also reported for the percent difference in peak-to-peak amplitude for 0.5 MHZ compared to 1.5 MHz.*

7.5 Discussion

The results of our experimental study showed that 30% of ultrasound signal amplitude was transmitted to the intracortical space. This suggests that it may be possible for a portion of the applied ultrasound energy to penetrate into the intra cortical space, delivering a dynamic mechanical signal. In previous chapters, we investigated the response of trabecular bone in this region to various applied ultrasound signals. The results of this ex vivo study support the hypothesis that ultrasound can deliver anti-catabolic signals to the trabecular region of the vertebral body.

Computational approaches offer a powerful tool, enabling a better understanding of the underlying physics of ultrasound wave propagation in biological systems. The highly nonlinear geometry and inhomogeneous composition of the system

make it difficult to predict ultrasound behavior using analytic techniques. Thus, computational approaches allow for the use of image based models to better understand the spatial and temporal distribution of applied ultrasound signals. Subsequently, this data can be used to better understand the relationship between bone's response and the locally transmitted ultrasound signals.

The findings presented in this study, show that ultrasound frequency affects both the magnitude and spatial distribution of transmitted signals. We found that given similar input signal amplitudes, 0.5MHz signals were capable of delivering 78% greater signal amplitude compared to 1.5MHz US signals. This is likely the result of an increased signal wavelength which could improve signal penetration. We also found that there was greater spatial variability in transmitted signal amplitudes at 1.5 MHz. For example, signal amplitude decreased between the posterior process and the anterior cortex 32% at 1.5MHZ, but only 24% for 0.5 MHz. As a result, in vivo studies using these two frequencies could expect to see greater spatial variability in bone's response.

Our findings support those of Nagatani et al., which found that for a 1MHz signal, up to 90% of signal amplitude was attenuated within the first 10mm of bovine cancellous bone [181]. Similar to our study, these results were obtained using a FDTD approach and were supported by experimental techniques [181].

7.6 Limitations

There are several limitations which should be considered in the interpretation of data presented in this chapter. In the first study, we measured ultrasound signal attenuation due to bone and soft tissue in the rat lumbar spine. While extreme care was taken in the preparation of these specimens, we recognize that removing a small portion of the anterior cortex undoubtedly alters the ultrasound transmission characteristics and therefore the measured response. Future studies could limit these factors by using a needle hydrophone, which has a smaller tip diameter and would, therefore, require a less invasive measurement.

There are several limitations associated with the implementation of the computational models. In this study, the intra-trabecular spaces and the volume surrounding the vertebra were assumed to be composed of water. In vivo, however, these regions are composed of marrow, fat, muscle, skin and other tissues. Compared to water, fat has lower density (100kg/m^3 vs. 937 kg/m^3) and velocity (1497 m/s vs. 1479 m/s). As a result, the distribution and magnitude of the transmitted ultrasound signal could be altered. In future studies, these tissues may be more accurately described with tissue-specific material properties. In addition, recent advances in μCT technology have shown that this imaging approach can provide three-dimensional volume information describing soft tissues including muscle and fat [182]. The image resolution used to describe bone geometry could also be a potential source of inaccuracy. In this study, our three-dimensional model was created at an isotropic resolution of 96μm. This number was chosen to satisfy a computational requirement which requires that the maximum image resolution should not exceed 10% of the smallest potential wavelength for the system [180]. In this case, the wavelength in water is 0.998mm; therefore, the maximum resolution is 99.8μm. Given the dimensions

of the lumbar vertebra in the rat, the use of image resolutions below 96μm would incur large computational costs requiring system memory exceeding 10GB and simulation times on the order of days. Future studies, which investigate the interactions between ultrasound and altered bone remodeling, will require higher resolutions in order to accurately capture the changes to bone morphology.

7.7 Conclusions

In conclusion, we showed that there is evidence to suggest that ultrasound signals with frequencies on the order of 0.5MHz and 1.5MHz are capable of penetrating the soft and bony tissues in the lumbar spine of the rat. Thus, verifying the transdermal ultrasound delivery of dynamic mechanical signals in the rat animal model.

7.6 Figures and Tables

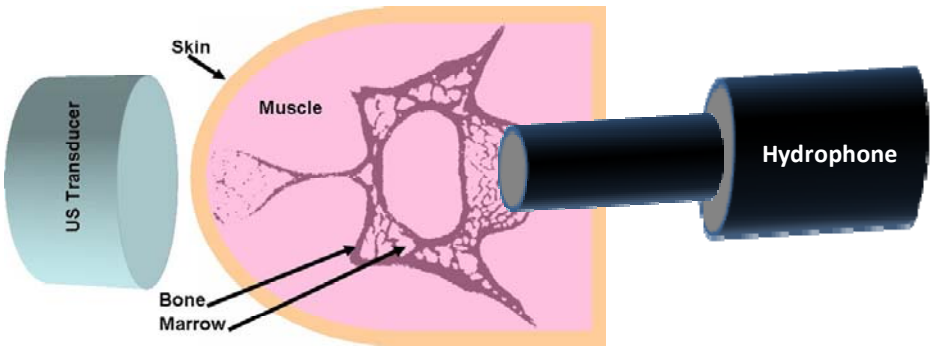

Figure 7.1: *Schematic of the experimental setup used in Experiment #1. An Ultrasound transducer was placed posteriorly and a sinusoidal 0.5 MHz US pulse was delivered to the system. The transmitted signal was then measured using a membrane hydrophone, which was placed inside the intracortical space of the vertebral body.*

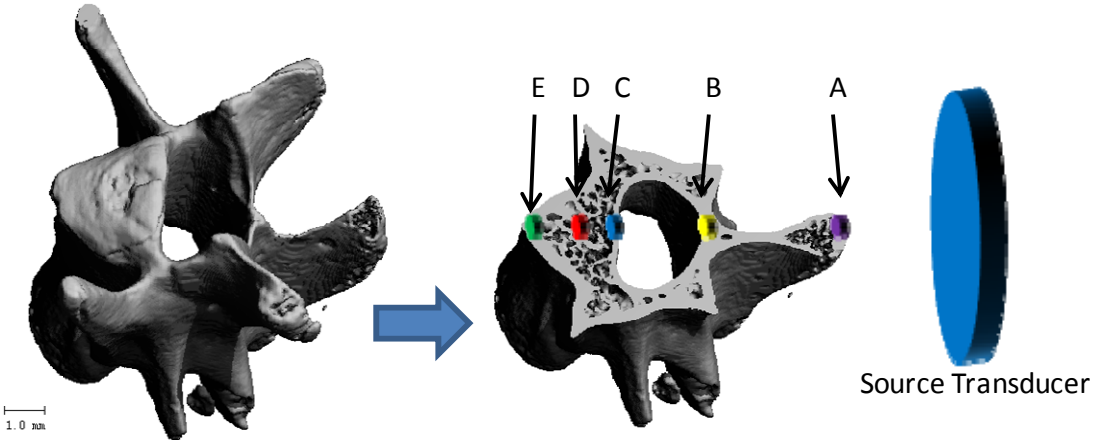

Figure 7.2: *(Left) A µCT rendering of the L5 vertebral body used in ultrasound simulations. (Right) An ultrasound signal is delivered posteriorly from the source transducer and the resulting signal is then measured at key sites away from the input signal. Each of the measurements was made on a single axial slice at the midpoint of the vertebral body. The sites are shown in the figure and labeled A thru E.*

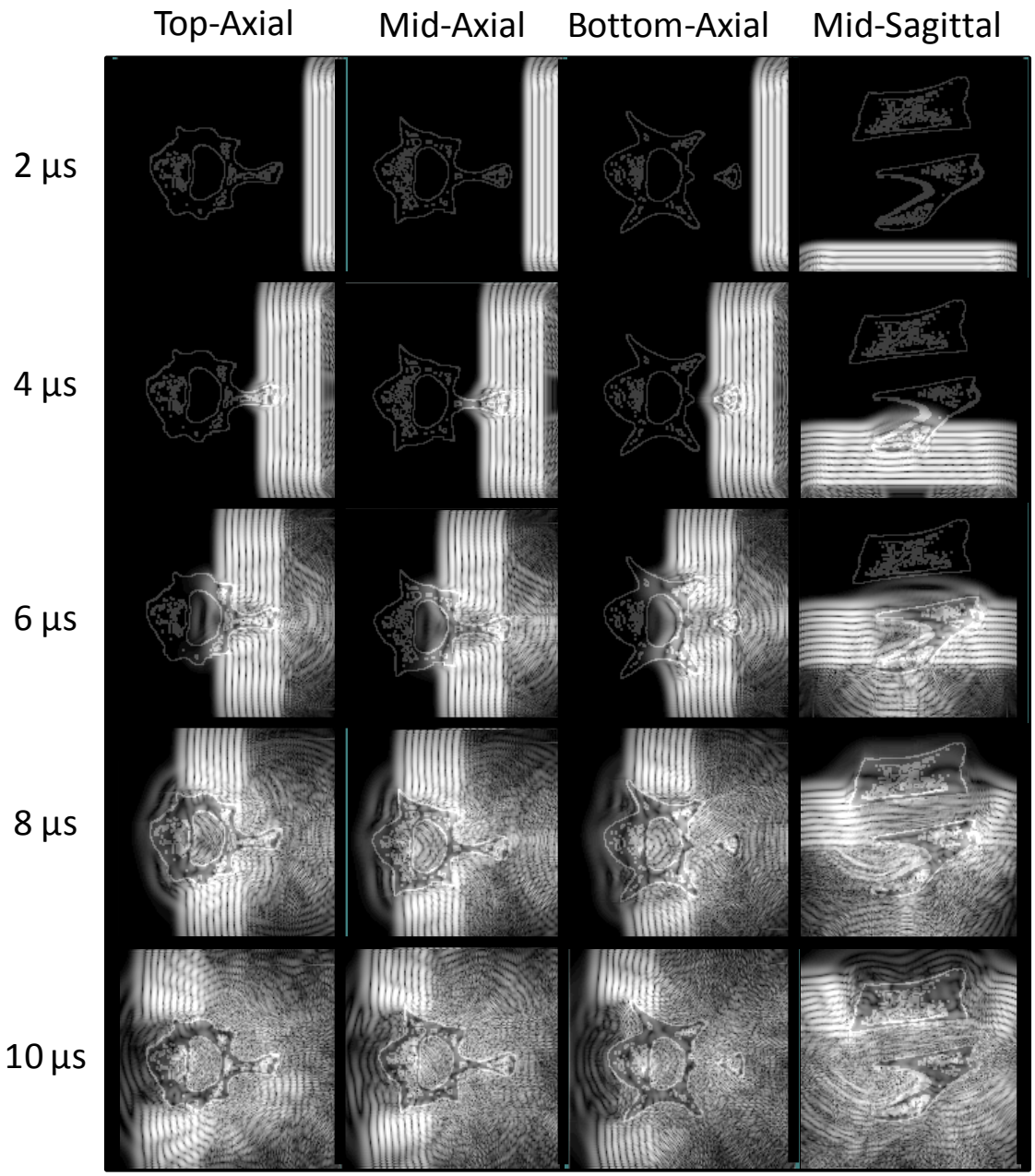

Figure 7.3: *Ultrasound signal amplitude distribution throughout 10µs of the simulation. Each column represents a slice through the bone-water system. The first three columns represent an axial slice through the top, middle and bottom portions of the vertebral body. The last column represents a sagittal slice taken at the midpoint of the vertebral body.*

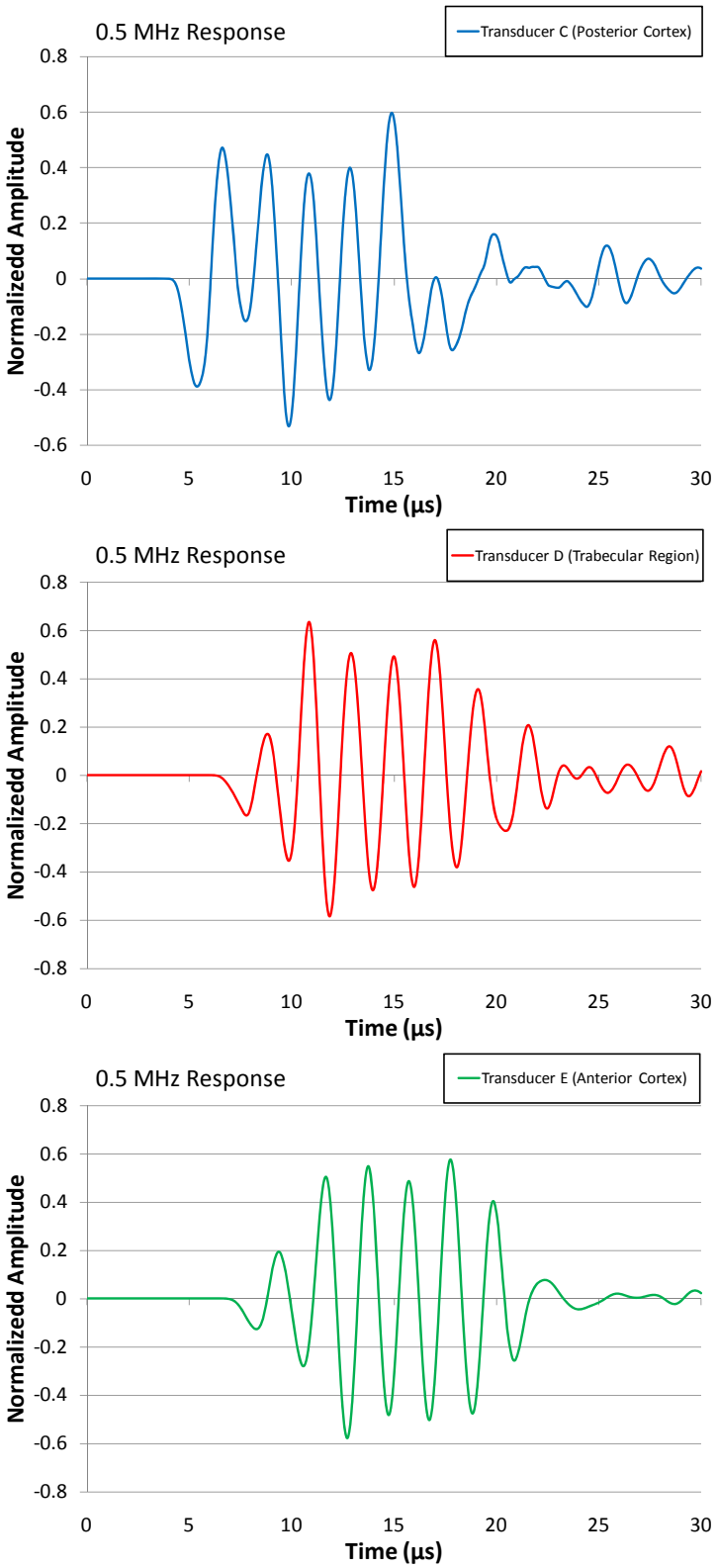

Figure 7.4: *Normalized ultrasound signal response to stimulation at 0.5MHz. The local response is plotted at the posterior cortex (Blue), Trabecular Region (Red) and in the anterior cortex (E). The amplitude values are normalized to the input amplitude.*

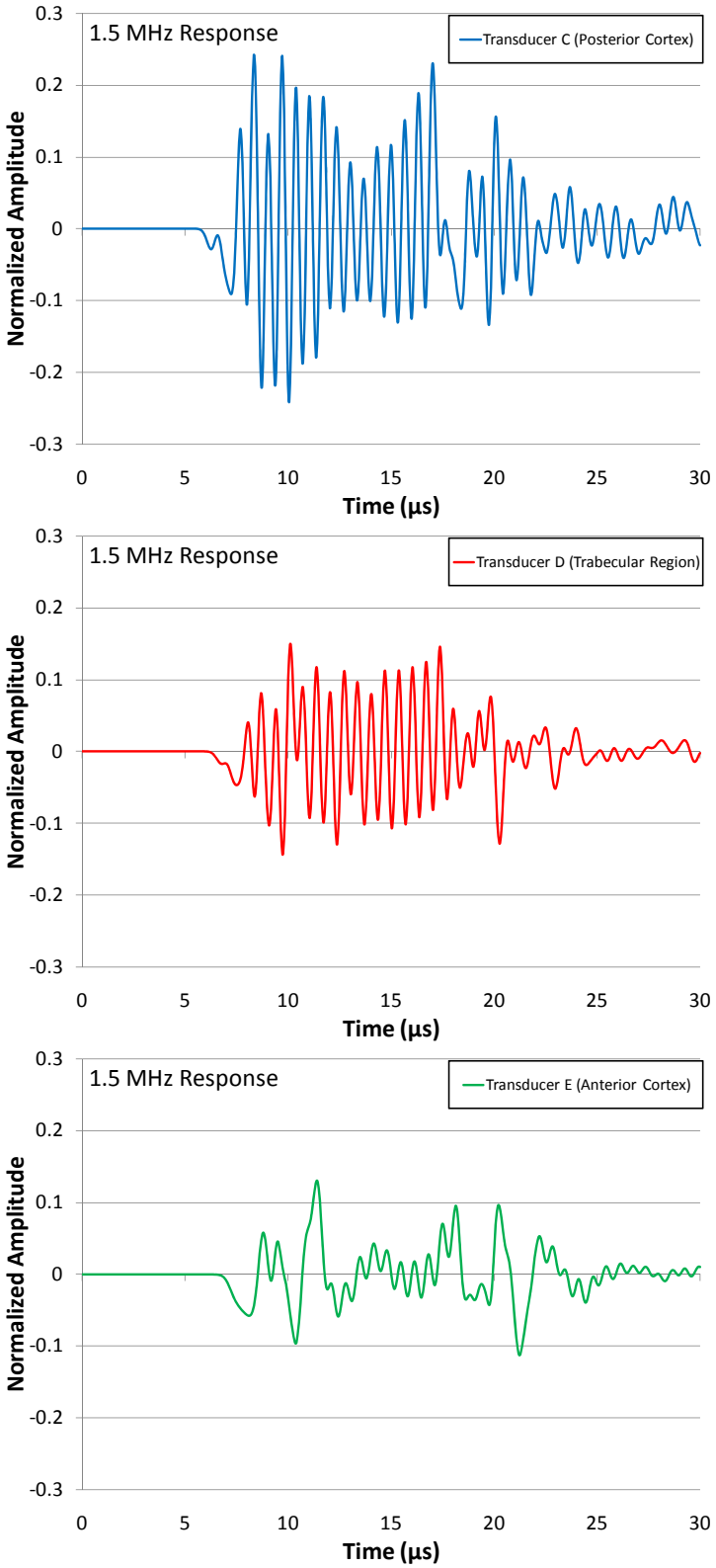

Figure 7.5: *Normalized ultrasound signal response to stimulation at 1.5MHz. The local response is plotted at the posterior cortex (Blue), Trabecular Region (Red) and in the anterior cortex (E). The amplitude values are normalized to the input amplitude.*

Chapter 8: Global Summary & Conclusions

The results from **Chapter III** show that dynamic mechanical signals delivered using low intensity (≤ 30mW/cm^2 I_{SATA}, 0.5MHz) ultrasound are capable of mediating changes to bone morphology and mechanical properties associated with estrogen deficient osteopenia. The decrease in bone volume fraction (BVF) resulting from ovariectomy (OVX) was reduced by half, from 40% to 19% in the group treated with 800μs pulse durations. Ultrasound intervention resulted in improved bone quality when compared to untreated and OVX controls. For some parameters, there was no significant difference compared to age-matched counterparts. Additionally, there were no significant differences in the response between each of the ultrasound treated groups. This suggests that ultrasound pulse duration plays a minor role in regulating bone's adaptive responses.

In **Chapter IV**, we show that low intensity (0.5MHz) ultrasound increases tissue level viscoelasticity, but has no effect on elastic mechanical properties. One explanation for this finding is that the reduced Elastic Modulus could be an indication of locally undermineralized tissue. Under dynamically applied loads, collagen content could play a more dominant role in bone's response to loading, resulting in increased tissue viscoelasticity. A second explanation is that low intensity pulsed ultrasound (LIPUS) could alter bone remodeling, contributing to an imbalance which may result in a net increase in tissue level micro-porosities. When filled with fluid, these micro-porosities could increase damping and tissue level viscoelasticity.

In **Chapter V** we address the role of ultrasound signal intensity on mediation of bone loss associated with estrogen deficient osteopenia. We show that bone's response is well correlated with signal intensity and, measures of bone morphology and mechanical competence were significantly improved over OVX controls in the 30mW/cm^2 and 100mW/cm^2 US signal groups. We also noted significant improvements in bone's response to 100mW/cm^2 US signals over that of the 5mW/cm^2 US signals, suggesting that signal intensity plays an important role in regulating bone's response. Finally, we determined that ultrasound signals delivered at the lumbar spine have no effect on bone's response in the distal femur. This suggests that the ultrasound signal is site specific, and does not cause a systemic osteogenic response.

In **Chapter VI**, we address the effects of ultrasound signal intensity on bone's tissue level mechanical properties. We found that bone's response was well correlated to ultrasound signal intensity resulting in increased Elastic Modulus and decreased loss tangent. We also noted spatial differences in bone's elastic material properties. Elastic Modulus was significantly increased over OVX controls in the posterior and trabecular regions, but not in the anterior region. While we found no significant differences in Elastic Modulus between regions, this trend suggests that signal attenuation in 1.5MHz plays a role in the transmission of energy in the vertebral body.

In **Chapter VII,** we used experimental and computational models to investigate the effects of ultrasound wave propagation in the lumbar vertebra. The results of our experimental study suggest that transdermal application of ultrasound is capable of delivering 30% of the applied ultrasound signal to the anterior portion of the vertebral body. Using computational models, we showed that the interaction between

ultrasound waves and the highly nonlinear geometry of the vertebral body resulted in large amounts if signal attenuation, particularly with 1.5MHz frequencies.

How do our findings relate to in vivo performance?

Low intensity ultrasound therapy is a promising new technology which could prove to be a potent prophylaxis treatment for osteopenia. The data presented in this dissertation suggests that LIPUS can affect measures of bone quality at both the whole bone and tissue levels. It is important to recognize that if similar results were found in a human model, these enhancements could have a significant impact on mechanical performance in vivo, resistance to fracture and overall bone quality. Finite element [183-186] and nanoindentation [187] studies have emphasized the sensitivity of bulk mechanical response to tissue level material properties. The 20% improvements we observed in tissue level modulus with LIPUS treatment could suggest a comparable increase in bulk modulus [186]. Conversely, for cases where we did not observe an improvement in tissue level modulus, as we saw in Chapter IV with the 0.5MHz signal, improvements in bone morphology with 0.5MHz (Chapter III) would only partially restore bone's structural integrity at the whole bone level.

In Chapters III and V, we looked at how changes to trabecular morphology affect the magnitude and distribution of mechanical loads. These studies isolated the effects of altered bone morphology by assuming that bone's tissue level material properties remained unchanged by OVX or ultrasound intervention. We showed that ultrasound treatment could significantly improve BVF 33% ($P<0.001$), Tb.Th. 13% ($P<0.05$) and subsequently Elastic Modulus 42% ($P<0.05$). This increase in mechanical performance may have a significant impact on bone's resistance to fracture during a fall. Recently, a study in human femoral head specimens showed shown that similar reductions in BVF and Tb.Th. were risk factors for traumatic fracture [188]. Therefore, the findings of the in vivo studies presented in this dissertation suggest that LIPUS technology could enhance current standards of care for postmenopausal bone loss.

How does morphology effect bone's susceptibility to therapeutic ultrasound?

Ultrasound behaves as a mechanical wave; as a result, bone's physical characteristics, such as size and shape, play an important role in the transmission of dynamic mechanical signals throughout the tissue. In our in vivo experiments we addressed ultrasounds' ability to protect against bone loss by, introducing treatment immediately after ovariectomy. As a result, ultrasound waves were passed into a system with a relatively high BVF. However, over the course of the four week study, untreated OVX controls experienced a net loss in BVF of 40%. This substantial decrease in BVF would likely have a substantial impact on the transmission of ultrasound waves and the subsequent signals perceived by the affected tissue. While we did not specifically address the ability of ultrasound to recover bone already lost due to OVX in the aims of this dissertation, it is plausible that the altered bone morphology would have introduced a confounding factor. Skeletal sites or disease states with different bone morphologies may require different ultrasound signals to produce similar effects regardless of the underlying biochemical status.

Trabecular morphology may also influence the adaptation of the signals presented in this dissertation into a clinically relevant therapy. Ultrasound propagation in trabecular bone occurs primarily along the trabeculae themselves [189]; therefore, there exists a potential for large amounts of dispersion and attenuation in structures where trabeculae are not aligned with the direction of the propagating wave [181]. This could prove to be an important factor if the ultrasound signals presented in this dissertation were translated to the case of an osteopenic human vertebra. In human vertebra, osteoporosis preferentially targets transverse trabeculae, leaving fewer structures available to transmit a signal applied in the anterior-posterior direction. The OVX rat model used in or studies had a relatively high BVF, even after 4 weeks of OVX, which may have made it increasingly susceptible to therapeutic ultrasound signals. In addition, this may explain why some studies did not find improvements in bone quality at the proximal tibia or distal femur using similar ultrasound signals [59-61]. The interactions between ultrasound and bone are highly sensitive to the composition and organization of the underlying tissue and therefore, should be carefully considered in future studies.

Understanding the complex interactions between ultrasound and bone morphology could prove crucial in the adaptation of the ultrasound signals pursued in this dissertation to other skeletal sites or between species.

What is the mechanism of ultrasound action in bone?

While the precise mechanism by which LIPUS acts in bone remains unclear, several possibilities have been proposed. First, ultrasound may act to generate a pulsed electromagnetic field (PEMF), which could then drive an osteogenic adaptation [113]. While we did not specifically address this issue in our study, an in vitro study has shown that ultrasound could generate an electric field in the range believed to be anabolic to bone tissue [112]. A second possible mechanism could involve acoustic streaming. Since ultrasound behaves as a mechanical wave, it could generate local pressure gradients within bone's micro vasculature [96, 97]. As the ultrasound wave propagates through bone, regions of dissimilar pressure would be created within bone's micro porosities. The magnitude and distance over which these pressures act would be a function of signal intensity and wavelength. Several recent studies have suggested that fluid movement within these structures could generate the mechanical signals required of an osteogenic response [27, 29]. If acoustic microstreaming plays a role in mechanotransduction of ultrasound signals, bone's response would be sensitive to parameters affecting the pressure gradient (signal intensity) and distance over which that gradient acts (wavelength). In this dissertation, we showed that bone's response was sensitive to differences in signal intensity. This supports our hypothesis that microvasculature plays a role in bone's response and suggests that a minimum pressure gradient is required to regulate bone's response. We also showed that signals with different frequencies, and therefore wavelengths, produced anti-catabolic responses at substantially different intensities. This indicates that wavelength plays an important role in regulating bone's response and, could be partially explained by the mechanisms

of acoustic microstreaming. These findings further indicate acoustic microstreaming as an important factor regulating bone's response to low intensity ultrasound.

How might ultrasound generate local bone fluid flow?

We have proposed that ultrasound induced pressure gradients could affect bone fluid flow. Subsequently, fluid movement within bone's microvasculature could initiate molecular events with the osteocyte. Therefore, it is crucial to draw a relationship between an applied pressure and the fluid movement in bone's micro porosities. While it is difficult or perhaps impossible to measure pressure gradients within the lacular-canalicular system, it may be possible to describe the relationship between pressure in bone (a porous medium) and local fluid velocity using Darcy's Law.

We can calculate fluid velocity within any of bone's hierarchal porosities using Darcy's law, where κ is the permeability (m^2), μ is the viscosity (Pa s) and ΔP and L are the peak-to-peak pressure amplitude and ½ wavelength shown in Figure 8.1.

$$q = \frac{-\kappa}{\mu}\frac{\Delta P}{L}$$

We may estimate ΔP to be 1.5 kPa, assuming a hydrostatic state of 0.1 με in cortical bone with an Elastic Modulus of 15 GPa. In water, the maximum pressure gradient is achieved over one half wavelength; thus, under ideal conditions, L would be equal to 0.1mm. The intrinsic properties of water give a μ of 0.798 at 30◦C. One may also note that for cases where ultrasound waves interact with bone structures, L may vary, thus affecting local velocity profiles. Modeling approaches similar to those used in Chapter VII could improve our prediction of L and ΔP. Permeability exists as a function of hierarchal porosity and in haversion systems may be on the order of 1 x 10^{-8} [190]. Using the equation described above, we may estimate that fluid velocity within the haversion systems may reach 0.16 m/s. In this way, bone fluid flow could induce mechanosensation by perturbing integrins [191] of affecting primary cilia [192, 193]. This three-dimensional approach may be useful as a tool to investigate more complex systems such as those found in in*vivo* and in*vitro* applications of ultrasound perturbation.

Conclusions

In summary, we found low intensity ultrasound is capable of attenuating changes to bone morphology which result from OVX. Bone is responsive to optimized low intensity signals on the order of 0.1mW/cm^2 delivered at 0.5MHz and higher intensity signals above 30mW/cm^2 delivered at 1.5MHz. We found that bone's response is sensitive to changes in signal intensity but not pulse duration. At the tissue level only, higher intensity signals, above 30mW/cm^2, are capable of increasing bone's Elastic Modulus. While Elastic Modulus was not recovered under lower intensity signals (~0.1mW/cm^2), significant improvements were observed in loss tangent, suggesting an adaptive response which could improve resistance to fracture. The development of future ultrasound technologies should consider the complex interactions between ultrasound and the highly nonlinear geometry of bone. Furthermore, computational approaches may offer a means for developing individualized, site specific and targeted therapies

which consider a patient's individuals bone status in the optimization of a treatment protocol.

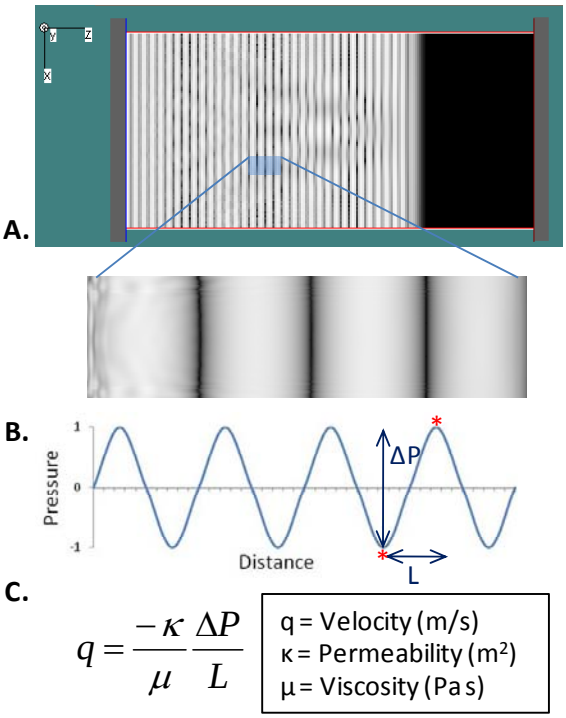

Figure 8.1: *(A) A representative series of ultrasound pulses (B) An expanded view of an ultrasound signal (C) Equation of Darcy's Law.*

Bibliography

1. ABPI. 2007 [cited 2007 May]; Available from: http://www.abpi.org.uk/publications/publication_details/azResearch/o3.asp
2. Gray, H., et al., *Gray's anatomy : the anatomical basis of clinical practice*. 39th ed. 2005, Edinburgh ; New York: Elsevier Churchill Livingstone. xx, 1627 p.
3. Fung, Y.C., *Biomechanics: mechanical properties of living tissues*. 1993, New York: Springer Verlag. 568.
4. NIH. *Osteoporosis prevention, diagnosis and therapy. National Institutes of health concensus development conference statement*. 2000.
5. Melton, L.J., *Excess mortality following vertebral fracture.* J Am Geriatr Soc, 2000. **48**(3): p. 338-9.
6. NOF, N., *Disease facts*. 2005.
7. Riggs, B. and L. Melton, *The worldwide problem of osteoporosis: insights affprded by epidemiology.* Bone, 1995. **17**(5 Suppl): p. 505S-511S.
8. Senanayake, P., *Women and reproductive health in a graying world.* Int J Gynaecol Obstet, 2000. **70**(1): p. 59-67.
9. Riggs, B.L., et al., *Population-based study of age and sex differences in bone volumetric density, size, geometry, and structure at different skeletal sites.* J Bone Miner Res, 2004. **19**: p. 1945-54.
10. NOF, N., *Disease Statistics: Osteoporosis*. 2003.
11. Day, J.S., et al., *Bisphosphonate treatment affects trabecular bone apparent modulus through micro-architecture rather than matrix properties.* J Orthop Res, 2004. **22**(3): p. 465-71.
12. Rubin, C., et al., *Anabolism. Low mechanical signals strengthen long bones.* Nature, 2001. **412**(6847): p. 603-4.
13. Bonewald, L.F., *Osteocyte biology: its implications for osteoporosis.* J Musculoskelet Neuronal Interact, 2004. **4**(1): p. 101-4.
14. Forwood, M.R. and C.H. Turner, *Skeletal adaptations to mechanical usage: results from tibial loading studies in rats.* Bone, 1995. **17**(4 Suppl): p. 197S-205S.
15. Lanyon, L.E. and C.T. Rubin, *Static vs dynamic loads as an influence on bone remodelling.* J Biomech, 1984. **17**(12): p. 897-905.
16. Rubin, C.T. and L.E. Lanyon, *Regulation of bone mass by mechanical strain magnitude.* Calcif Tissue Int, 1985. **37**(4): p. 411-7.
17. Gross, T.S., et al., *Strain gradients correlate with sites of periosteal bone formation.* J Bone Miner Res, 1997. **12**(6): p. 982-8.
18. Judex, S., T.S. Gross, and R.F. Zernicke, *Strain gradients correlate with sites of exercise-induced bone-forming surfaces in the adult skeleton.* J Bone Miner Res, 1997. **12**(10): p. 1737-45.
19. Judex, S. and R.F. Zernicke, *High-impact exercise and growing bone: relation between high strain rates and enhanced bone formation.* J Appl Physiol, 2000. **88**(6): p. 2183-91.
20. Mosley, J.R., et al., *Strain magnitude related changes in whole bone architecture in growing rats.* Bone, 1997. **20**(3): p. 191-8.
21. Turner, C.H., *Three rules for bone adaptation to mechanical stimuli.* Bone, 1998. **23**(5): p. 399-407.
22. Rubin, C.T., *Skeletal strain and the functional significance of bone architecture.* Calcif Tissue Int, 1984. **36 Suppl 1**: p. S11-8.
23. Batra, N.N., et al., *Effects of short-term recovery periods on fluid-induced signaling in osteoblastic cells.* J Biomech, 2005. **38**(9): p. 1909-17.
24. LaMothe, J.M. and R.F. Zernicke, *Rest insertion combined with high-frequency loading enhances osteogenesis.* J Appl Physiol, 2004. **96**(5): p. 1788-93.
25. Srinivasan, S., et al., *Low-magnitude mechanical loading becomes osteogenic when rest is inserted between each load cycle.* J Bone Miner Res, 2002. **17**(9): p. 1613-20.
26. Cowin, S.C., *Mechanosensation and fluid transport in living bone.* J Musculoskelet Neuronal Interact, 2002. **2**(3): p. 256-60.

27. Han, Y., et al., *Mechanotransduction and strain amplification in osteocyte cell processes.* Proc Natl Acad Sci U S A, 2004. **101**(47): p. 16689-94.
28. Riddle, R.C. and H.J. Donahue, *From streaming-potentials to shear stress: 25 years of bone cell mechanotransduction.* J Orthop Res, 2009. **27**(2): p. 143-9.
29. Weinbaum, S., P. Guo, and L. You, *A new view of mechanotransduction and strain amplification in cells with microvilli and cell processes.* Biorheology, 2001. **38**(2-3): p. 119-42.
30. Wang, L., et al., *On bone adaptation due to venous stasis.* J Biomech, 2003. **36**(10): p. 1439-51.
31. Nolte, P.A., J. Klein-Nulend, and G.H. Albers, *Low intensity ultrasound stimulates in vitro endochondral ossification.* Calcif Tissue Int, 1999. **64**(Supp V): p. S62.
32. Nolte, P.A., et al., *Low-intensity ultrasound stimulates endochondral ossification in vitro.* J Orthop Res, 2001. **19**(2): p. 301-7.
33. Doan, N., et al., *In vitro effects of therapeutic ultrasound on cell proliferation, protein synthesis and cytokine production by human fibroblasts, osteoblasts and monocytes.* J Oral Maxillofac Surg, 1999. **57**: p. 409-19.
34. Reher, P., et al., *Therapeutic ultrasound for osteonecrosis: An in vitro comparison between 1MHz and 45 kHz machines.* Eur J Cancer, 1998. **34**: p. 1962-1968.
35. Saito, M., et al., *Effect of low- and high-intensity pulsed ultrasound on collagen post-translational modifications in MC3T3-E1 osteoblasts.* Calcif Tissue Int, 2004. **75**(5): p. 384-95.
36. Saito, M., et al., *Intensity-related differences in collagen post-translational modification in MC3T3-E1 osteoblasts after exposure to low- and high-intensity pulsed ultrasound.* Bone, 2004. **35**(3): p. 644-55.
37. Pan, H., et al., *Study of sonoporation dynamics affected by ultrasound duty cycle.* Ultrasound Med Biol, 2005. **31**(6): p. 849-56.
38. Harle, J., et al., *Effects of therapeutic ultrasound on osteoblast gene expression.* J Mater Sci Mater Med, 2001. **12**(10-12): p. 1001-4.
39. Li, J.G., et al., *Optimum intensities of ultrasound for PGE(2) secretion and growth of osteoblasts.* Ultrasound Med Biol, 2002. **28**(5): p. 683-90.
40. Reher, P., et al., *The stimulation of bone formation in vitro by therapeutic ultrasound.* Ultrasound Med Biol, 1997. **23**(8): p. 1251-8.
41. Sun, J.S., et al., *In vitro effects of low-intensity ultrasound stimulation on the bone cells.* J Biomed Mater Res, 2001. **57**(3): p. 449-56.
42. Heckman, J.D., et al., *Acceleration of tibial fracture-healing by non-invasive, low-intensity pulsed ultrasound.* J Bone Joint Surg Am, 1994. **76**(1): p. 26-34.
43. Heckman, J.D. and J. Sarasohn-Kahn, *The economics of treating tibia fractures. The cost of delayed unions.* Bull Hosp Jt Dis, 1997. **56**(1): p. 63-72.
44. Cook, S.D., et al., *Acceleration of tibia and distal radius fracture healing in patients who smoke.* Clin Orthop Relat Res, 1997(337): p. 198-207.
45. Kristiansen, T.K., et al., *Accelerated healing of distal radial fractures with the use of specific, low-intensity ultrasound. A multicenter, prospective, randomized, double-blind, placebo-controlled study.* J Bone Joint Surg Am, 1997. **79**(7): p. 961-73.
46. Mayr, E., et al., *[Does low intensity, pulsed ultrasound speed healing of scaphoid fractures?].* Handchir Mikrochir Plast Chir, 2000. **32**(2): p. 115-22.
47. Ito, M., Y. Azuma, and Y. Harada, *Low intensity pulsed ultrasound accelerates fracture-healing by non-invasive, low-intensity pulsed ultrasound.* J Bone Joint Surg Am, 1998. **76A**: p. 26-34.
48. Wang, S.J., et al., *Low intensity ultrasound treatment increases strength in a rat femoral fracture model.* J Orthop Res, 1994. **12**(1): p. 40-7.
49. Pilla, A.A., et al., *Non-invasive low-intensity pulsed ultrasound accelerates bone healing in the rabbit.* J Orthop Trauma, 1990. **4**(3): p. 246-53.
50. Chan, C.W., et al., *Dose-dependent effect of low-intensity pulsed ultrasound on callus formation during rapid distraction osteogenesis.* J Orthop Res, 2006. **24**(11): p. 2072-9.
51. Malizos, K.N., et al., *Transosseous application of low-intensity ultrasound for the enhancement and monitoring of fracture healing process in a sheep osteotomy model.* Bone, 2006. **38**(4): p. 530-9.

52. Gebauer, D., et al., *Low-intensity pulsed ultrasound: effects on nonunions.* Ultrasound Med Biol, 2005. **31**(10): p. 1391-402.
53. Duarte, L.R., *The stimulation of bone growth by ultrasound.* Arch Orthop Trauma Surg, 1983. **101**(3): p. 153-9.
54. Frankel, V.H., *Results of Prescription Use of Pulse Ultrasound Therapy in Fracture Management.* Surg Technol Int, 1998. **VII**: p. 389-393.
55. Gold, S.M. and R. Wasserman, *Preliminary results of tibial bone transports with pulsed low intensity ultrasound (Exogen).* J Orthop Trauma, 2005. **19**(1): p. 10-6.
56. Jones, C.P., M.J. Coughlin, and P.S. Shurnas, *Prospective CT scan evaluation of hindfoot nonunions treated with revision surgery and low-intensity ultrasound stimulation.* Foot Ankle Int, 2006. **27**(4): p. 229-35.
57. Lerner, A., H. Stein, and M. Soudry, *Compound high-energy limb fractures with delayed union: our experience with adjuvant ultrasound stimulation (exogen).* Ultrasonics, 2004. **42**(1-9): p. 915-7.
58. Warden, S.J., et al., *Efficacy of low-intensity pulsed ultrasound in the prevention of osteoporosis following spinal cord injury.* Bone, 2001. **29**(5): p. 431-6.
59. Spadaro, J.A. and S.A. Albanese, *Application of low-intensity ultrasound to growing bone in rats.* Ultrasound Med Biol, 1998. **24**(4): p. 567-73.
60. Yang, R.S., et al., *The effects of low-intensity ultrasound on growing bone after sciatic neurectomy.* Ultrasound Med Biol, 2005. **31**(3): p. 431-7.
61. Warden, S.J., et al., *Skeletal effects of low-intensity pulsed ultrasound on the ovariectomized rodent.* Ultrasound Med Biol, 2001. **27**(7): p. 989-98.
62. Carvalho, D.C. and A. Cliquet Junior, *The action of low-intensity pulsed ultrasound in bones of osteopenic rats.* Artif Organs, 2004. **28**(1): p. 114-8.
63. Arai, T., et al., *The effects of ultrasound stimulation on disuse osteoporisis.* Trans Bioelectr Repair Growth Soc, 1993. **13**: p. 17.
64. Yang, K.H., et al., *Exposure to low-intensity ultrasound increases aggrecan gene expression in a rat femur fracture model.* J Orthop Res, 1996. **14**(5): p. 802-9.
65. Tsai, C.L., W.H. Chang, and T.K. Liu, *Preliminary studies of duration and intensity of ultrasonic treatments on fracture repair.* Chin J Physiol, 1992. **35**(1): p. 21-6.
66. Ito, M., et al., *Differences in three-dimensional trabecular microstructure in osteopenic rat models caused by ovariectomy and neuroectomy.* Bone, 2002. **30**(4): p. 594-8.
67. Laib, A., et al., *The temporal changes of trabecular architecture in ovariectomized rats assessed by MicroCT.* Osteoporos Int, 2001. **12**(11): p. 936-41.
68. Ikeda, S. and e.a. H. Tsurukami, *Effect of trabecular bone contour on ultimate strength of lumbar vertebra after bilateral ovariectomy in rats.* Bone, 2001. **28**(6): p. 625-33.
69. Yamaura, M., et al., *Local bone turnover in the metaphysis of the proximal tibia and the lumbar vertebra during the early periods after ovariectomy in rats.* Calcif Tissue Int, 1996. **58**(1): p. 52-9.
70. Li, C.Y., et al., *Estrogen and "exercise" have a synergistic effect in preventing bone loss in the lumbar vertebra and femoral neck of the ovariectomized rat.* Calcif Tissue Int, 2003. **72**(1): p. 42-9.
71. Pytlik, M., J. Folwarczna, and W. Janiec, *Effects of doxycycline on mechanical properties of bones in rats with ovariectomy-induced osteopenia.* Calcif Tissue Int, 2004. **75**(3): p. 225-30.
72. Mosekilde, L., C.C. Danielsen, and U.B. Knudsen, *The effect of aging and ovariectomy on the vertebral bone mass and biomechanical properties of mature rats.* Bone, 1993. **14**(1): p. 1-6.
73. Samnegard, E., M.P. Akhter, and R.R. Recker, *Maintenance of vertebral body bone mass and strength created by human parathyroid hormone treatment in ovariectomized rats.* Bone, 2001. **28**(4): p. 414-22.
74. Jiang, Y., et al., *Long-term changes in bone mineral and biomechanical properties of vertebrae and femur in aging, dietary calcium restricted, and/or estrogen-deprived/-replaced rats.* J Bone Miner Res, 1997. **12**(5): p. 820-31.
75. Smit, T.H., *The use of a quadruped as an in vivo model for the study of the spine - biomechanical considerations.* Eur Spine J, 2002. **11**(2): p. 137-44.

76. Hoffler, C.E., et al., *Heterogeneity of bone lamellar-level elastic moduli.* Bone, 2000. **26**(6): p. 603-9.
77. Hengsberger, S., A. Kulik, and P. Zysset, *Nanoindentation discriminates the elastic properties of individual human bone lamellae under dry and physiological conditions.* Bone, 2002. **30**(1): p. 178-84.
78. Rho, J.Y., et al., *The anisotropic Young's modulus of equine secondary osteons and interstitial bone determined by nanoindentation.* J Exp Biol, 2001. **204**(Pt 10): p. 1775-81.
79. Rho, J.Y., et al., *Elastic properties of microstructural components of human bone tissue as measured by nanoindentation.* J Biomed Mater Res, 1999. **45**(1): p. 48-54.
80. Rho, J.Y., et al., *Variations in the individual thick lamellar properties within osteons by nanoindentation.* Bone, 1999. **25**(3): p. 295-300.
81. Ferguson, V.L., A.J. Bushby, and A. Boyde, *Nanomechanical properties and mineral concentration in articular calcified cartilage and subchondral bone.* J Anat, 2003. **203**(2): p. 191-202.
82. Hengsberger, S., A. Kulik, and P. Zysset, *A combined atomic force microscopy and nanoindentation technique to investigate the elastic properties of bone structural units.* Eur Cell Mater, 2001. **1**: p. 12-7.
83. Ho, S.P., et al., *The effect of sample preparation technique on determination of structure and nanomechanical properties of human cementum hard tissue.* Biomaterials, 2004. **25**(19): p. 4847-57.
84. Pelled, G., et al., *Structural and nanoindentation studies of stem cell-based tissue-engineered bone.* J Biomech, 2007. **40**(2): p. 399-411.
85. Xu, J., et al., *Atomic force microscopy and nanoindentation characterization of human lamellar bone prepared by microtome sectioning and mechanical polishing technique.* J Biomed Mater Res A, 2003. **67**(3): p. 719-26.
86. Zhang, Y., et al., *Mechanical properties of skeletal bone in gene-mutated stopsel(dtl28d) and wild-type zebrafish (Danio rerio) measured by atomic force microscopy-based nanoindentation.* Bone, 2002. **30**(4): p. 541-6.
87. Hofmann, T., et al., *Assessment of composition and anisotropic elastic properties of secondary osteon lamellae.* J Biomech, 2006. **39**(12): p. 2282-94.
88. Busa, B., et al., *Rapid establishment of chemical and mechanical properties during lamellar bone formation.* Calcif Tissue Int, 2005. **77**(6): p. 386-94.
89. Muller, R., T. Hildebrand, and P. Ruegsegger, *Non-invasive bone biopsy: a new method to analyse and display the three-dimensional structure of trabecular bone.* Phys Med Biol, 1994. **39**(1): p. 145-64.
90. Van Rietbergen, B., et al., *Tissue stresses and strain in trabeculae of a canine proximal femur can be quantified from computer reconstructions.* J Biomech, 1999. **32**(2): p. 165-73.
91. Mittra, E., S. Akella, and Y.X. Qin, *The effects of embedding material, loading rate and magnitude, and penetration depth in nanoindentation of trabecular bone.* J Biomed Mater Res A, 2006. **79**(1): p. 86-93.
92. Oliver, W.C. and G.M. Pharr, *An improved technique for determining hardness and elastic modulus using load and displacement sensing indentation experiments.* J Mater Res Soc, 1992. **7**(6): p. 1564-1583.
93. Oliver, W.C. and G.M. Pharr, *Measurement of hardness and elastic modulus by instrumented indentation: Advances in understanding and refinements to methodology.* J Mater Res Soc, 2004. **19**(1): p. 3-20.
94. Johnell, O. and J. Kanis, *Epidemiology of osteoporotic fractures.* Osteoporos Int, 2005. **16 Suppl 2**: p. S3-7.
95. NationalInstitutesofHealth. *Osteoporosis prevention, diagnosis and therapy. National Institutes of health concensus development conference statement*. 2000.
96. Pohl, P., Y.N. Antoneko, and E. Rosenfeld, *Effects of ultrasound on the pH profiles in the unstirred layers near bilayer lipid membranes measured by microelectrodes.* Biochim Biophys Ata, 1993. **1152**: p. 155-60.

97. Pohl, P., E. Rosenfeld, and R. Millner, *Effects of ultrasound on the steady-state transmembrane pH grardient and th epermeability of acetic acid through bilayer lipid membranes.* Biochim Biophys Ata, 1993. **1145**: p. 279-83.
98. Qin, Y.X., et al., *Fluid pressure gradients, arising from oscillations in intramedullary pressure, is correlated with the formation of bone and inhibition of intracortical porosity.* J Biomech, 2003. **36**(10): p. 1427-37.
99. Wimsatt, J., et al., *Ultrasound therapy for the prevention and correction of contractures and bone mineral loss associated with wing bandaging in the domestic pigeon (Columba livia).* J Zoo Wildl Med, 2000. **31**(2): p. 190-5.
100. Boonen, S., et al., *Recent developments in the management of postmenopausal osteoporosis with bisphosphonates: enhanced efficacy by enhanced compliance.* J Intern Med, 2008. **264**(4): p. 315-32.
101. Recker, R.R., et al., *Safety of bisphosphonates in the treatment of osteoporosis.* Am J Med, 2009. **122**(2 Suppl): p. S22-32.
102. Li, J., T. Mashiba, and D.B. Burr, *Bisphosphonate treatment suppresses not only stochastic remodeling but also the targeted repair of microdamage.* Calcif Tissue Int, 2001. **69**(5): p. 281-6.
103. Mashiba, T., et al., *Effects of suppressed bone turnover by bisphosphonates on microdamage accumulation and biomechanical properties in clinically relevant skeletal sites in beagles.* Bone, 2001. **28**(5): p. 524-31.
104. Greenspan, S.L., L. Maitland-Ramsey, and E. Myers, *Classification of osteoporosis in the elderly is dependent on site-specific analysis.* Calcif Tissue Int, 1996. **58**(6): p. 409-14.
105. Stoch, S.A., et al., *Classification of osteoporosis and osteopenia in men is dependent on site-specific analysis.* J Clin Densitom, 2000. **3**(4): p. 311-7.
106. Varney, L.F., et al., *Classification of osteoporosis and osteopenia in postmenopausal women is dependent on site-specific analysis.* J Clin Densitom, 1999. **2**(3): p. 275-83.
107. Azuma, Y., et al., *Low-intensity pulsed ultrasound accelerates rat femoral fracture healing by acting on the various cellular reactions in the fracture callus.* J Bone Miner Res, 2001. **16**(4): p. 671-80.
108. Rawool, N.M., et al., *Power Doppler assessment of vascular changes during fracture treatment with low-intensity ultrasound.* J Ultrasound Med, 2003. **22**(2): p. 145-53.
109. Cook, S.D., et al., *Low-intensity pulsed ultrasound improves spinal fusion.* Spine J, 2001. **1**(4): p. 246-54.
110. Leung, K.S., et al., *Complex tibial fracture outcomes following treatment with low-intensity pulsed ultrasound.* Ultrasound Med Biol, 2004. **30**(3): p. 389-95.
111. Hadjiargyrou, M., et al., *Enhancement of fracture healing by low intensity ultrasound.* Clin Orthop Relat Res, 1998(355 Suppl): p. S216-29.
112. Montalibet, A., et al., *Electric current generated by ultrasonically induced Lorentz force in biological media.* Med Biol Eng Comput, 2001. **39**(1): p. 15-20.
113. Pilla, A.A., *Low-intensity electromagnetic and mechanical modulation of bone growth and repair: are they equivalent?* J Orthop Sci, 2002. **7**(3): p. 420-8.
114. Nahirnyak, V., T.D. Mast, and C.K. Holland, *Ultrasound-induced thermal elevation in clotted blood and cranial bone.* Ultrasound Med Biol, 2007. **33**(8): p. 1285-95.
115. Duck, F.A., *Hazards, risks and safety of diagnostic ultrasound.* Med Eng Phys, 2008. **30**(10): p. 1338-48.
116. Myers, M.R., *Transient temperature rise due to ultrasound absorption at a bone/soft-tissue interface.* J Acoust Soc Am, 2004. **115**(6): p. 2887-91.
117. Stratmeyer, M.E., et al., *Fetal ultrasound: mechanical effects.* J Ultrasound Med, 2008. **27**(4): p. 597-605; quiz 606-9.
118. Carstensen, E.L., S. Gracewski, and D. Dalecki, *The search for cavitation in vivo.* Ultrasound Med Biol, 2000. **26**(9): p. 1377-85.
119. Dalecki, D., *Mechanical bioeffects of ultrasound.* Annu Rev Biomed Eng, 2004. **6**: p. 229-48.
120. ter Haar, G., *Therapeutic applications of ultrasound.* Prog Biophys Mol Biol, 2007. **93**(1-3): p. 111-29.

121. Yang, K.H. and S.J. Park, *Stimulation of fracture healing in a canine ulna full-defect model by low-intensity pulsed ultrasound.* Yonsei Med J, 2001. **42**(5): p. 503-8.
122. Hill, C.R., J.C. Bamber, and G.R. ter Haar, *Physical Principles of Medical Ultrasonics*, ed. C.R. Hill, J.C. Bamber, and G.R. ter Haar. 2002.
123. Carter, D.R. and W.C. Hayes, *The compressive behavior of bone as a two-phase porous structure.* J Bone Joint Surg., 1977. **59**: p. 954-962.
124. Rice, J.C., S.C. Cowin, and J.A. Bowman, *On the dependence of the elasticity and strength of cancellous bone on apparent density.* J Biomech, 1988. **21**(2): p. 155-68.
125. Burr, D.B., *Bone material properties and mineral matrix contributions to fracture risk or age in women and men.* J Musculoskelet Neuronal Interact, 2002. **2**(3): p. 201-4.
126. Ferreri, S. and Y.X. Qin, *Anabolic Role of Therapeutic Ultrasound in Mediation of Bone Loss in an OVX Induced Osteopenia Rat Model* in *Transactions of the Orthopaedic Research Society*. 2008, Transactions Vol.33, San Francisco, CA, 2008: San Francisco, CA.
127. Bembey, A.K., et al. *Contribution of collagen, mineral and water phases to the nanomechanical properties of bone*. 2005. Boston, MA, United States: Materials Research Society, Warrendale, PA 15086, United States.
128. Burr, D.B., *The contribution of the organic matrix to bone's material properties.* Bone, 2002. **31**(1): p. 8-11.
129. Evans, G.P., et al., *Microhardness and Young's modulus in cortical bone exhibiting a wide range of mineral volume fractions, and in a bone analogue* J Mater Sci Mater Med, 1990. **1**(1): p. 38-43.
130. Hengsberger, S., et al., *Intrinsic bone tissue properties in adult rat vertebrae: modulation by dietary protein.* Bone, 2005. **36**(1): p. 134-41.
131. Roy, M.E., et al., *Correlations between osteocalcin content, degree of mineralization, and mechanical properties of C. carpio rib bone.* J Biomed Mater Res, 2001. **54**(4): p. 547-53.
132. Tai, K., H.J. Qi, and C. Ortiz, *Effect of mineral content on the nanoindentation properties and nanoscale deformation mechanisms of bovine tibial cortical bone.* J Mater Sci Mater Med, 2005. **16**(10): p. 947-59.
133. Loubet, J.L., *Some measurements of viscoelastic properties with the help of nanoindentation.* NIST Special Publication, 1996: p. 31-34.
134. Rho, J.Y., et al., *Relationship between ultrastructure and the nanoindentation properties of intramuscular herring bones.* Ann Biomed Eng, 2001. **29**(12): p. 1082-8.
135. Bembey, A.K., et al., *Viscoelastic properties of bone as a function of hydration state determined by nanoindentation.* Philosophical Magazine, 2006. **86**(33): p. 5691-5703.
136. Fan, Z. and J.Y. Rho, *Effects of viscoelasticity and time-dependent plasticity on nanoindentation measurements of human cortical bone.* J Biomed Mater Res A, 2003. **67**(1): p. 208-14.
137. Sirola, J., et al., *Factors related to postmenopausal muscle performance: a cross-sectional population-based study.* Eur J Appl Physiol, 2004. **93**(1-2): p. 102-7.
138. Zimmermann, C.L. and T.M. Cook, *Effects of vibration frequency and postural changes on human responses to seated whole-body vibration exposure.* Int Arch Occup Environ Health, 1997. **69**(3): p. 165-79.
139. Westgaard, R.H., *Measurement and evaluation of postural load in occupational work situations.* Eur J Appl Physiol Occup Physiol, 1988. **57**(3): p. 291-304.
140. Swadener, J.G., J.Y. Rho, and G.M. Pharr, *Effects of anisotropy on elastic moduli measured by nanoindentation in human tibial cortical bone.* J Biomed Mater Res, 2001. **57**(1): p. 108-12.
141. Fan, Z., et al., *Anisotropic properties of human tibial cortical bone as measured by nanoindentation.* J Orthop Res, 2002. **20**(4): p. 806-10.
142. Rubin, C., S. Judex, and Y.X. Qin, *Low-level mechanical signals and their potential as a non-pharmacological intervention for osteoporosis.* Age Ageing, 2006. **35 Suppl 2**: p. ii32-ii36.
143. Garman, R., et al., *Low-level accelerations applied in the absence of weight bearing can enhance trabecular bone formation.* J Orthop Res, 2007. **25**(6): p. 732-40.
144. Garman, R., C. Rubin, and S. Judex, *Small oscillatory accelerations, independent of matrix deformations, increase osteoblast activity and enhance bone morphology.* PLoS ONE, 2007. **2**(7): p. e653.

145. Qin, Y.X., C.T. Rubin, and K.J. McLeod, *Nonlinear dependence of loading intensity and cycle number in the maintenance of bone mass and morphology.* J Orthop Res, 1998. **16**(4): p. 482-9.
146. Heybeli, N., et al., *Diagnostic ultrasound treatment increases the bone fracture-healing rate in an internally fixed rat femoral osteotomy model.* J Ultrasound Med, 2002. **21**(12): p. 1357-63.
147. NEMA, N., *Acoustic Output Measurement Standard for Diagnostic Ultrasound Equipment, Revision3 NEMA UD 2-2004.* 2004.
148. Chang, W.H., et al., *Study of thermal effects of ultrasound stimulation on fracture healing.* Bioelectromagnetics, 2002. **23**(4): p. 256-63.
149. Chen, H., X. Li, and M. Wan, *Spatial-temporal dynamics of cavitation bubble clouds in 1.2 MHz focused ultrasound field.* Ultrason Sonochem, 2006. **13**(6): p. 480-6.
150. Gilsanz, V., et al., *Low-level, high-frequency mechanical signals enhance musculoskeletal development of young women with low BMD.* J Bone Miner Res, 2006. **21**(9): p. 1464-74.
151. Rubin, C., et al., *Prevention of postmenopausal bone loss by a low-magnitude, high-frequency mechanical stimuli: a clinical trial assessing compliance, efficacy, and safety.* J Bone Miner Res, 2004. **19**(3): p. 343-51.
152. Rubin, C., et al., *Mechanical strain, induced noninvasively in the high-frequency domain, is anabolic to cancellous bone, but not cortical bone.* Bone, 2002. **30**(3): p. 445-52.
153. Xie, L., et al., *Low-level mechanical vibrations can influence bone resorption and bone formation in the growing skeleton.* Bone, 2006. **39**(5): p. 1059-66.
154. Christiansen, B.A. and M.J. Silva, *The effect of varying magnitudes of whole-body vibration on several skeletal sites in mice.* Ann Biomed Eng, 2006. **34**(7): p. 1149-56.
155. Ferreri, S., et al. *Mediation of Bone Loss with Ultrasound Induced Dynamic Mechanical Signals in an OVX Induced Rat Model of Osteopenia*. in *Transactions of the American Society of Bone and Mineral Research*. 2008.
156. Misra, S.K., et al., *Fabrication and Characterization of Biodegradable Poly(3-hydroxybutyrate) Composite Containing Bioglass.* Biomacromolecules, 2007. **8**(7): p. 2112-2119.
157. Foschia, R., M. Jobin, and S. Hengsberger, *Local dynamic mechanical analysis.* Micron, 2009. **40**(1): p. 51-55.
158. Donnelly, E., et al., *Effects of surface roughness and maximum load on the mechanical properties of cancellous bone measured by nanoindentation.* J Biomed Mater Res A, 2006. **77**(2): p. 426-35.
159. Donnelly, E., et al., *Quasistatic and dynamic nanomechanical properties of cancellous bone tissue relate to collagen content and organization.* J Mater Res Soc, 2006. **21**(8): p. 2106-2117.
160. Doi, M., *Materials Science and Technology: A Comprehensive Treatment, Vol. 12, Structure and Properties of Polymers* ed. E.L. Thomas. 1993: Wiley-VCH.
161. Yeni, Y.N., et al., *The effect of yield damage on the viscoelastic properties of cortical bone tissue as measured by dynamic mechanical analysis.* J Biomed Mater Res A, 2007. **82**(3): p. 530-7.
162. Les, C.M., et al., *Long-term ovariectomy decreases ovine compact bone viscoelasticity.* J Orthop Res, 2005. **23**(4): p. 869-76.
163. Junro Yamashita, B.R.F.H.R.R.X.W.C.M.A., *The use of dynamic mechanical analysis to assess the viscoelastic properties of human cortical bone.* Journal of Biomedical Materials Research, 2001. **58**(1): p. 47-53.
164. Junro Yamashita, X.L.B.R.F.H.R.R.X.W.C.M.A., *Collagen and bone viscoelasticity: A dynamic mechanical analysis.* Journal of Biomedical Materials Research, 2002. **63**(1): p. 31-36.
165. Lakes, R.S., J.L. Katz, and S.S. Sternstein, *Viscoelastic properties of wet cortical bone--I. Torsional and biaxial studies.* J Biomech, 1979. **12**(9): p. 657-78.
166. Riekkinen, O., et al., *Influence of overlying soft tissues on trabecular bone acoustic measurement at various ultrasound frequencies.* Ultrasound Med Biol, 2006. **32**(7): p. 1073-83.
167. Xia, Y., W. Lin, and Y.X. Qin, *The influence of cortical end-plate on broadband ultrasound attenuation measurements at the human calcaneus using scanning confocal ultrasound.* J Acoust Soc Am, 2005. **118**(3 Pt 1): p. 1801-7.
168. Chaffai, S., et al., *In vitro measurement of the frequency-dependent attenuation in cancellous bone between 0.2 and 2 MHz.* J Acoust Soc Am, 2000. **108**(3 Pt 1): p. 1281-9.

169. Langton, C.M., S.B. Palmer, and R.W. Porter, *The measurement of broadband ultrasonic attenuation in cancellous bone.* Eng Med, 1984. **13**(2): p. 89-91.
170. Wear, K.A., *Ultrasonic attenuation in human calcaneus from 0.2 to 1.7 MHz.* IEEE Trans Ultrason Ferroelectr Freq Control, 2001. **48**(2): p. 602-8.
171. Warden, S., et al., *Can conventional therapeutic ultrasound units be used to accelerate fracture repair?* Phys Ther Rev, 1999. **4**: p. 117–126.
172. Biot, M.A., *Theory of Propagation of Elastic Waves in a Fluid-Saturated Porous Solid I. Low-Frequency Range.* The Journal of the Acoustical Society of America, 1956. **28**(2): p. 168-178.
173. Biot, M.A., *Theory of propagation of elastic waves in a fluid saturated porpus solid II. Higher frequency range.* The Journal of the Acoustical Society of America, 1956. **28**(2): p. 179-191.
174. Hosokawa, A., *Simulation of ultrasound propagation through bovine cancellous bone using elastic and Biot's finite-difference time-domain methods.* J Acoust Soc Am, 2005. **118**(3 Pt 1): p. 1782-9.
175. Sebaa, N., et al., *Application of the Biot model to ultrasound in bone: inverse problem.* IEEE Trans Ultrason Ferroelectr Freq Control, 2008. **55**(7): p. 1516-23.
176. Bossy, E., et al., *Attenuation in trabecular bone: A comparison between numerical simulation and experimental results in human femur.* J Acoust Soc Am, 2007. **122**(4): p. 2469-75.
177. Bossy, E., et al., *Three-dimensional simulation of ultrasound propagation through trabecular bone structures measured by synchrotron microtomography.* Phys Med Biol, 2005. **50**(23): p. 5545-56.
178. Padilla, F., et al., *Numerical simulation of wave propagation in cancellous bone.* Ultrasonics, 2006. **44 Suppl 1**: p. e239-43.
179. Kaufman, J.J., G. Luo, and R.S. Siffert, *Ultrasound simulation in bone.* IEEE Trans Ultrason Ferroelectr Freq Control, 2008. **55**(6): p. 1205-18.
180. Luo, G., et al., *Computational methods for ultrasonic bone assessment.* Ultrasound Med Biol, 1999. **25**(5): p. 823-30.
181. Nagatani, Y., et al., *Numerical and experimental study on the wave attenuation in bone--FDTD simulation of ultrasound propagation in cancellous bone.* Ultrasonics, 2008. **48**(6-7): p. 607-12.
182. Luu, Y.K., et al., *In vivo quantification of subcutaneous and visceral adiposity by micro-computed tomography in a small animal model.* Med Eng Phys, 2009. **31**(1): p. 34-41.
183. Beillas, P., et al., *Sensitivity of the tibio-femoral response to finite element modeling parameters.* Comput Methods Biomech Biomed Engin, 2007. **10**(3): p. 209-21.
184. Taddei, F., et al., *Subject-specific finite element models of long bones: An in vitro evaluation of the overall accuracy.* J Biomech, 2006. **39**(13): p. 2457-67.
185. Taddei, F., et al., *Finite-element modeling of bones from CT data: sensitivity to geometry and material uncertainties.* IEEE Trans Biomed Eng, 2006. **53**(11): p. 2194-200.
186. Verhulp, E., et al., *Micro-finite element simulation of trabecular-bone post-yield behaviour--effects of material model, element size and type.* Comput Methods Biomech Biomed Engin, 2008. **11**(4): p. 389-95.
187. Silva, M.J., et al., *Nanoindentation and whole-bone bending estimates of material properties in bones from the senescence accelerated mouse SAMP6.* J Biomech, 2004. **37**(11): p. 1639-46.
188. Tanck, E., et al., *Predictive value of femoral head heterogeneity for fracture risk.* Bone, 2009.
189. Cardoso, L., et al., *In vitro acoustic waves propagation in human and bovine cancellous bone.* J Bone Miner Res, 2003. **18**(10): p. 1803-12.
190. Beno, T., et al., *Estimation of bone permeability using accurate microstructural measurements.* J Biomech, 2006. **39**(13): p. 2378-87.
191. Salter, D.M., J.E. Robb, and M.O. Wright, *Electrophysiological responses of human bone cells to mechanical stimulation: evidence for specific integrin function in mechanotransduction.* J Bone Miner Res, 1997. **12**(7): p. 1133-41.
192. Malone, A.M., et al., *Primary cilia in bone.* J Musculoskelet Neuronal Interact, 2007. **7**(4): p. 301.
193. Malone, A.M., et al., *Primary cilia mediate mechanosensing in bone cells by a calcium-independent mechanism.* Proc Natl Acad Sci U S A, 2007. **104**(33): p. 13325-30.

Appendix A: Validation of μCT Image-based Finite Element Technique

A.1 Introduction

Finite element techniques have been widely used in the field of orthopaedic mechanics to study how changes in bone's microarchitecture and tissue level material properties affect bone's response to mechanical loading. The principal advantage of using these types of models is that they offer a non invasive method for investigating mechanical properties. This allows the researcher to investigate a variety of mechanical loading scenarios using a single "virtual" sample. For example, one may investigate the effects of loading in both the axial and transverse directions using a single sample whereas with traditional physical mechanical testing, separate samples would be needed due to the potential for local tissue fatigue and failure. This can offer a tremendous advantage in the design of experiments in that it allows one to obtain a larger body of data without the need for more animals.

Finite element techniques in general are sensitive to the quality of the input parameters, including: geometry, mesh quality, material property definitions, boundary constraints and loading conditions. The trabecular bone finite element modeling studies used in this dissertation implement a custom meshing tool developed in out lab. In addition they use a commercial finite element solver to solve the finite element equations.

The goal of this appendix was to validate the finite-element techniques used in this dissertation by comparing the results acquired through simulation to those obtained experimentally.

A.2 Methods

Human cadaveric samples were obtained from the anatomy lab of the department of anatomical sciences at Stony Brook University. The samples were obtained from individuals with a mean age of 79±9 years and a mean BVF of 12.6% ±4.1%. Samples are extracted from embalmed human calcanei using a diamond wheel saw under constant irrigation. The samples were approximately 15mm x 15mm x 20 mm in size and were aligned along the principal load bearing axis.

Three-dimensional image data from each ROI was used to generate specimen specific finite-element models, which were then used to evaluate the load bearing capabilities for each sample. Voxel based finite element meshes were created using custom software based on the pixel-to-voxel technique, in which each pixel is represented by an eight-noded cuboid element. Disassociated regions of the model, which did not intersect virtual-cut plane surfaces, were removed to ensure convergence. Trabecular tissue was assumed to behave as a homogenous, linear elastic isotropic solid (E=12GPa & ν=0.3) and full friction boundary conditions were assigned at the superior and inferior surfaces. Trabecular samples were subjected to 0.5% compressive strain in the cranio-caudal direction and a commercial, nonlinear finite element solver (ABAQUS v6.4, Dassault Systemes, Inc., Providence, RI) was used to solve for apparent and tissue level stresses and strains.

Mechanical strain testing was then performed on the samples (858 Minibionix II, MTS Systems, Co.). Steel disks were glued to the superior and inferior surfaces and a

dome shaped disk was placed on the superior surface to ensure even load distribution. Uni-axial compression testing was then performed to failure under displacement control at a loading rate of 5με/s. Elastic modulus, yield strength (calculated by 0.2% strain offset method), and ultimate strength (maximum stress bone sample can hold) were then calculated from the loading-displacement curve.

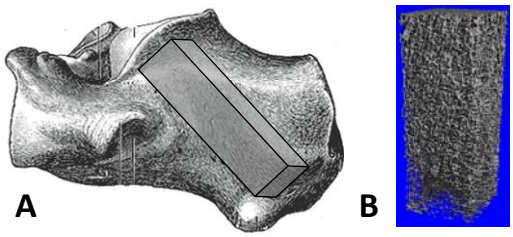

Figure A.1: *(A) A cubiodal specimen was removed from a human calcaneus and oriented along the principal load bearing direction. The samples were then imaged using a μCT scanner at 34μm resolution. The image in (B) depicts an extracted cuboidal sample of human calcaneal bone.*

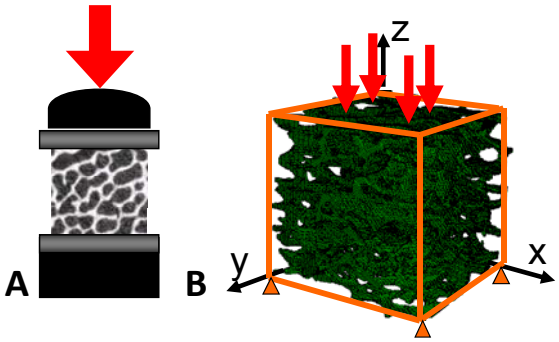

Figure A.2: *Each sample was subjected to both physical mechanical testing and finite element simulations. The mechanical test setup is depicted in (A). Steel disks were glued to the superior and inferior surfaces and a dome shaped disk was placed on the superior surface to ensure even load distribution. Finite element simulations (B) were performed on a 5 x 5 x 5mm cube which was virtually removed from the center of the sample. Boundary and loading conditions are also shown in (B).*

A.3 Results

We found a strong linear correlation (r^2 = 0.89) between Elastic Modulus obtained using experimental and finite element methods.

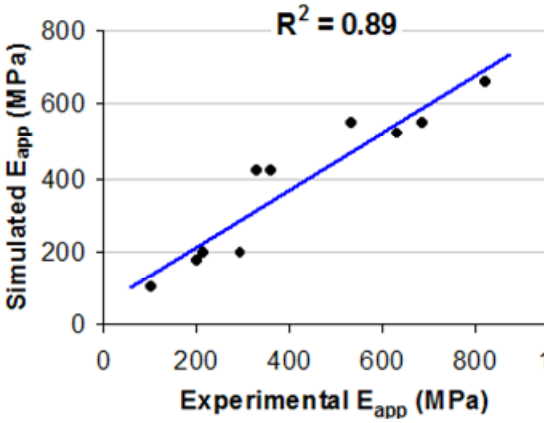

Figure A.3: *Simulated Apparent Young's Modulus found using the finite-element technique presented here was shown to be in good correlation with experimentally derived Apparent Young's Modulus.*

A.4 Discussion

The results of this study suggest that the finite element techniques developed in our group are representative experimental mechanical testing techniques. Therefore, they may be used as an analog to experimental methods. This is particularly advantageous for cases where we are interested in mechanical testing at the tissue level using nanoindentation and for which bulk mechanical testing could alter the tissue level properties.